

# Online Research @ Cardiff

This is an Open Access document downloaded from ORCA, Cardiff University's institutional repository: <https://orca.cardiff.ac.uk/id/eprint/104478/>

This is the author's version of a work that was submitted to / accepted for publication.

Citation for final published version:

Hopkins, Jenni L., Wilson, Colin J. N., Millet, Marc-Alban ORCID: <https://orcid.org/0000-0003-2710-5374>, Leonard, Graham S., Timm, Christian, McGee, Lucy E., Smith, Ian E. M. and Smith, Euan G. C. 2017. Multi-criteria correlation of tephra deposits to source centres applied in the Auckland Volcanic Field, New Zealand. *Bulletin of Volcanology* 79 (7) , 55. 10.1007/s00445-017-1131-y file

Publishers page: <http://dx.doi.org/10.1007/s00445-017-1131-y>  
<<http://dx.doi.org/10.1007/s00445-017-1131-y>>

Please note:

Changes made as a result of publishing processes such as copy-editing, formatting and page numbers may not be reflected in this version. For the definitive version of this publication, please refer to the published source. You are advised to consult the publisher's version if you wish to cite this paper.

This version is being made available in accordance with publisher policies.

See

<http://orca.cf.ac.uk/policies.html> for usage policies. Copyright and moral rights for publications made available in ORCA are retained by the copyright holders.



# **Multi-criteria correlation of tephra deposits to source centres applied in the Auckland Volcanic Field, New Zealand**

**Jenni L. Hopkins**<sup>\*a</sup>, Colin, J.N. Wilson<sup>a</sup>, Marc-Alban Millet<sup>b</sup>, Graham S. Leonard<sup>c</sup>,  
Christian Timm<sup>c</sup>, Lucy E. McGee<sup>d</sup>, Ian E.M. Smith<sup>e</sup>, Euan G.C. Smith<sup>a</sup>.

<sup>\*</sup>Corresponding author: jenni.hopkins@vuw.ac.nz

<sup>a</sup>School of Geography, Environment and Earth Sciences, Victoria University, PO Box 600, Wellington 6140, New Zealand

<sup>b</sup>School of Earth and Ocean Sciences, Cardiff University, Cardiff CF10 3AT, UK

<sup>c</sup>GNS Science, PO Box 30368, Lower Hutt 5040, New Zealand

<sup>d</sup>Department of Earth and Planetary Sciences, E&A 424, Macquarie University, Sydney, NSW 2109, Australia.

<sup>e</sup>School of Environment, Auckland University, Private Bag 92019, Auckland 1142, New Zealand

***Manuscript revised for Bulletin of Volcanology.***

## ***Keywords***

Basalt; correlation; tephra; Auckland Volcanic Field; monogenetic volcanic field;  
tephrochronology;

## ***Highlights***

- Outlines a method to correlate proximal whole rock samples with distal tephra deposits
- Uses this correlation with new age data to reconstruct an age order for AVF eruptions
- Discusses the spatial, temporal, and geochemical evolution of the AVF

## Abstract

Linking tephra back to their source centre(s) in volcanic fields is crucial not only to reconstruct the eruptive history of the volcanic field but also to understand tephra dispersal patterns and thus the potential hazards posed by a future eruption. Here we present a multi-disciplinary approach to correlate distal basaltic tephra deposits from the Auckland Volcanic Field (AVF) to their source centres using proximal whole-rock geochemical signatures. In order to achieve these correlations, major and trace element tephra-derived glass compositions are compared with published and newly obtained whole-rock geochemical data for the entire field. The results show that incompatible trace element ratios (e.g.  $(\text{Gd}/\text{Yb})_{\text{N}}$ ,  $(\text{La}/\text{Yb})_{\text{N}}$ ,  $(\text{Zr}/\text{Yb})_{\text{N}}$ ) vary widely across the AVF (e.g.  $(\text{La}/\text{Yb})_{\text{N}} = 5$  to 40) but show a more restricted range within samples from a single volcanic centre (e.g.  $(\text{La}/\text{Yb})_{\text{N}} = 5$  to 10). These ratios are also the least affected by fractional crystallisation and are therefore the most appropriate geochemical tools for correlation between tephra and whole rock samples. However, findings for the AVF suggest that each volcanic centre does not have a unique geochemical signature in the field as a whole, thus preventing unambiguous correlation of tephra to source centre using geochemistry alone. A number of additional criteria are therefore combined to further constrain the source centres of the distal tephra including age, eruption scale, and location (of centres, and sites where tephra were sampled). The combination of tephrostratigraphy,  $^{40}\text{Ar}/^{39}\text{Ar}$  dating and morphostratigraphic constraints allow, for the first time, the relative and absolute ordering of 48 of 53 volcanic centres of the Auckland Volcanic Field to be resolved. Eruption frequencies are shown to

51 vary between 0.13-1.5 eruptions/kyr and repose periods between individual  
52 eruptions vary from <0.1 to 13 kyr, with 23 of the 48 centres shown to have pre-  
53 eruptive repose periods of <1000 years. No spatial evolutionary trends are  
54 noted, although a relationship between short repose periods and closely spaced  
55 eruption locations is identified for a number of centres. In addition no temporal-  
56 geochemical trends are noted, but a relationship between geochemical signature  
57 and eruption volume is highlighted.  
58

## 59    **Introduction**

60            The eruptive histories of basaltic volcanic fields can be reconstructed by  
61    the dating of lava and scoria deposits. These reconstructions are critical for  
62    understanding the temporal, geochemical and spatial evolution of the fields in  
63    order to better understand their potential future behaviour. However, within  
64    young fields the errors associated with current dating techniques (e.g.  $^{40}\text{Ar}/^{39}\text{Ar}$   
65    or  $^{14}\text{C}$ ) are often larger than the repose periods, and thus hinder establishment of  
66    a definitive stratigraphic age order of the centres (e.g. Briggs et al. 1994; Cook et  
67    al. 2005; Fleck et al. 2014; Leonard et al. 2017). Similarly, due to the restricted  
68    subaerial distribution of scoria and lavas from small monogenetic centres, field-  
69    wide stratigraphic relationships are often difficult to establish, and cannot  
70    resolve ambiguities that arise from the dating techniques. In these circumstances  
71    distal airfall deposits (tephras) can more reliably resolve the chronological  
72    uncertainties due to their higher preservation potential, and often  
73    stratigraphically restricted relationships.

74            Tephra correlation is used on a number of levels from simply correlating  
75    tephra deposit across cores or outcrops (Hopkins et al. 2015), to defining  
76    stratigraphic marker horizons (e.g. Molloy et al. 2009), or matching horizons to  
77    volcanic source or provenance through comparison of distal and proximal tephra  
78    deposit characteristics (e.g. Alloway et al. 2004; Allan et al. 2008; Zawalna-Geer  
79    et al. 2016). Linking tephtras to their source volcanic centre can be  
80    straightforward where the potential number of sources is limited, the eruptive  
81    episodes (and tephtras) are precisely dated, stratigraphic successions are  
82    established in proximal tephra layering, and/or the tephtras (and sources) have

83 distinctive geochemical signatures (Lowe 2011). Where these criteria are not  
84 met, however, difficulties arise in accurately linking distal tephras to their  
85 sources. In cases where there are multiple potential sources and where proximal  
86 deposits are poorly characterised, or poorly preserved, there is currently no  
87 established method to resolve the origin of identified distal tephras.

88         There are a number of processes and features that should be taken into  
89 account when attempting to correlate tephra deposits. The key ones important  
90 for this study are those that can potentially produce differences in the  
91 geochemistry of glass shards in distal tephra horizons. For example, these could  
92 include atmospheric sorting of components during transportation (e.g. Lirer et  
93 al. 1973), or geochemical variation of magma produced during single eruptions  
94 (e.g. Shane et al. 2008), or the presence of micro-inclusions within individual  
95 glass shards (Lowe 2011). In addition, post-eruption processes such as  
96 reworking of deposits can produce repeated sequences (Hopkins et al. 2015),  
97 whereas poor preservation can result in inconsistent deposit thicknesses; both  
98 make the record harder to interpret (e.g. Davies et al. 2001; Pyne O'Donnell  
99 2011). Methodological discrepancies also need to be considered. In general  
100 different sample types and size fractions are not compared (e.g. Larsson 1937),  
101 nor are analyses using different analytical methods. Many of these issues can be  
102 resolved through methodological, statistical or technical practises that we  
103 discuss below. Overall, if distal deposits could be confidently linked to their  
104 source(s), the chronology of a volcanic region could be better resolved.

105         The Auckland Volcanic Field (AVF) is an example of a volcanic region  
106 where climate and urbanization have resulted in the loss or obscuration of  
107 proximal tephra deposits. The spatial density of centres (53 centres distributed

over an area of ca. 600 km<sup>2</sup>; **Fig. 1**) adds further complexity because a given tephra deposit could have come from a number of possible sources (e.g. Shane and Smith 2000). In addition, because of the rapid thinning of basaltic tephra away from source, evidence of stratigraphic successions is often limited to well preserved basinal deposits, for example in the maar crater infillings (e.g. Hopkins et al. 2015). The tephrostratigraphy of six cores from the maar craters in the AVF (Pupuke, Onepoto, Orakei Basin, Glover Park, Hopua, Pukaki; highlighted in red on **Fig. 1**) has been extensively assessed (e.g. Sandiford et al. 2001; Shane and Hoverd 2002; Molloy et al. 2009; Shane et al. 2013; Hopkins et al. 2015; Zawalna-Geer et al. 2016). The tephrostratigraphic framework developed by the careful cross correlation of the tephra deposits between individual cores, and the geochemistry of the tephra-derived glass is used as a basis for this study (e.g. Molloy et al. 2009; Hopkins et al. 2015).

Proximal lava and coarse-grained scoria cone-forming deposits in the AVF (defined here as whole-rock samples) have a higher preservation potential than proximal airfall tephra, and therefore the sources of these materials can be more easily defined (e.g. Hayward et al. 2011). In addition a large number of whole-rock analyses already exist for the AVF centres, characterising their geochemical signatures (**Table 1**). Traditional tephrochronology links distal to proximal tephra deposits, but in the AVF this process is not possible due to the lack of unambiguously sourced proximal tephra beyond the cones themselves. Here we therefore develop and present a method for correlating distal tephra (from cored maar-lake deposits, represented by glass geochemical analyses) to proximal deposits (represented by whole-rock geochemical analyses of lava or large fragments), in order to better constrain the relative and absolute eruption

history of the AVF. Here we define “tephra” as the bulk airfall deposits of material explosively erupted from the volcanoes, now found as unconsolidated pyroclastic horizons within the maar-lake cores (cf. Lowe 2011). Geochemical analyses for this study were undertaken on the juvenile glass shards derived from within these tephra horizons. The term “whole rock” is used here to refer to analyses of individual pieces of solid rock, from lava flows or from individual bombs or lapilli.

## **Methodology**

To provide the most complete basis for tephra-to-source correlations a critical requirement is an extensive database of characteristics for all volcanic centres and tephra deposits in the field. For the AVF a large dataset already exists, including geochemistry of proximal whole-rock samples (e.g. McGee et al. 2013) and geochemistry of distal tephra-derived glass samples (e.g. Hopkins et al. 2015), ages of eruptive centres (e.g. Leonard et al. 2017), and scale of eruptions (e.g. Kereszturi et al. 2013). Currently lacking, however, is a collated field-wide suite of geochemical data of whole-rock compositions, up-to-date estimates of the ages of the tephra horizons in the maar-lake cores, and estimates of tephra volumes for the individual centres. Below we present the methods by which these pre-existing data were collated, and our new data collected.



***Collation of pre-existing data***

***Whole-rock geochemistry for individual centres***

A large amount of unpublished whole-rock geochemical data exists for the AVF. This includes datasets from MSc theses (Bryner 1991; Miller 1996; Franklin 1999; Hookway 2000; Spargo 2007; Eade 2009; see **Table 1**), and the unpublished data of I.E.M. Smith and co-workers at the University of Auckland. We also include here data from McGee (2012), the majority of which is published in McGee et al. (2011, 2012, 2013). For the newly discovered centres of Puhinui Craters and Cemetery Hill (B. Hayward *pers. comm.*), no geochemical or age data exist and therefore these centres are not included in this study. The collated whole-rock major and trace-element dataset can be found in the **supplementary material**.

***Glass geochemistry for individual tephra horizons***

Hopkins et al. (2015) analysed major and trace element geochemistry for glass shards from tephra horizons found in the lacustrine maar cores using Electron Microprobe Analysis (EMPA) and Laser Ablation-ICP-MS (LA-ICP-MS) at Victoria University of Wellington (VUW). Glass shards from only forty-nine basaltic horizons from five maar cores could be analysed for trace element concentrations because glass shard sizes were too small or the samples were no longer available. These data are combined with previously published major element data (Sandiford et al. 2001; Shane and Hoverd 2002; Hoverd et al. 2005; Molloy et al. 2009) reported in Hopkins et al. (2015) and outlined in the **supplementary material**.

*Compatibility of pre-existing and new data*

To ensure compatibility between the data sets, and as a quality control measure, we assessed the analytical methods, accuracy and precision of all data used in this contribution. For all pre-existing whole-rock analyses (outlined above), the methods and standardisation procedures were the same. XRF analyses for major elements were undertaken at the University of Auckland (UoA), and (where applicable) trace elements were analysed using laser ablation (LA)-ICP-MS on the XRF glass discs at the Australian National University (ANU). For XRF methods in-house rock standards were used (see **Supplementary Material**), and the Si concentrations obtained from XRF analysis were used for the trace element calibration. In addition duplicate analyses were undertaken by this study to ensure compatibility of the old and new data sets (see **Supplementary Material**).

For tephra-derived glass chemistry all sample preparation followed the same standard procedures. Major-element geochemistry presented in Sandiford et al (2001) was acquired at VUW on an older instrument than that used by Hopkins et al (2015); both of these studies however used wavelength dispersive X-ray spectroscopy (WDS) techniques. Data presented in Molloy et al (2009), Shane and Hoverd (2002) and Hoverd et al (2005) were obtained by EMPA at University of Auckland (UoA), using energy dispersive X-ray spectroscopy (EDS) techniques. No previous trace-element analysis had been undertaken on these samples prior to work by Hopkins et al (2015). Accuracy and precision of these methods is detailed in the **Supplementary Material**. Duplicate analyses from the same horizons, and from the same shards, were run in order to compare the newly acquired data with the existing data sets (example reported in

**Supplementary Material**). All aspects of these methods for both glass and whole-rock analyses, and the accuracy and precision reported for the standards are comparable to the methods used by this study.

#### *Ages for individual centres*

To maximise the amount of available age data from individual eruptive centres, data from three methods have been collated. These methods include morphostratigraphic evidence (e.g. Hayward et al. 2011),  $^{40}\text{Ar}/^{39}\text{Ar}$  dating of groundmass material (e.g. Cassata et al. 2008; Leonard et al. 2017), and  $^{14}\text{C}$  dating of organic materials contained within or bounding the volcanic deposits (compiled in Lindsay et al. 2011). These are detailed in **Table 2**. Modelled ages for the AVF centres suggested by Bebbington and Cronin (2011) are excluded from this study, as they are based on tephra horizon ages given by Molloy et al. (2009), which are superseded by those in Lowe et al. 2013 (for rhyolitic tephra ages) and Hopkins et al. 2015 (for basaltic tephra horizon thicknesses and depths).

Morphostratigraphy is here defined as the inter-relationships exhibited by the surface landforms, for example where tephra or lava deposits from one centre overlie another. Due to the proximity of the centres to one another within the field (cf. **Fig. 1**), 35 of 53 centres have morphostratigraphic constraints associated with them (outlined in **Table 2**). These morphostratigraphic constraints give optimum relative ages, which need to be combined with the absolute ages derived from  $^{40}\text{Ar}/^{39}\text{Ar}$  or  $^{14}\text{C}$  dating. In all cases the morphostratigraphic constraints are consistent with the absolute radiometric age ranges.

The  $^{40}\text{Ar}/^{39}\text{Ar}$  ages presented in Leonard et al. (2017) are here given as age ranges (the 2sd error on the age, reported in **Table 2**). This is because any age within the range is considered appropriate for the centre, with no extra emphasis given to the mean ages. For the 20 centres with no  $^{40}\text{Ar}/^{39}\text{Ar}$  or  $^{14}\text{C}$  ages, the relative ages of 14 centres were derived by morphostratigraphy (see **Table 2**). For the remaining six centres (Otuataua, Pigeon Mt., Robertson Hill, Boggust Park, Cemetery Hill, and Puhinui Craters) no radiometric ages or morphostratigraphic relationships are evident. As previously mentioned Cemetery Hill and Puhinui Craters are not considered in this study, and therefore Otuataua, Pigeon Mt., Robertson Hill, and Boggust Park are still included as possible correlatives for any dated horizon during the correlation process.

## ***New data acquisition***

### ***Geochemical whole rock data***

Prior to this study, 28 of the 53 AVF centres had three or more pre-existing major and trace element analyses, fifteen centres had less than three, and ten had no geochemical data at all (see **Table 1**). Volcanic centres with less than three existing whole rock analyses were targeted in this study. Seventeen centres had sufficient exposure to be sampled including: Boggust Park, Little Rangitoto, Mt Albert, Mt Cambria, Mt Hobson, Mt Roskill, Mt Smart, Onepoto, Otuataua, Pigeon Mt, Pukaki, Pukeiti, Pupuke, Mt Robertson, St Heliers, Taylors Hill and Te Pou Hawaiki (**Fig. 1**). For an additional seven centres major element data existed (Miller 1996), but no trace element data were reported. Thus, for these seven centres (**Fig. 1**; Green Mt, Hampton Park, Mangere Mt, McLaughlins Mt,

Mclennan Hills, Mt Victoria, and Otara), samples collected by Miller (1996) were re-analysed for both major and trace elements by this study. For six centres (Ash Hill, Kohuora, Mangere Lagoon, Styaks Swamp, Cemetery Hill, and Tank Farm; **Fig. 1**), there are currently no exposures suitable for sampling (due to urbanisation and erosion), and therefore, no geochemical data exists.

Whole rock samples were crushed to <15 mm in a Rocklabs Boyd crusher, then powdered using a Rocklabs tungsten-carbide TEMA swing mill at VUW. Powders were made into fused lithium metaborate glass discs and analysed for major element oxide concentrations at the Open University, Milton Keynes, UK using X-ray Fluorescence (XRF) analysis following the methods of Ramsey et al. (1995). Internal standards WS-E (Whin Sill Dolerite) and OU-3 (Nanhoron microgranite) were analysed to monitor precision and accuracy. Major element oxides were accurate to within 2.0% of the recommended values for the internal standards and analytical precision ( $2\sigma$ ) was 1.5% or better for all elements.

For trace element analysis, 50 mg of whole rock powder was treated using conventional methods of HF-HNO<sub>3</sub> digestion, and analysed on an Agilent 7500CS ICP-MS (VUW) in solution mode. Trace element abundances were calculated using the reduction program Iolite (Paton et al. 2011), using BHVO-2 as a bracketing standard, and BCR-2 as a secondary standard. <sup>43</sup>Ca was used as an internal standard using CaO contents measured by XRF. Trace element analyses were accurate to within <6% of the recommended values for the secondary standard (BCR-2) and precision ( $2\sigma$ ) was <6.5 % with the exceptions of Cr  $\pm$ 10.4 %, Nb  $\pm$ 22 %, Cs  $\pm$ 12.2 %, Ba  $\pm$ 11.8 %, Ta  $\pm$ 20.9 % and Pb  $\pm$ 31 %.

## 274 *Tephra horizon ages*

275        Within the Auckland maar cores as well as the locally derived basaltic tephra  
276 horizons, there are also distal andesitic and rhyolitic tephra deposits from  
277 various other sources within North Island (**Fig. 1B**). These “foreign” tephra can  
278 be used as stratigraphic marker horizons to aid both the absolute and relative  
279 dating of the basaltic deposits. The ages of the basaltic horizons within the cores  
280 are modelled by interpolating ages as a function of deposit depth, with the mean  
281 time interval per millimetre of core (**Fig. 2**). This principle assumes that tephra  
282 represent instantaneous events (Shane 2005), and therefore, their thicknesses  
283 are subtracted from the total sediment thickness. We use the most recent  
284 published ages for the rhyolitic marker horizons (RMHs; e.g. Lowe et al. 2013),  
285 and couple them with the most recent published thicknesses for the basaltic,  
286 andesitic and rhyolitic deposits in the maar cores. For basaltic deposits at Orakei  
287 and Glover Park we use data from Hopkins et al. (2015), and for the Onepoto  
288 core, all tephra thicknesses and depths are adapted from Shane and Hoverd  
289 (2002). Rhyolitic and andesitic deposit thicknesses at Orakei, Hopua, Pupuke,  
290 and lower Pukaki cores (below the Kawakawa/Oruanui RMH (Kk)) are from  
291 Molloy (2008) and in the upper Pukaki core (above Kk) from Sandiford et al.  
292 (2001).

293        Ages and uncertainties for all deposits found above the Maketu RMH are  
294 obtained by Monte Carlo simulation as follows. One thousand simulated sets of  
295 measured ages were found by adding the age’s Gaussian noise with the standard  
296 deviations of the determined ages. Any resulting set of ages out of stratigraphic  
297 order were rejected, that is, the 1000 simulations were conditional on the ages  
298 produced being in decreasing order. The simulations were then used to produce

1000 sets of interpolations with the lower 5 and upper 95 percentiles of the distribution giving the interpolated age uncertainties in  $2\sigma$  (see **Table 3**).

Sedimentation rate calculations are used to estimate the ages of the basaltic deposits found below the Rotoehu RMH (AVF3 to AVFc; no basaltic deposits are found between Maketu and Rotoehu RMHs). The age of the Rotoehu RMH itself is currently contentious, with published estimates ranging from ca. 40 to ca. 70 ka, associated with a range of different dating techniques (e.g. Lowe and Hogg 1995; Lian and Shane 2000; Charlier et al. 2003; Wilson et al. 2007; Danišík et al. 2012; Flude and Storey 2016). Here, we use an age estimate of  $52 \pm 7$  ka (D.J. Lowe *pers. comm.*), in order to accommodate the most likely range. In addition, because there are no dated RMHs below the Rotoehu, these calculations often assume constant sedimentation rates for a large proportion of the cores, which is probably unrealistic, and thus they are taken as a guide only (**Table 3**).

The basaltic deposit AVFd, was used as a lower constraint for the sedimentation rate between the Rotoehu and the base of the Onepoto core. This deposit contains lava and scoriaceous blocks interpreted to represent the Onepoto maar crater floor (Shane and Hoverd 2002). Although no age exists from the Onepoto eruption, morphostratigraphy suggests that it is just younger than Pupuke (Hayward et al. 2011), and we therefore use the mean age measured for Pupuke ( $193.2 \pm 2.8$  ka by  $^{40}\text{Ar}/^{39}\text{Ar}$  dating: Leonard et al. 2017) as a maximum age for the eruption of Onepoto. The respective calculated sedimentation rate of 0.19 mm/yr is comparable to those recorded previously for younger core sections (0.18 mm/yr: Shane and Hoverd 2002). In addition, the calculated basaltic tephra horizon ages are comparable to those calculated

for the correlated horizons AVF2 and AVF1 in the Orakei Basin core, suggesting that the assumptions made to calculate these values are realistic (**Table 3**).

In the Glover Park core, for the horizons correlated to other cores (AVF2 and AVF1), ages are assigned from an average of the values calculated from these core deposits. For horizon AVFa, which is only found at Glover Park, an age estimate was obtained through calculating the sedimentation rate between the bounding basaltic horizons, AVF1 and AVFb. The ages for these horizons were assigned based on the ages calculated for these deposits in Orakei Basin (AVF1) and Onepoto cores (AVF1 and AVFb). Calculated ages based on sedimentation rate for all basaltic tephra horizons and their associated errors are outlined in **Table 3**.

#### *Estimated tephra volumes*

Previous studies have estimated total eruptive volumes for the centres of the AVF (Allen and Smith 1994; Kereszturi et al. 2013) although, distal tephra volumes were not reported due to limited measurable material. Other studies (e.g. Kawabata et al. 2015) suggest that tephra volumes for small-scale eruptions can be estimated from the volumes of the tuff and scoria cones using the following equation:

$$V_{DRE} = 0.5V_{tuff} + 1.5V_{scoria}$$

where V is volume, and DRE is dense rock equivalent values (where volumes are corrected for void spaces, detailed in Kereszturi et al. 2013). In order to estimate tephra volume we use the most recently published DRE values for tuff and scoria from Kereszturi et al. (2013). Volume estimates are detailed in **Table 2**.



## Results

### *Whole-rock and glass geochemistry*

#### *Whole-rock geochemistry*

Following the rock classification of LeMaitre et al. (2002), the AVF samples range from basanitic/nephelinitic to basaltic in composition (e.g. SiO<sub>2</sub> = 39-49 wt.%; Mg# = 50-72. Broad positive trends exist between wt.% MgO and wt.% CaO, and wt.% MgO and wt.% Al<sub>2</sub>O<sub>3</sub>. Although less obvious, there are discernable broad negative trends exhibited in the AVF data between wt.% MgO and wt.% SiO<sub>2</sub>, TiO<sub>2</sub>, Fe<sub>2</sub>O<sub>3</sub><sup>tot</sup> and P<sub>2</sub>O<sub>5</sub> (not shown). These elements are more variable within a single centre than are MgO vs. CaO or Al<sub>2</sub>O<sub>3</sub>. For example the eruptive products of Motukorea show an almost flat trend for wt.% MgO vs. wt.% TiO<sub>2</sub>, whereas the Crater Hill samples show a strong positive trend. Although all samples from the AVF seem to follow the overall major element trends on variation diagrams, samples from individual AVF centres can define separate trends (c.f. **Fig. 3**) within this, as previously described by McGee et al. (2013).

Trace-element contents in the AVF samples vary substantially, for example, La 10-90 ppm, Nb 10-80 ppm and Sr 300-1000 ppm (see **Supplementary Material**). Similar to the major elements, some of the trace elements show overall general trends for the field, as well as trends specific to each centre (**Fig. 3**). There is a strong positive trend for wt.% MgO and ppm Cr and Sc, and a general negative trend of variable slope exists between wt.% MgO and ppm Th, Nb, Sr, and La (**Fig. 3**).

Mantle-normalised trace-element data for near primitive AVF samples (e.g. Mg# ≥ 60) are broadly similar and are characterised by a positive Nb

anomaly and a negative sloping light to heavy rare earth element profile (e.g. La/Yb range 4 to 40; **Fig. 4**), characteristics that are similar to ocean island basalts (OIBs). Some centres (e.g. Rangitoto 2 and Te Pou Hawaiiiki) have geochemical signatures that are less enriched in trace elements than others, characterised by a shallower rare earth element (REE) pattern gradient (e.g. La/Yb  $\leq 7.5$ ), and a positive Sr anomaly (e.g.  $Sr^* \geq 1.2$ ). In contrast, samples from trace element-enriched centres (e.g. Mt Cambria, Mt Hobson, St Heliers) have a relatively steep REE pattern gradient (e.g. La/Yb  $\geq 20$ ), show a small trough at Zr-Hf, exhibit no Sr anomaly (e.g.  $Sr^* \leq 1.0$ ), and display a negative K anomaly (e.g.  $K^* \leq 0.7$ ; **Fig. 4**). These major and trace element signatures for the field are discussed in detail by McGee et al. (2013), and are attributed to mixing during ascent of magma from three mantle sources.

#### *Glass geochemistry*

The geochemical composition of glass shards found in the AVF tephras are discussed in detail in Hopkins et al. (2015; see Fig 4 therein). In general they show a consistent range in MgO (ca. 2 to 7.5 wt.%), CaO (ca. 7 to 15 wt.%), FeO (ca. 9 to 15 wt.%), K<sub>2</sub>O (ca. 1 to 4 wt %), and TiO<sub>2</sub> (ca. 2 to 4.5 wt.%) between samples from across all cores. Al<sub>2</sub>O<sub>3</sub> concentrations are shown to be consistently lower at given MgO values in the Orakei and Onepoto cores, and SiO<sub>2</sub> is consistently lower at given MgO values in the Onepoto core. Glass shards from individual horizons have mostly similar major element concentrations with variations within <1 wt. % for MgO, SiO<sub>2</sub>, FeO, and TiO<sub>2</sub>, and <3 wt. % for CaO, Al<sub>2</sub>O<sub>3</sub>, Na<sub>2</sub>O, and K<sub>2</sub>O, with minor numbers of horizons showing bimodal or

systematic ranges in concentrations of major elements (as discussed in Hopkins et al. 2015).

In addition to major oxides, Hopkins et al. (2015) analysed trace elements on individual  $\geq 30 \mu\text{m}$  diameter glass shards. Their results showed (similar to whole-rock analyses) high variability in concentrations for trace elements, for example La ca. 5-100 ppm, Nb ca. 20-175 ppm, and Sr 140-1500 ppm. In general, glass shard primitive-mantle normalised multi-element plots show comparable signatures to the whole rock geochemical patterns (**Fig. 4**). Glass shards from individual tephra horizons have a more limited range in trace-element concentrations when compared to the whole field, and in many cases show relatively distinct trace element patterns for each individual tephra horizon (**Fig. 4**).

#### ***Tephra horizon ages***

Age estimates for all tephra horizons used in this study are outlined in **Table 3** and summarised in **Figure 2**. Basaltic tephra horizons found within 6 cores span a large age range in the field from 0.54 to ca. 143 ka (AVF24 in Pupuke core and AVFc in Onepoto core respectively). Fourteen horizons have ages calculated at  $<28$  ka, nine horizons are found between ca. 28 and 35 ka, and only 6 horizons have ages of ca. 59-143 ka. Overall the estimated ages are in good agreement where multiple deposits are correlated across cores (**Fig. 2**). Two discrepancies, however, arise (highlighted in **Table 3**): 1) The calculated age for AVF17 appears too young within the AVF number sequence, and 2) the calculated age of AVF16 appears too old for the AVF number sequence and

suspiciously similar to the age of AVF13. These results are potentially problematic, and are therefore discussed below.

The age of AVF17 when estimated using only the Orakei Basin core (23.35 ka), rather than averaging all ages across the cores, is not chronologically out of place (e.g. AVF18 is 23.2 ka and AVF15 is 24.5 ka). However, using the average age for AVF18, which is calculated as the average of correlated units from multiple cores (deposits from within Hopua 25.2 ka, Pukaki 24.6 ka and Orakei 23.35 ka cores) it appears too old (**Table 3**). This is because the ages for the deposits in the Pukaki and Hopua core are slightly older than those estimated for just the Orakei Basin core. But, within this section (Okareka to Te Rere), all of the horizon ages calculated are within error of each other, and therefore stratigraphic constraints in the cores are required to resolve the absolute ordering. AVF19 is found above the andesitic horizon Eg36 (**Fig. 2**; Molloy 2008), which is found in all the cores, and therefore acts as a marker horizon to place AVF19 as the youngest horizon. AVF18 is found above AVF17 within the Orakei Basin core, further restricting the ordering of these two horizons. The ordering and correlation of these horizons will therefore be maintained, however, the errors on the ages must be taken into account during the correlation process.

The ages calculated for AVF16 (Pukaki core only) and AVF13 (Orakei core only) are identical ( $25.23 \pm 0.86$  ka and  $25.23 \pm 0.31$  ka respectively). The age estimate for AVF16 implies that it is older than suggested by the original position in the AVF nomenclature sequence, and there is a strong possibility that the horizons represent the same deposit. Stratigraphically, there are limited constraints on the relationship of AVF16 with the other deposits from other

cores. The andesitic deposit Eg34 is found below AVF16 but is not found in any other cores and therefore provides no further regional stratigraphic constraints. The Te Rere and the Kawakawa/Oruanui RHM's stratigraphically constrain horizon AVF16 (above and below respectively), but there are no other age constraints (Te Rere tephra is not found in the Orakei Basin core). In addition there are limited geochemical data for the deposit AVF16 to confirm or deny its relationship with AVF13 (Sandiford et al. 2001; Hopkins et al. 2015). Therefore due to the lack of distinct evidence to suggest these deposits are not the same, and the overwhelming similarity in the ages, we assume AVF16 and AVF13 record the same event and will be referred to as 'AVF13' with an age of  $25.23 \pm 0.86$  ka in the following discussion.

## Discussion

### *Discriminatory geochemical elements for the AVF*

Previous studies on the petrogenesis of AVF eruptive products have shown that each magma batch feeding a single centre is generated by mixing of contributions from differing degrees of partial melting of multiple mantle sources at different depths (Huang et al. 1997; McGee et al. 2013, 2015; Hopkins et al. 2016). The resulting geochemical signatures of the erupted volcanic products demonstrate that although there is overlap for many elements, combinations of some major element ( $\text{SiO}_2$ ,  $\text{MgO}$ ,  $\text{CaO}$ ,  $\text{FeO}$ ,  $\text{P}_2\text{O}_5$ ) and trace element (Sc, Sr, Zr, Gd, La, Sm, Nd, Nb, Ce) concentrations or ratios (e.g.  $(\text{La}/\text{Yb})_N$  or  $(\text{La}/\text{Y})_N$ ) can be used to discriminate single trends for individual centres (**Fig.**

3). The selected elements also show the widest range in concentrations in eruptive products from the AVF.

The rare-earth elements (REEs) are especially useful because fractional crystallisation of the common silicate phases has only a minor effect on their concentrations. They can therefore be used to discriminate between melts from a deep (garnet-bearing mantle = high light REE/heavy REE) or shallow (spinel-bearing mantle = low light REE/heavy REE) source (e.g. McKenzie and O’Nions 1991; Robinson and Wood 1998; McGee et al. 2013, 2015; Hopkins et al. 2016; McGee and Smith 2016). As a result of these variations, and of the discriminatory nature of certain elements and element ratios within the AVF, we show that geochemical fingerprinting can be used as a method to correlate distal tephra deposits to their source centre. Below we discuss the techniques by which this method was tested and developed.

### ***Geochemical correlation***

A key issue in correlating the geochemistry of glass shards in distal tephra to whole-rock geochemistry of proximal lavas and pyroclastic particles is that most whole-rock samples contain mineral inclusions (e.g. olivine), whereas small volcanic glass shards (in tephra) do not. Hence, the concentration of elements that strongly partition into mineral phases (e.g. Mg, Ni or Cr into olivine) in whole-rock samples will not be comparable to the respective element contents in the glass shards (e.g. **Fig. 5A**). Conversely, elements that preferentially remain in the melt (e.g. those that are incompatible with mineral phases commonly found in alkali basalts, such as the REE) are likely to have comparable concentrations in whole-rock and glass shards. In addition, mineral-free groundmass glass from

whole-rock samples is likely to have a comparable geochemical signature to the glass shards forming distal tephra deposits (e.g. Lowe 2011; Allan et al. 2008; Lowe and Alloway 2015; **Fig. 5B**).

These hypotheses were tested initially on samples from a known source by comparing the geochemical composition of (a) a proximal whole-rock sample and (b) the matrix-derived glass from that sample to (c) glass shards from a distal tephra deposit. The whole-rock lava sample Mt. Wellington AU62394 was chosen for two reasons, 1) it has a fresh, glassy groundmass and, 2) distal tephra from Mt. Wellington has been unambiguously identified in the Hopua core based on age and thickness (Molloy et al. 2009). The lava sample was processed first as a whole-rock sample (XRF and ICP-MS, see methodology). It was also processed to produce a 'matrix-derived glass' sample by crushing the rock and separating shards of matrix glass that were of comparable size (30-100  $\mu\text{m}$ ) to the glass shards found in the tephra horizon from the Hopua core (Molloy et al. 2009). These separated matrix-derived glass shards were then analysed by EMPA and LA-ICP-MS using methods outlined in Hopkins et al. (2015).

#### *Geochemical correlation of glass shards from distal tephra deposits with matrix derived glass*

**Figure 6** shows MgO vs. Al<sub>2</sub>O<sub>3</sub> (in wt. %, [**Fig. 6A**]) and Gd vs. Zr (in ppm [**Fig. 6B**]) for matrix-derived glass and the glass from its known distal correlative from the Hopua core, the overlap in the data demonstrates that their compositions are comparable. This is the case for a wide range of both major and trace elements (including, MgO vs. full major element suite plus trace elements Rb, Zr, Cs, Ni, Cr, Y, and Er; SiO<sub>2</sub> vs. Al<sub>2</sub>O<sub>3</sub>, Na<sub>2</sub>O, K<sub>2</sub>O, and CaO vs. Al<sub>2</sub>O<sub>3</sub>, Na<sub>2</sub>O).

Limited variability exists between trace elements (e.g. Rb, Zr, Ni, Cr and Y, and the REE) when plotted against each other, or against  $\text{Al}_2\text{O}_3$  or  $\text{MgO}$ .

For some elements, however, the glass from the distal tephra has larger variations than does the matrix-derived glass (**Fig. 6A**). This is attributed to either 1), the matrix-derived glass being made from a single clast and thus having minimal compositional variation, and/or 2) glass shards from the distal tephra showing a higher variability due to initial differences in composition of the erupted magma creating variability in the glass shard composition throughout the eruption (e.g. McGee et al. 2012). This test proves that matrix-derived glass from proximal samples can be successfully correlated with glass shards in distal tephtras using trace elements and trace element ratios (**Fig. 6B**).

Geochemical analysis using EMPA and LA-ICP-MS techniques are for individual glass shards, ensuring phenocrysts and microlites are not analysed. Accordingly matrix-derived glass from proximal samples can be correlated with glass shards from within distal tephra deposits using both elements that are highly compatible and elements that are incompatible. Compatible elements are preferentially incorporated in key crystallising minerals within the whole rock (e.g. olivine) and therefore result in comparable glass chemistries between matrix-derived glass and tephra-derived glass. The incompatible trace elements can also be used because they are not preferentially taken into the crystal phases. We therefore conclude that matrix-derived glass from whole-rock samples can be correlated to glass shards from the distal tephra deposits, with some minor caveats. For example, this method relies on the existence and ability to extract glass from the groundmass of proximal whole-rock samples, which is not always possible.



### *Correlation of glass shards from distal tephra with whole-rock samples*

In general, when the entire suite of whole-rock and glass geochemical datasets are compared, MgO, Cr, and Ni all show distinctly higher concentrations in whole-rock samples than in the glasses (e.g. MgO in whole rock range from ca. 6-16 wt.%; in glass ca. 2-6 wt.%: **Fig. 5A**). Compared to whole-rock analyses, all glasses contain higher (but slightly overlapping) wt.% SiO<sub>2</sub>, Al<sub>2</sub>O<sub>3</sub>, Na<sub>2</sub>O, and K<sub>2</sub>O contents (e.g. SiO<sub>2</sub> in whole rock ca. 38-50 wt.%; glass ca. 42-52 wt.%). CaO, FeO, TiO<sub>2</sub>, and P<sub>2</sub>O<sub>5</sub> have comparable ranges between whole rock and glass, as do the trace elements, including REEs (**Fig. 5B**). The REEs in general do show comparable but slightly wider ranges in concentrations in the glass than in the whole rock (e.g. Sr in glass = 140-1500 ppm vs. Sr in whole-rock = 300-1000).

In addition to the presence of phenocrystic material combined into a bulk rock analysis, correlating major-element compositions of proximal whole-rock samples to those of glass shards in distal tephra has proved difficult, due to the effect that fractional crystallization has on the concentrations of some elements (e.g. Pearce et al. 2008; Ukstins Peate et al. 2008; Dunbar and Kurbatov 2011; Óladóttir et al. 2012). Plotting element concentrations (for whole-rock samples from a single centre or glass shard analyses from one tephra horizon) against other elements that are compatible with certain crystals (e.g. MgO for olivine, CaO and Al<sub>2</sub>O<sub>3</sub> for pyroxene or plagioclase) can be used to monitor the effect of crystal removal on these elements in the glass. If an element shows a positive or negative correlation ( $r^2 \geq 0.6$ , where no single point is responsible for the trend), with key compatible major elements (MgO, CaO, Al<sub>2</sub>O<sub>3</sub>) then that element is significantly affected by crystal removal and therefore not useful for correlation purposes. In addition to key major elements, trace elements with high partition

coefficients for olivine and pyroxene (e.g. Ni, Cr, Sc) are also affected. For example, **Fig. 7** shows that for MgO vs. Ni, the whole rock  $r^2 = 0.75$ , and for tephra-derived glass  $r^2 = 0.61$ . Conversely, high field strength elements (HFSE), such as Nb, Zr, and REE, show no trend with elements tracing fractional crystallisation (e.g. for MgO vs. La;  $r^2 = 0.02$  for tephra-derived glass, and  $r^2 = 0.11$  for whole rock. This exercise discussed above was repeated for all glass-shard analyses from all tephra horizons and for all whole-rock samples from all centres using MgO, CaO, Al<sub>2</sub>O<sub>3</sub>, Ni, Mn, and Sr on the x-axis (and all other major and trace elements on the y-axis). These results suggest that HFSEs are incompatible with major crystallising phases and are therefore well suited for geochemical fingerprinting (e.g. **Fig. 6E-F; Fig. 7**). Respective trace element ratios (e.g. (La/Yb)<sub>N</sub>, (Gd/Yb)<sub>N</sub>, (Zr/Yb)<sub>N</sub>, (Ce/Yb)<sub>N</sub>, (Nb/Yb)<sub>N</sub>, and (Nd/Yb)<sub>N</sub>) also showed no correlation with any of the x-axis elements. Therefore, these ratios are considered best for geochemical correlation between glass shards and whole rocks. Such ratios show a broad range in the AVF as a whole, but a relatively restricted range in samples from each single centre, and no relationship with indices of fractional crystallisation.

When applied to the known Mt Wellington samples, a comparison of proximal whole rock, matrix-derived glass (of the same whole rock sample), and distal tephra-derived glass show the expected results. **Figure 6C** shows an example of element combinations that are comparable for glass-glass correlations but not for glass-whole rock correlations (e.g. MgO vs. Al<sub>2</sub>O<sub>3</sub>, K<sub>2</sub>O, Ni, Cr, and the REE). In contrast, some major element combinations do appear to correlate the whole-rock with glass of the distal tephra (**Fig. 6D**; including SiO<sub>2</sub> vs. TiO<sub>2</sub> and FeO, and CaO vs. TiO<sub>2</sub>, FeO and Al<sub>2</sub>O<sub>3</sub>). In these cases, however, the

strong correlation is mainly due to the small variability observed in the Mt Wellington samples; it may not be applicable for other centres within the AVF. **Figure 6E** illustrates an example of incompatible trace elements in glasses that show slightly more variability than the whole-rock samples do; this discrepancy is, however, minimised when trace element ratios for the two sample types are compared (see **Fig. 6F**). The incompatible trace element ratios are sufficiently distinctive to allow independent correlation to be made between the field-wide suite of proximal whole-rock and distal glass data, especially  $(\text{La}/\text{Yb})_{\text{N}}$ ,  $(\text{Gd}/\text{Yb})_{\text{N}}$ , and  $(\text{Zr}/\text{Yb})_{\text{N}}$ , all of which show a wide range of values in the field as a whole. It is therefore concluded that by using incompatible-element and LREE/HREE ratios, it is possible to geochemically correlate individual glass shards from distal tephra deposits with proximal whole-rock samples. There are, however, some additional limitations for the AVF.

#### *Limitations on geochemical correlations*

Previous studies have demonstrated that the geochemical composition of the erupted products within some of the AVF centres (e.g. Crater Hill: Smith et al. 2008; Motukorea: McGee et al. 2012), change as the eruptions progress from initially phreatomagmatic to magmatic eruption styles (**Table 2**). These centres consistently show, for example, initially low wt.%  $\text{SiO}_2$  and Mg/Fe ratios and higher incompatible element contents that evolve to final products with higher wt.%  $\text{SiO}_2$ , Mg/Fe ratios and lower incompatible element abundances (e.g. Reiners 1998; Smith et al. 2008; McGee et al. 2012). Such variability may complicate correlation of proximal units to their related distal tephra deposits

because directions and distances of eruptive dispersal may not be constant through an eruption.

For AVF centres, most of the eruptive phases are explosive (**Table 2**), and therefore, if centres show geochemical evolution through an eruption (e.g. Motukorea, Crater Hill), there is the potential for tephra deposits (from early phreatomagmatic phases) to have higher trace element ratios (LREE/HREE) than their subsequent lava or scoria deposits (from later magmatic phases). This bias may hinder correlation of some distal tephras to their source centre.

To address this issue, **Fig. 8** shows the geochemical progression through the eruption of Motukorea (data from McGee et al. 2012), compared with the correlated Motukorea tephra horizon found in the Orakei Basin core. Distal tephra-derived glass shards appear to show slightly higher SiO<sub>2</sub> concentrations at given Zr concentrations (due to fractional crystallisation processes), but do show the full evolutionary geochemical trend for the entire eruption. For the incompatible trace element ratios the glass shards appear to be geochemically comparable and again have signatures that are the same as all phases of the eruption from tuff (explosive early phases), to lava and scoria (less-explosive later phases) (**Fig. 8**). Although these results generally validate our method, we still cannot discount the possibility of a mismatch, due to the limited geochemical data available for the evolution of individual centres.

Another limitation of using geochemistry to correlate tephras to their source centres is that not all the 53 AVF centres show distinct geochemical signatures. Geochemical composition alone cannot unambiguously fingerprint a centre if there are either a large number of centres with relatively similar geochemical compositions, or a general lack of geochemical data (either whole

rock or glass). It is therefore essential to include additional criteria (discussed below) to allow confident correlations to be made.

#### ***Multi-criteria correlation of tephra horizons to source centres***

We combine four key factors to correlate distal tephra deposits to their source centres: age, geochemistry, scale of eruption, and location of sources. Where applicable, wind direction is also taken into account.

A shortlist of potential source centres (**Table 2**) is created based primarily on the restrictions provided by the age estimates of the tephra deposits and the age estimates of the centres. For those shortlisted centres, the major, trace, and trace element ratios of the proximal whole rock analyses are compared to the distal tephra derived-glass compositions, focussing on incompatible trace element ratios (**Fig. 9**). To strengthen potential correlations, other criteria such as the eruption scale and styles, and the location of the relevant source centre(s), and the relevant core(s) are also taken into account, as discussed below.

Because fall deposits thin systematically with distance (Pyle 1989; Lowe 2011), eruptions with a large estimated tephra volume (ETV) and a dominant phreatomagmatic component are likely to produce a larger tephra output and hence a greater dispersal footprint and deposit. Therefore, very thick (primary) tephra deposits (>100 mm) in a core (Hopkins et al. 2015) require a source centre that is either 1) close to the deposition site (less than a few kilometres: Brand et al. 2014), and/or 2) has a predominantly phreatomagmatic eruption style, and/or 3) has a large magma supply and thus a long eruption duration.

Due to the relatively small size of the AVF volcanoes, the tephra dispersed by single eruption is not thought to cover the entire field for any single event (Kermode 1992). Therefore, the distribution and thickness of tephra deposits can be indicative of the region within the field where the source centre is located. For example, tephra deposits that are only found in the northern maar sites (Onepoto, Pupuke, Orakei, Glover Park) are inferred to indicate sources in the north or central AVF (based on the dominant wind direction, discussed below). Conversely a deposit only found in the southern maar site (Pukaki) is suggestive of sources in the south of the field. Tephra deposits found in both northern and southern maar sites are likely to have been derived from the central part of the field, and/or reflect an eruption large enough to widely disperse tephra from any source site within the field.

Wind direction is also considered, where possible, when making source correlations, because it has a controlling influence on tephra dispersal. For the Auckland region, evidence of prevailing past wind directions can be inferred from the morphology of the volcanic centres, for example, asymmetric tuff rings or scoria cones (e.g. Motukorea, Hayward et al. 2011). Such morphological indications are not however definitive for the majority of centres because there has often been post-depositional erosion, so present cone morphology is not seen as a definitive wind-direction indicator for an individual eruption. The dominant prehistoric wind patterns (westerly/south-westerly) are, however, still the dominant patterns for today (Houghton et al. 2006). This wind direction generally has resulted in more frequent tephra deposition in the northeast and east of the field, confirmed by the high number of deposits found within the Orakei Basin core, situated north-east of most centres (**Fig. 1**). Tephra deposits

are therefore more readily traced back to sources to the west and southwest. Conversely, centres found to the east or north east of the maar sites (e.g. Pigeon Mt., Hampton Park, Otara, Green Mt., and Styaks Swamp; **Fig. 1**) are less likely to be represented in the maar-lake tephra record.

Hopkins et al. (2015) detailed twenty-eight tephra horizons within six cores. Eleven of the horizons are cross-correlated between cores, linking two or more deposits, and seventeen tephra horizons are single deposits found only within single cores. We here have reduced the number of single horizons to sixteen, and increased the number of cross-correlated horizons to twelve based on the correlation of horizons AVF16/AVF13 as previously discussed.

For correlation purposes, we assess each tephra horizon individually; all potential sources are accounted for and discussed, without bias from any other correlations made (see **Supplementary Material**). A ‘confidence value’ is assigned for each correlation based on the number of supporting criteria that are satisfied (i.e. age, geochemistry, scale and location). In general, if all four criteria are satisfied a confidence level of 1 is given, when three are satisfied a confidence level of 2 is given, and if only two are satisfied a confidence level of 3 is given (detailed in **Table 4**). Each of these criteria is variably weighted in importance with age  $\geq$  geochemistry  $\gg$  locality  $\geq$  eruptive scale. In some cases the confidence level is skewed to reflect this weighting of criteria, and this skew is detailed for each individual case in the supplementary material.

Discussion of the correlation of all 28 horizons to their proposed source can be found in the **supplementary material**, with an example of the discussion outlined below for a single representative tephra horizon (AVF5). For each of the horizons the proposed source centres are given in **Table 4** along with

alternatives that were considered. Of the twenty-eight horizons, eight have been given a correlation with confidence level of 1, eleven have been given a confidence level of 2, and seven have been given a confidence level of 3, with two horizons remaining uncorrelated (**Table 4**).

*Example of multi-criteria discussion for a level 3 correlation*

**AVF5** is a thick (110 mm) geochemically homogeneous deposit found only in the Orakei Basin core at a depth of 57.44 m. The bulk tephra sample contains coarse glass shards (>250  $\mu\text{m}$ ) and abundant country-rock lithic grains. The source is thus inferred to be relatively close to Orakei Basin in the north of the field. Its modelled sedimentation rate age is of  $34.2 \pm 0.9$  ka (**Table 2**). Mt. Cambria is the only candidate with the appropriate age and location, however it is one of the smallest centres in the field with an estimated tephra volume (ETV) of  $0.44 \times 10^6 \text{ m}^3$  (**Table 2**). It is located ca. 5 km away from Orakei Basin, and therefore, it is highly improbable that it would have produced a 110 mm thick tephra deposit within the basin. Several other centres have appropriate locations and eruption scales, but are older than 35 ka ( $^{40}\text{Ar}/^{39}\text{Ar}$  age ranges [95 % confidence] from Leonard et al. 2017): Mt. Hobson (45.3-68.5 ka), Mt. St John (71.9-78.7 ka), Mt. Victoria (AVF4) (42.8-72.4 ka), and North Head (72.3-102.7 ka), or conversely, too young; Little Rangitoto (AVF14) (16.3-25.1 ka), Taylors Hill (AVF10) (24.2-30.6 ka), and Panmure Basin (AVF13) (>17.5 ka). Of these centres only Mt. Victoria and Mt. Hobson have a similar (overlapping within error) geochemical signature to the tephra-derived glass within the AVF5 horizon. Mt. Victoria has an ETV of  $3.9 \times 10^6 \text{ m}^3$  and is located 4.7 km to the northwest of Orakei. In comparison Mt. Hobson has an ETV of  $1.8 \times 10^6 \text{ m}^3$  and is



2.5 km downwind to the south west of Orakei basin. Based on this, Mt. Hobson is more likely than Mt. Victoria to have produced a thick deposit with large shards in Orakei Basin. The  $^{40}\text{Ar}/^{39}\text{Ar}$  age for Mt. Hobson (44.9-66.9 ka) is older than the modelled AVF5 tephra horizon age, but the only morphostratigraphic constraint is that **Mt. Hobson** is older than Three Kings (consistent with this correlation). We therefore discount the age constraints, which are separated by 9.8 kyr beyond error bounds. This correlation is predominantly based on the locality and scale of eruption and the deposit, with inconclusive geochemistry; it is therefore given a confidence level of 3.

#### ***Tephra dispersal in the AVF***

Using confident correlations (level 1 and 2 only, which depend primarily on age and geochemistry) of tephra horizons from cores to their source centres, inferences can be made about the dispersal distances and thickness of the deposits from the AVF eruptions. **Table 5** outlines the distance (from source to depositional core site), thickness (primary horizon thickness identified by Hopkins et al. 2015), and (where applicable) the estimated shard sizes (based on grain sieving during glass shard extraction) for each of the centres that have been assigned a correlation with confidence level 1 or 2. There are no contemporaneous subaerial deposits in Auckland (cf. Hopkins et al. 2015), and the recorded thicknesses are here considered to be minima due to potential post-depositional compaction and erosion (Óladóttir et al. 2012).

For all correlations with a confidence level of 1, the maximum dispersal is of 13.5 km, for the Three Kings eruption recorded in Pupuke maar in a deposit 2

mm thick with shards of 50-100  $\mu\text{m}$ . For both confidence level 1 and 2 correlations, the thickest deposits ( $\geq 100$  mm) are all found within 6 km from source, with a sharp decrease in deposit thickness (all  $< 80$  mm) at distances  $> 6$  km (**Fig. 10A**). The maximum tephra thickness recorded in the cores is 510 mm; the tephra is from the One Tree Hill eruption in Orakei Basin, 4.6 km from the core site, suggesting that for a relatively large eruption ( $\text{DRE}^{\text{tot}} = 0.26 \text{ km}^3$  Kereszturi et al. 2013) tephra deposits can be  $> 500$  mm thick at distances of  $> 4$  km. The correlation results also show that shard size decreases with distance from source (**Fig. 10B**), with 60% of deposits  $< 6$  km from source having shards  $> 200 \mu\text{m}$ , which reduces to 45% of deposits 6-12 km away and 0%  $> 12$  km from source. These findings are particularly applicable as inputs for tephra dispersal model simulations, evacuation and 'clean-up' forecasting, planning, and management (e.g. Tomsen et al. 2014; Wilson et al. 2014; Hayes et al. 2015).

Tephra horizon AVF12 correlates to Mt. Eden (**Fig. 1**), and is one of the most widely dispersed (and thus best preserved) tephra horizons;  $> 10$  mm thick in both Pupuke and Pukaki cores, which are 11 km and 12 km from source respectively. The Mt. Eden event also correlates with some of the thickest tephra deposits in the cores; 410 mm in Orakei (4.5 km from source), and 460 mm in Hopua (6 km from source). **Figure 11A** shows the decrease in tephra thickness away from source, coupled with the decrease in tephra shard size. Mt. Eden is also used as an example to show how the core-to-core and core-to-source centre correlations can be used to build isopach maps for the dispersal pattern of the eruption (**Fig. 11B**). The impact of the prevailing westerly winds (Hayward et al. 2011) is considered and therefore produces an inferred elliptical tephra dispersal footprint. With a calculated total DRE volume of  $0.086 \text{ km}^3$ , the

eruption of Mt. Eden was one of the largest in the AVF, and therefore illustrates the impacts of a more extreme tephra dispersal event from a larger scale eruption.

Smaller eruptions produce more-restricted tephra dispersal; thirteen of the twenty-nine tephra horizons (45%) are only identified within single cores. Small eruptions can nevertheless result in near-source tephra horizons of substantial thickness. For example AVF10, now correlated to the eruption of Taylors Hill (DRE volume of  $0.0051 \text{ km}^3$ ), is restricted to the north of the field with cross-correlated deposits found in Orakei Basin (407 mm at ca. 5 km away), Onepoto (15 mm at ca. 12 km away) and Pupuke (3 mm at ca. 13 km away).

Deposits are not necessarily found in all maars along a dispersal pathway. For example AVF4 is found in Orakei Basin (41 mm) and Pupuke (15 mm) but is absent in Onepoto, which lies directly between the two. These dispersal patterns are most likely indicative of either discontinuous preservation and/or complex distal fallout (Molloy et al. 2009).

**Table 6** lists tephra dispersal information from selected basaltic volcanic fields worldwide together with those for some AVF centres. Monogenetic basaltic eruptions that show comparable total eruptive volumes, dispersal distances and thicknesses to some of the larger AVF centres include Mt. Gambier (Newer Volcanics, Australia) with an estimated  $\text{DRE}^{\text{tot}} = 0.20 \text{ km}^3$  (van Otterloo and Cas 2013) and measured tephra thicknesses  $\leq 5 \text{ cm}$  at 10-12 km distance (Lowe and Palmer 2005). In comparison One Tree Hill ( $\text{DRE}^{\text{tot}} = 0.26 \text{ km}^3$ ) of the AVF has a measured tephra thickness of 6 cm at 10 km from source (**Table 6**). Marcath Volcano (Lunar Crater volcanic field, Nevada, USA) is of a similar eruptive scale to the mid-range AVF volcanoes, with a  $\text{DRE}^{\text{tot}} = 0.06 \text{ km}^3$  (Johnson et al. 2014).

Its tephra is 2 cm thick 7 km from vent, comparable to many AVF eruptions of similar scale, e.g. Mt. Wellington and Three Kings (**Table 6**). It is difficult to find global comparisons for the smaller AVF eruptions, but some of the latter show equivalent values to the larger global examples, for example, Orakei Basin, with a DRE<sup>tot</sup> of 0.0067 km<sup>3</sup> depositing tephra 4 mm thick at 5 km from vent. A number of factors could potentially contribute to the apparent wider dispersal of tephra from the smaller AVF centres, including the high proportion of phreatomagmatic eruptions seen within the field (**Table 2**), the consistent prevailing wind directions, or the more favourable preservation conditions provided by the maar sites.

#### ***Eruption age order resolution for the AVF***

The correlation of tephra deposits to their source centres, coupled with <sup>40</sup>Ar/<sup>39</sup>Ar ages and morphostratigraphy, enables us to construct a relative age model for 48 of the 53 centres, thus allowing us to re-assess the absolute ages for all centres. As previously outlined, although the <sup>40</sup>Ar/<sup>39</sup>Ar age data (Leonard et al. 2017) provide improved age constraints for many of the AVF centres, the associated errors preclude ordering eruptive events. We reconstruct the relative temporal eruptive history for the AVF by combining; 1) the mean <sup>40</sup>Ar/<sup>39</sup>Ar (Cassata et al. 2008; Leonard et al. 2017) and <sup>14</sup>C ages (Lindsay et al. 2011; Needham et al. 2011), 2) the modelled sedimentation rate ages assigned based on tephra horizon correlations and, 3) the relative positions based on morphostratigraphic (cf. **Table 3**) or paleomagnetic constraints (Shibuya et al. 1992; Cassidy 2006; Leonard et al. 2017; **Fig. 12**). For five centres there is not

832 enough information to assign absolute or relative ages, and these centres are  
833 therefore not included in the following evaluations. **Table 7** and **Figure 13**  
834 present a new relative age order and absolute ages for 48 of the AVF centres as  
835 defined by this study. A full discussion of the proposed relative and absolute age  
836 order can be found in the **supplementary material**.

837         Two previous studies have attempted reconstructions using statistical  
838 methods. Bebbington and Cronin (2011) reconstructed the temporal history of  
839 the entire field through age simulations based on tephra horizon correlations,  
840 stratigraphic constraints, and radiometric ages. Kawabata et al. (2016) made  
841 improvements to this statistical approach but focussed solely on correlating the  
842 tephra horizons to sources. The input for the original model simulations of  
843 Bebbington and Cronin (2011) included deposit thicknesses and age estimates  
844 for basaltic tephra within maar cores (from Sandiford et al. 2001; Shane and  
845 Hoverd 2002; Molloy et al. 2009), and age estimates for the AVF centres (from  
846 Lindsay et al. 2011). In order to improve on Bebbington and Cronin (2011),  
847 Kawabata et al. (2016) used newly refined ages for the rhyolitic and andesitic  
848 marker horizons from Lowe et al. (2013) as tie points within their  
849 reconstruction, and added wind direction and estimated tephra volumes. This  
850 improved modelling showed only 3 correlations that were consistent with the  
851 previous research, suggesting how easily new data inputs can dramatically  
852 impact the outputs of statistical modelling.

853         When we compare our tephra correlations to those outlined by Kawabata  
854 et al. (2016; **Table 4** and **Fig. 13**), there are three common correlations; AVF1  
855 and Domain, AVF2 and One Tree Hill, and AVF12 and Mt Eden. There are  
856 however a large number of discrepancies that we attribute to differences in

input data, in most cases linked to differing tephra horizon characteristics and the improved age constraints provided by Leonard et al. (2017).

**Figure 14** shows a comparison of our field-wide absolute and relative chronology results to those of Bebbington and Cronin (2011). There is significant scatter around the 1:1 line, indicating the data sets, and thus the relative orders are significantly different (**Fig. 14A**). For example, Bebbington and Cronin (2011) model 21 centres as older, 18 as younger, and 9 in the same positions as our results show. There are, however only a few large discrepancies (>20 positions) between the two studies. Little Rangitoto, Motukorea, and Te Pou Hawaiki were all given much older positions (42<sup>nd</sup>, 35<sup>th</sup>, 43<sup>rd</sup> respectively) than those inferred in this study (13<sup>th</sup>, 12<sup>th</sup>, 16<sup>th</sup> respectively), and McLaughlins Mt., Mt. Mangere and Mangere Lagoon are given much younger positions (4<sup>th</sup>, 9<sup>th</sup>, 12<sup>th</sup> respectively from Bebbington and Cronin, 2011) than those inferred in this study (30<sup>th</sup>, 33<sup>rd</sup>, 34<sup>th</sup> respectively).

For absolute age estimates (**Fig. 14B&C**), variation between the data sets is apparently greater than for the relative age estimates. Only twenty centres show offsets of <5 kyr between the modelled ages and our inferred ages, with the remaining 28 showing larger offsets of between 6.1 kyr (Mt Hobson) up to 124 kyr (Te Pou Hawaiki). In addition, the modelled absolute ages (from Bebbington and Cronin 2011) cluster around 30 ka, whereas this study infers a broader spread between 20 and 35 ka for the same centres. The Bebbington and Cronin (2011) model is heavily weighted towards tephra horizons in the 30 ka age range, and this may impart a bias on the age constraints of their model's output. For all centres modelled by Bebbington and Cronin (2011) with ages between 45 and 75 ka, the ages appear to be younger than inferred in this study (e.g. One

Tree Hill, Mt. Albert, and Tank Farm). Conversely, modelled ages for centres older than 75 ka seem to be over estimates (e.g. Little Rangitoto, Orakei Basin and Onepoto). The conflicting results for both relative and absolute age estimates between the two studies (e.g. for Onepoto, Pupuke, and Tank Farm), is likely to reflect differences in the data inputs.

## ***Implications for the spatial, temporal and geochemical evolution of the Auckland Volcanic Field***

### ***Spatial and temporal evolution***

The newly estimated ages for 48 of the 53 centres suggest that 18 centres erupted in the first ca. 140 kyr of the AVF's history (190 – ca. 50 ka), with 30 erupting from ca. 50 ka to 0.5 ka. By using the rhyolitic marker horizons (RMHs) as definitive age constraints the number of eruptions per 1000 years (erup/kyr) can be calculated: present to Rerewhakaaitu (Rk) (0-17.5 ka) 0.3 erupt/kyr; Rk to Okareka (Ok) (17.5–21.5 ka) eruption rate of 1.0 erupt/kyr; Ok to Kawakawa/Oruanui (Kk) (21.5–25.4 ka) eruption rate of 1.5 erupt/kyr; Kk to Rotoehu (Re) (25.4–52 ka) eruption rate of 0.6 erupt/kyr and Re to inception (52-193 ka) eruption rate of 0.13 erupt/kyr. These results suggest that in general there was an increase in the eruption frequency through time until ca. 21.5 ka (Okareka RMH; **Table 7**), followed by a decrease since 21.5 ka. Field-repose periods show a wide range from <0.1–13 kyr (**Table 7**), however eruptions are not evenly distributed within this range. Only six centres show field-repose periods of 10-13 kyr, whereas, twenty-three centres erupted after field-repose periods of 1000 years or less (all except four of which are younger than 50 ka),

and eighteen of these twenty-three have field-repose periods of 500 years or less. In general the longer field-repose periods occur at the beginning of the field's history, with all of the six centres with field-repose periods of 10-13 kyrs appearing between 193–86 ka.

The distance between successive eruptions (**Table 7**) varies from <0.5 km to 14 km with two outliers events taking place 21 and 19 km from sites of preceding events. There is spatial but not temporal alignment of some centres for example McLaughlins Hill – Wiri Mt. – Ash Hill (**Fig. 1**); these alignments have previously been attributed to pre-existing crustal fractures and faults (Magill et al. 2005; von Veh and Németh 2009; Kereszturi et al. 2014). In general there is no obvious spatial progression or pattern in location of vents through time.

Previous studies (Bebbington 2013; Le Corvec et al. 2013) have suggested that the location of each centre is independent of that of the previous centre, and for the most part the results presented in this study support this suggestion. When centre location is linked with the temporal evolution, however, a number of centres appear to have erupted very closely in space *and* time. These 'coupled' centres are here defined as having a field-repose period of 1000 years or less and with centres erupting <1 km away from each other. For example Mt. Wellington and Purchas Hill are dated to 10.5 ka and 11 ka respectively and are located ca. 0.5 km apart. The other centres include Rangitoto 1 and 2 (Needham et al. 2011), Styaks Swamp and Green Mt., Mt. Eden and Te Pou Hawaiki, Otara and Hampton Park, and Wiri Mt. and Ash Hill (**Table 7**). It may also be possible to include Onepoto and Tank Farm, Mangere Mt. and Mangere Lagoon, and Domain and Grafton, although the age of one or both volcanoes in each of these pairs is poorly constrained.



## 931    *Geochemical evolution*

932            The collation of existing, and collection of new, whole rock and tephra-  
933    derived glass geochemical data presented here provides the most  
934    comprehensive geochemical dataset for the AVF to date (see **Table 1**). These  
935    data reveal a more complete view of the field as a whole, and further support the  
936    work of McGee et al. (2013, 2015), Hopkins et al. (2016), and McGee and Smith  
937    (2016) on the mantle source characteristics and the link between geochemical  
938    signatures of the erupted products (e.g.  $\text{SiO}_2$  vs.  $\text{CaO}/\text{Al}_2\text{O}_3$  (**Fig. 17A**), or  $\text{SiO}_2$  vs.  
939     $(\text{La}/\text{Yb})_N$  (**Fig. 17B**)) and the eruptive volume for the centres (from Kereszturi et  
940    al. 2013). The new field-wide data set produced by this study shows that for  $\text{SiO}_2$   
941    vs.  $\text{CaO}/\text{Al}_2\text{O}_3$  the trend in the data is less well defined in comparison to  $\text{SiO}_2$  vs.  
942     $(\text{La}/\text{Yb})_N$  (**Fig 17**). This greater scatter is attributed to the impact of minor  
943    amounts of fractional crystallisation on major elements during magma ascent  
944    (e.g. Hopkins et al. 2016). The  $(\text{La}/\text{Yb})_N$  ratio shows a much stronger trend  
945    because these two elements are incompatible, thus less effected by fractional  
946    crystallisation, and therefore are more reflective of the mantle source signature.

947            In addition, McGee et al. (2013) highlighted a relationship between the  
948    trends observed in trace element multi-plots and eruptive volumes, suggesting  
949    that K and Sr anomalies (c.f **Fig. 4**) are also linked to eruptive volume. This  
950    conclusion was, however, based on geochemical data for only 10 centres  
951    (spanning a wide range in eruptive volumes). The addition of our new data  
952    suggests that these relationships may be less clear-cut. For example, the  
953    geochemical data for whole-rock samples from Te Pou Hawaiki shows a highly  
954    subdued K anomaly, coupled with a large Sr anomaly. This signature was linked  
955    by McGee et al. (2013) to centres with large eruptive volumes (e.g. Rangitoto

DRE<sup>tot</sup> = 0.6 km<sup>3</sup>), yet Te Pou Hawaiki has a relatively small estimated volume (DRE<sup>tot</sup> = 0.028 km<sup>3</sup>). Similarly, Mt Cambria has one of the smallest eruptive volumes (DRE<sup>tot</sup> = 0.00029 km<sup>3</sup>), much smaller than Purchas Hill (DRE<sup>tot</sup> = 0.0017 km<sup>3</sup>), yet does not have a more extreme geochemical signature than Purchas Hill (e.g. it lacks a more pronounced K anomaly, or Zr-Hf trough; **Fig. 4**).

If the McGee et al. (2013, 2015) correlations are accepted, then a number of the newly analysed centres exhibit geochemical signatures that are suggestive of larger magma batches than fit their inferred eruptive volumes (e.g. Te Pou Hawaiki; **Fig. 15**). There are three possible explanations for these discrepancies: 1) volume estimates are inaccurate, 2) magma volume is 'lost' on ascent, or 3) the mantle source is heterogeneous.

Volume estimates by Kereszturi et al. (2013) are considered more reliable than those of Allen and Smith (1994), but the same relationships are seen with either data set (**Fig. 15**). Distal tephra is not accounted for in either model, potentially leading to volume underestimates (Kereszturi *pers. comm.*). This underestimate is not, however, enough to account for the observed discrepancies between the geochemical signatures and the erupted volumes. It is possible that there is a loss of magma during ascent, due to either or both of 1) fractional crystallisation of ascending melt, or 2) trapping of magma within the crust as an intrusion. Losses through fractional crystallisation are supported by the less well-defined relationship between the major elements and the erupted volumes as discussed previously. However, because many of the AVF lavas have a very primitive geochemical signature, there is only evidence of very limited fractional crystallisation (e.g. Smith et al. 2008; McGee et al. 2013; Hopkins et al. 2016), which is again not enough to account for the discrepancies. It is therefore most

likely that a heterogeneous mantle source, coupled with minor amounts of fractional crystallisation and retention of magma in the crust, may affect the final proportion of magma that is erupted. When geochemical data are combined with the temporal ordering, there are no obvious patterns identifiable through the history of the field. The lack of systematic change in the geochemical signatures through time suggests that the mantle source is not evolving in any systematic manner. Instead, the magma batches for each eruption are formed through the variable tapping and mixing of these heterogeneous mantle sources.

## **Conclusions**

The collation of whole rock major and trace element data for the AVF has (with a few exceptions) facilitated the development and testing of a method to correlate distal tephra samples to their source volcanic centres. Geochemical correlation between distal tephra-derived glass and the glassy matrix of whole rocks at the source volcano is proved to be reliable. The method produces reasonable results based on major element signatures alone, with correlations strengthened by the use of trace-element signatures. Furthermore, incompatible trace elements and their ratios (particularly versus Yb; e.g.  $(\text{Gd}/\text{Yb})_{\text{N}}$ ,  $(\text{La}/\text{Yb})_{\text{N}}$ ,  $(\text{Zr}/\text{Yb})_{\text{N}}$ ) are representative for individual centres and can therefore be used to geochemically correlate distal basaltic tephra to proximal whole-rock samples in the AVF. Specifically the ratios listed above are proven to be most useful in assigning individual geochemical fingerprints because they are highlighted to be the most variable across the field, yet the least variable within any given centre, and the least affected by fractional crystallisation processes.

This study has demonstrated geochemistry to be an effective tephra correlation tool, but we stress that geochemical compositions are not always sufficiently distinct to provide a definitive result. To efficiently correlate tephra layers to their source centres, a multi-criteria approach is required. For greatest correlation confidence, this approach combines age data (of both distal tephras and proximal whole rock deposits) and eruption characteristics (e.g. scale and locality), to assign the source centre to tephra deposits. Of the twenty eight basaltic tephra horizons in the AVF maar-lake cores, all but two (newA and newB) are correlated to a source; eight with a confidence level of 1, eleven with a confidence level of 2, and seven with a confidence level of 3.

The correlations with confidence levels of 1 and 2 are used to determine tephra dispersal and thickness (e.g. footprint) from the AVF eruptions. The maximum tephra dispersal distance is 13.5 km with a primary deposit thickness within the core of 2 mm, and for all primary core deposits with a thickness >100 mm the source is <6 km away. In a number of cases the deposits are restricted to sites in close proximity to the source centre, suggesting that in the event of a future small-scale eruption, damaging thicknesses of tephra will not inundate the entire Auckland area.

Our correlations also provide a clearer picture of the temporal evolution of the AVF. Using the stratigraphic relationships of the tephra horizons within the cores and their association with the rhyolitic marker horizons, the absolute age order of the centres can be resolved. Because of the errors associated with dating techniques ( $^{40}\text{Ar}/^{39}\text{Ar}$  and  $^{14}\text{C}$ ) a relative sequencing of the AVF centres was previously not possible. Using our new method we provide high-confidence relative and absolute eruption age estimates for 48 centres, leaving only five

1030 centres with uncertain ages (Pukaki, Pukewairiki, Boggust Park, Cemetery Hill  
1031 and Puhinui Craters). Our reconstruction of the relative ages of the centres also  
1032 allows the temporal, spatial, and geochemical evolution of the AVF to be  
1033 assessed, confirming that there is no simple temporal pattern in the spatial and  
1034 geochemical evolution of the field.

1035

## 1036 **Acknowledgements**

1037 JLH is funded by the DEVORA (DEtermining VOLcanic Risk in Auckland) project,  
1038 led by Jan Lindsay and Graham Leonard. JLH would like to thank Elaine Smid and  
1039 Shaun Eaves for field assistance, and David Lowe, Monica Handler and Stephen  
1040 Blake for valuable discussion and advice during the early stages of this  
1041 manuscript. The authors wish to thank Neville Hudson at the University of  
1042 Auckland collections for assistance in finding pre-existing samples, and Bruce  
1043 Hayward for invaluable advice on site locations for new samples.

## References

- Affleck DK, Cassidy J, Locke CA (2001) Te Pou Hawaiki volcano and pre-volcanic topography in central Auckland: volcanological and hydrogeological implications. *NZ J Geol Geophys* 44:313-321
- Agustín-Flores J, Németh K, Cronin SJ, Lindsay JM, Kereszturi G (2015) Construction of the North Head (Maungauika) tuff cone: a product of Surtseyan volcanism, rare in the Auckland Volcanic Field, New Zealand. *Bull Volcanol* 77:11
- Allan ASR, Baker JA, Carter L, Wysoczanski RJ (2008) Reconstructing the Quaternary evolution of the world's most active silicic volcanic system: insights from an ~1.65 Ma deep ocean tephra record sourced from the Taupo Volcanic Zone, New Zealand. *Quat Sci Rev* 27:2341-2360
- Allen SR, Smith IEM (1994) Eruption styles and volcanic hazard in the Auckland Volcanic Field, New Zealand. *Geosci Rep Shizuoka Univ* 20:5-14
- Alloway BV, Westgate JA, Pillans, BJ, Pearce NJG, Newnham RM, Byrami, ML, Aarburg SE (2004) Stratigraphy, age and correlation of middle Pleistocene silicic tephras in the Auckland region, New Zealand: a prolific distal record of Taupo Volcanic Zone volcanism. *NZ J Geol Geophys* 47:447-479
- Bebbington MS (2013) Assessing probabilistic forecasts of volcanic eruption onsets. *J Volcanol Geotherm Res* 252:14-28
- Bebbington MS, Cronin SJ (2011) Spatio-temporal hazard estimation in the Auckland Volcanic Field, New Zealand, with a new event-order model. *Bull Volcanol* 73:55-72
- Brand BD, Gravley DM, Clarke AB, Lindsay JM, Bloomberg SH, Agustín-Flores J, Németh K (2014) A combined field and numerical approach to understanding

1076 dilute pyroclastic density current dynamics and hazard potential: Auckland  
 1077 Volcanic Field, New Zealand. *J Volcanol Geotherm Res* 276:215-232  
 1078  
 1079 Briggs RM, Okada T, Itaya T, Shibuya H, Smith IEM (1994) K-Ar ages,  
 1080 paleomagnetism, and geochemistry of South Auckland volcanic field, North  
 1081 Island, New Zealand. *NZ J Geol Geophys* 37:143-153  
 1082  
 1083 Bryner V (1991) Motukorea: the evolution of an eruption centre in the Auckland  
 1084 Volcanic Field. MSc thesis, University of Auckland, New Zealand.  
 1085  
 1086 Cassata WS, Singer BS, Cassidy J (2008) Laschamp and Mono Lake geomagnetic  
 1087 excursions recorded in New Zealand. *Earth Planet Sci Lett* 268:76-88  
 1088  
 1089 Cassidy J (2006) Geomagnetic excursion captured by multiple volcanoes in a  
 1090 monogenetic field. *Geophys Res Lett* 33:L21310  
 1091  
 1092 Charlier BLA, Peate DW, Wilson CJN, Lowestern JB, Storey M, Brown SJA (2003)  
 1093 Crystallisation ages in coeval silicic magma bodies:  $^{238}\text{U}$ - $^{230}\text{Th}$  disequilibrium  
 1094 evidence from the Rotoiti and Earthquake Flat eruption deposits, Taupo Volcanic  
 1095 Zone, New Zealand. *Earth Planet Sci Lett* 206:441-457  
 1096  
 1097 Cook C, Briggs RM, Smith IEM, Maas R (2005) Petrology and geochemistry of  
 1098 intraplate basalts in the South Auckland volcanic field, New Zealand: Evidence  
 1099 for two coeval magma suites from distinct sources. *J Petrol* 46:473-503  
 1100  
 1101 Danišík M, Shane P, Schmitt AK, Hogg A, Santos GM, Storm S, Evans NJ, Fifield LK,  
 1102 Lindsay JM (2012) Re-anchoring the late Pleistocene tephrochronology of New  
 1103 Zealand based on concordant radiocarbon ages and combined  $^{238}\text{U}/^{230}\text{Th}$   
 1104 disequilibrium and (U-Th)/He zircon ages. *Earth Planet Sci Lett* 349-350:240-  
 1105 250  
 1106

1107 Davies SM, Turney CSM, Lowe JJ (2001) Identification and significance of a  
 1108 visible , basalt-rich Vedde Ash layer in a Late-glacial sequence on the Isle of Skye,  
 1109 Inner Hebrides, Scotland. J Quat Sci 16:99-104  
 1110  
 1111 Dunbar NW, Kurbatov AV (2011) Terphrochronology of the Siple Dome ice core,  
 1112 West Antarctica: correlations and sources. Quat Sci Rev 30:1602-1614  
 1113  
 1114 Eade J (2009) Petrology and correlation of lava flows from the central part of the  
 1115 Auckland Volcanic Field. MSc thesis, University of Auckland, New Zealand.  
 1116  
 1117 Fleck RJ, Hagstrum JT, Calvert AT, Evarts RC, Conrey RM (2014)  $^{40}\text{Ar}/^{39}\text{Ar}$   
 1118 geochronology, paleomagnetism, and evolution of the Boring volcanic field,  
 1119 Oregon and Washington, USA. Geosphere 10:1483-1314  
 1120  
 1121 Flude S, Storey M (2016)  $^{40}\text{Ar}/^{39}\text{Ar}$  age of the Rotoiti Breccia and Rotoehu Ash,  
 1122 Okataina Volcanic Complex, New Zealand, and identification of heterogeneously  
 1123 distributed excess  $^{40}\text{Ar}$  in supercooled crystals. Quat Geochronol 33:13-23  
 1124  
 1125 Franklin JT (1999) Geology of the Orakei Basin area. MSc thesis, University of  
 1126 Auckland, New Zealand.  
 1127  
 1128 Hayes JL, Wilson TM, Magill C (2015) Tephra fall clean-up in urban  
 1129 environments. J Volcanol Geotherm Res 304:237-252  
 1130  
 1131 Hayward BW (2008) Ash Hill Volcano, Wiri. Geocene, Geoscience Society of New  
 1132 Zealand, 3:8-9  
 1133  
 1134 Hayward BW, Hopkins, JL, Smid, ER (2016) Mangere Lagoon predated Mangere  
 1135 Mt. Geocene, Geoscience Society of New Zealand, 14:4-5  
 1136  
 1137 Hayward BW, Murdoch G, Maitland G (2011) Volcanoes of Auckland, The  
 1138 Essential Guide. Auckland University Press, Auckland, New Zealand.  
 1139



1140 Heming RF, Barnet PR (1986) The petrology and petrochemistry of the Auckland  
 1141 volcanic field. In: Smith IEM (Ed), Late Cenozoic Volcanism in New Zealand. Roy  
 1142 Soc NZ Bull 23:64-75  
 1143  
 1144 Hill BE, Connor CB, Jarzempa MS, La Femina PC, Navarro M, Strauch W (1998)  
 1145 1995 Eruptions of Cerra Negro Volcano, Nicaragua, and risk assessment for  
 1146 future eruptions Geol Soc Am Bull 110:1231-1241  
 1147  
 1148 Hookway M (2000) The geochemistry of Rangitoto. MSc thesis, University of  
 1149 Auckland, New Zealand  
 1150  
 1151 Hopkins JL, Millet, M-A, Timm C, Wilson CJN, Leonard GS, Palin JM, Neil H (2015)  
 1152 Tools and techniques for developing tephra stratigraphies in lake cores: a case  
 1153 study from the Auckland Volcanic Field, New Zealand. Quat Sci Rev 123:58-75.  
 1154  
 1155 Hopkins JL, Timm C, Millet M-A, Poirier A, Wilson CJN, Leonard GS (2016) Os  
 1156 isotopic constraints on crustal contamination in Auckland Volcanic Field basalts,  
 1157 New Zealand. Chem Geol 439:83-97  
 1158  
 1159 Houghton BF, Bonadonna C, Gregg CE, Johnston DM, Cousins WJ, Cole JW, Del  
 1160 Carlo P (2006) Proximal tephra hazards: recent eruptions studies applied to  
 1161 volcanic risk in the Auckland Volcanic Field, New Zealand. J Volcanol Geotherm  
 1162 Res 155:138-149  
 1163  
 1164 Hoverd JL, Shane PA, Smith IEM, Smith VC, Wilson CJN (2005) Towards an  
 1165 improved understanding of local and distal volcanic stratigraphy in Auckland:  
 1166 stratigraphy of a long core from Glover Park (St Helier's Volcano) in Auckland.  
 1167 Institute of Geological & Nuclear Sciences Science Report 2005/31:45p  
 1168  
 1169 Huang Y, Hawkesworth C, van Calsteren P, Smith I, Black P (1997) Melt  
 1170 generation models for the Auckland volcanic field, New Zealand: constraints  
 1171 from U-Th isotopes. Earth Planet Sci Lett 149:67-84  
 1172

1173 Johnson PJ, Valentine GA, Cortés JA, Tadini A (2014) Basaltic tephra from  
 1174 monogenetic Marcath Volcano, central Nevada. *J Volcanol Geotherm Res* 281:27-  
 1175 33  
 1176  
 1177 Kawabata E, Cronin S, Bebbington M, Moufti M, El-Masry N, Wang T (2015)  
 1178 Identifying multiple eruption phases from a compound tephra blanket: an  
 1179 example of the AD1256 Al-Madinah eruption, Saudi Arabia. *Bull Volcanol* 77:6  
 1180  
 1181 Kawabata E, Bebbington MS, Cronin SJ, Wang T (2016) Optimal likelihood-based  
 1182 matching of volcanic sources and deposits. *J Volcanol Geotherm Res* 323:194-  
 1183 208  
 1184  
 1185 Kereszturi G, Németh K, Cronin SJ, Agustín-Flores J, Smith IEM, Lindsay J (2013)  
 1186 A model for calculating eruptive volumes for monogenetic volcanoes –  
 1187 Implication for the Quaternary Auckland Volcanic Field, New Zealand. *J Volcanol*  
 1188 *Geotherm Res* 266:16-33  
 1189  
 1190 Kereszturi G, Németh K, Cronin SJ, Procter J, Agustín-Flores J (2014) Influences  
 1191 on the variability of eruption sequences and style transitions in the Auckland  
 1192 Volcanic Field, New Zealand. *J Volcanol Geotherm Res* 286:101-115  
 1193  
 1194 Kermode LO (1992) Geology of the Auckland urban area. Scale 1:50,000.  
 1195 Institute of Geological and Nuclear Sciences geological map 2. Institute of  
 1196 Geological and Nuclear Sciences Ltd, Lower Hutt, New Zealand  
 1197  
 1198 Larsson W (1937) Vulkanische asche vom ausbruch des Chilenischen vulkans  
 1199 Quizapú (1932) in Argentina gesammelt. *Bulletin Geological Institution of*  
 1200 *Uppsala* 26:27-52.  
 1201  
 1202 Le Corvec N, Bebbington MS, Lindsay JM, McGee LE (2013) Age, distance and  
 1203 geochemical evolution within a monogenetic volcanic field: Analysing patterns in  
 1204 the Auckland Volcanic Field eruption sequence. *Geochem Geophys Geosyst*  
 1205 14:3648-3665  
 1206

1207 LeMaitre RW (2002) Igneous Rocks: Classification and Glossary of Terms. 2<sup>nd</sup>  
 1208 Edition, Cambridge University Press, Cambridge, UK, pp236.  
 1209  
 1210 Leonard GS, Calvert AT, Hopkins JL, Wilson CJN, Smid E, Lindsay J, Champion D  
 1211 (2017) High precision <sup>40</sup>Ar-<sup>39</sup>Ar dating of late Quaternary basalts from Auckland  
 1212 Volcanic Field, New Zealand, with implications for eruption rates and  
 1213 paleomagnetic correlations. Earth Planet Sci Lett (in press)  
 1214  
 1215 Lian OB, Shane P (2000) Optical dating of paleosols bracketing the widespread  
 1216 Rotoehu tephra North Island, New Zealand. . Quat Sci Rev 19:1649-1662  
 1217  
 1218 Lindsay JM, Leonard GS, Smid ER, Hayward BW (2011) Age of the Auckland  
 1219 Volcanic Field: a review of existing data. NZ J Geol Geophys 54:379-401  
 1220  
 1221 Lirer L, Pescatore T, Booth B, Walker GPL (1973) Two plinian pumice-fall  
 1222 deposits from Somma-Vesuvius, Italy. Geol. Soc. Am. Bull. 84:759-772  
 1223  
 1224 Lowe DJ (2011) Tephrochronology and its application: a review. Quat  
 1225 Geochronol 6:107-153  
 1226  
 1227 Lowe DJ, Hogg AG (1995) Age of the Rotoehu Ash. NZ J Geol Geophys 38:399-402  
 1228  
 1229 Lowe DJ, Palmer DJ (2005) Andisols of New Zealand and Australia. J Integr Field  
 1230 Sci 2:39-65  
 1231  
 1232 Lowe DJ, Alloway BV (2015) Tephrochronology. In Rink WJ, Thompson JW (Eds)  
 1233 Encyclopedia of Scientific Dating methods. Springer, Dordrecht 733-799.  
 1234  
 1235 Lowe DJ, Blaauw M, Hogg AG, Newham RM (2013) Ages of 24 widespread  
 1236 tephras erupted since 30,000 years ago in New Zealand, with re-evaluation of the  
 1237 timing and palaeoclimatic implications of the Late Glacial cool episode recorded  
 1238 in the Kaipo bog. Quat Sci Rev 74:170-194  
 1239

1240 Magill CR, McAneney KJ, Smith IEM (2005). Probabilistic assessment of vent  
 1241 locations for the next Auckland Volcanic Field event. *Math Geol* 37:227-242.  
 1242  
 1243 McDonough WF, Sun S-s (1995) The composition of the Earth. *Chem Geol*  
 1244 120:223-253  
 1245  
 1246 McGee LE (2012) Melting processes in small basaltic systems: the Auckland  
 1247 Volcanic Field, New Zealand. Ph.D. thesis, University of Auckland, New Zealand.  
 1248  
 1249 McGee LE, Smith IEM (2016) Interpreting chemical compositions of small scale  
 1250 basaltic systems: A review. *J Volcanol Geotherm Res* 325:45-60  
 1251  
 1252 McGee LE, Beier C, Smith IEM, Turner S (2011) Dynamics of melting beneath a  
 1253 small-scale basaltic system: a U-Th-Ra study from Rangitoto volcano, Auckland  
 1254 Volcanic Field, New Zealand. *Contrib Mineral Petr* 162:547-563  
 1255  
 1256 McGee LE, Millet M-A, Smith IEM, Németh K, Lindsay JM (2012) The inception  
 1257 and progression of melting in a monogenetic eruption: Motukorea Volcano, the  
 1258 Auckland Volcanic Field, New Zealand. *Lithos* 156:360-374  
 1259  
 1260 McGee LE, Smith IEM, Millet M-A, Handley H, Lindsay JM (2013) Asthenospheric  
 1261 control of melting processes in a monogenetic basaltic system: a case study of  
 1262 the Auckland Volcanic Field, New Zealand. *J Petrol* 54:2125-2153  
 1263  
 1264 McGee LE, Millet M-A, Beier C, Smith IEM, Lindsay JM (2015) Mantle  
 1265 heterogeneity controls on small-volume basaltic eruption characteristics.  
 1266 *Geology* 43:551-554  
 1267  
 1268 McKenzie D, O'Nions RK (1991) Partial melt distributions from inversion of rare  
 1269 earth element concentrations. *J Petrol* 32:1021-1091  
 1270  
 1271 Miller CA (1996) Geophysical and geochemical characteristics of the Auckland  
 1272 Volcanic Field. MSc thesis, University of Auckland, New Zealand.

1273

1274 Molloy CM (2008) Tephrostratigraphy of the Auckland maar craters. MSc thesis,  
 1275 University of Auckland, New Zealand.

1276

1277 Molloy C, Shane P, Augustinus P (2009) Eruption recurrence rates in a basaltic  
 1278 volcanic field based on tephra layers in maar sediments: implications for hazards  
 1279 in the Auckland volcanic field. *Geol Soc Am Bull* 121:1666-1677

1280

1281 Needham AJ, Lindsay JM, Smith IEM, Augustinus P, Shane PA (2011) Sequential  
 1282 eruption of alkaline and subalkaline magmas from a small monogenetic volcano  
 1283 in the Auckland Volcanic Field, New Zealand. *J Volcanol Geotherm Res* 201:126-  
 1284 142

1285

1286 Newnham RM, Lowe DJ, Giles T, Alloway BV (2007) Vegetation and climate of  
 1287 Auckland, New Zealand, since ca. 32000 cal. yr ago: support for an extended  
 1288 LGM. *J Quat Sci* 22:517-534

1289

1290 Óladóttir BA, Larsen G, Sigmarsson O (2012) Deciphering eruption history and  
 1291 magmatic processes from tephra in Iceland. *Jökull* 62:21-38

1292

1293 Ort MH, Elson MD, Anderson KC, Duffield WA, Hooten JA, Champion DE, Waring G  
 1294 (2008) Effects of scoria-cone eruptions upon nearby human communities. *Geol*  
 1295 *Soc Am Bull* 120:476-486

1296

1297 Paton C, Hellstrom J, Paul B, Woodhead J, Hergt J (2011) Iolite, freeware for the  
 1298 visualisation and processing of mass spectrometric data. *J Anal Atom Spectrom*  
 1299 26:2508-2518

1300

1301 Pearce NJ, Alloway BV, Westgate JA (2008) Mid-Pleistocene silicic tephra beds in  
 1302 the Auckland region, New Zealand: their correlation and origins based on the  
 1303 trace element analyses of single glass shards. *Quaternary International* 178:16-  
 1304 43

1305

1306 Pyle DM (1989) The thickness, volume and grain size of tephra fall deposits. Bull  
 1307 Volcanol 51:1-15  
 1308  
 1309 Pyne O'Donnell S (2011) The taphonomy of Last Glacial-Interglacial Transition  
 1310 (LGIT) distal volcanic ash in small Scottish lakes. Boreas 40:131-145  
 1311  
 1312 Ramsey MH, Potts PJ, Webb PC, Watkins P, Watson JS, Coles BJ (1995) An  
 1313 objective assessment of analytical method precision: comparison of ICP-AES and  
 1314 XRF for the analysis of silicate rocks. Chem Geol 124:1-19  
 1315  
 1316 Reiners PW (1998) Reactive melt transport in the mantle and geochemical  
 1317 signatures of mantle-derived magmas. J Petrol 39:1039-1061  
 1318  
 1319 Robinson JA, Wood BJ (1998) The depth of the spinel to garnet transition at the  
 1320 peridotite solidus. Earth Planet Sci Lett 164:277-284  
 1321  
 1322 Sandiford A, Alloway B, Shane P (2001) A 28,000-6600 cal yr record of local and  
 1323 distal volcanism preserved in a paleolake, Auckland, New Zealand. NZ J Geol  
 1324 Geophys 44:323-336  
 1325  
 1326 Sandiford A, Horrocks M, Newnham R, Ogden J, Alloway B (2002) Environmental  
 1327 change during the last glacial maximum (c. 25000 – c. 16500 years BP) at Mt  
 1328 Richmond, Auckland Isthmus, New Zealand. J Roy Soc New Zeal 32:155-167  
 1329  
 1330 Shane P (2005) Towards a comprehensive distal andesitic tephrostratigraphic  
 1331 framework for New Zealand based on eruptions from Egmont Volcano. J Quat Sci  
 1332 20:45-57  
 1333  
 1334 Shane P, Hovard J (2002) Distal record of multi-sourced tephra in Onepoto Basin,  
 1335 Auckland, New Zealand: implications for volcanic chronology, frequency and  
 1336 hazards. Bull Volcanol 64:441-454  
 1337

1338 Shane P, Smith IEM (2000) Geochemical fingerprinting of basaltic tephra  
 1339 deposits in the Auckland Volcanic Field. *NZ J Geol Geophys* 43:569-577  
 1340  
 1341 Shane P, Gehrels M, Zawalna-Geer A, Augustinus P, Lindsay J, Chaillou I (2013)  
 1342 Longevity of a small shield volcano revealed by crypto-tephra studies (Rangitoto  
 1343 volcano, New Zealand): Change in eruptive behaviour of a basaltic field. *J*  
 1344 *Volcanol Geotherm Res* 257:174-183  
 1345  
 1346 Shibuya H, Cassidy J, Smith IEM, Itaya T (1992) A geomagnetic excursion in the  
 1347 Brunhes epoch recorded in New Zealand basalts. *Earth Planet Sc Lett* 111:41-48  
 1348  
 1349 Smith IEM, Blake S, Wilson CJN, Houghton BF (2008) Deep-seated fractionation  
 1350 during the rise of a small-volume basalt magma batch: Crater Hill, Auckland, New  
 1351 Zealand. *Contrib Mineral Petrol* 155:511-527  
 1352  
 1353 Spargo SRW (2007) The Pupuke volcanic centre: polygenetic magmas in a  
 1354 monogenetic field. MSc thesis, University of Auckland, New Zealand  
 1355  
 1356 Tomsen E, Lindsay JM, Gahegan M, Wilson TM, Blake DM (2014) Evacuation  
 1357 planning in the Auckland Volcanic Field, New Zealand: a spatio-temporal  
 1358 approach for emergency management and transportation network decisions.  
 1359 *Journal of Applied Volcanology* 3:6  
 1360  
 1361 Ukstins Peate I, Kent AJR, Baker JA, Menzies MA (2008) Extreme geochemical  
 1362 heterogeneity in Afro-Arabian Oligocene tephras: preserving fractional  
 1363 crystallisation and mafic recharge processes in silicic magma chambers. *Lithos*  
 1364 102:260-278  
 1365  
 1366 Valentine GA, Krier D, Perry FV, Heiken G (2008) Eruptive and geomorphic  
 1367 processes at the Lathrop Wells scoria cone volcano. *J Volcanol Geotherm Res*  
 1368 161:57-80  
 1369

1370 van Otterloo J, Cas RAF (2013) Reconstructing the eruption magnitude and  
 1371 energy budgets for the pre-historic eruption of the monogenetic ~5 ka Mt.  
 1372 Gambier Volcanic Complex, south-eastern Australia. Bull Volcanol 75:769  
 1373  
 1374 von Veh MW, Németh K (2009) An assessment of the alignments of vents based  
 1375 on geostatistical analysis in the Auckland Volcanic Field, New Zealand.  
 1376 Géomorphologie: relief, processus, environment 15:175-186.  
 1377  
 1378 Wilson CJN, Rhoades DA, Lanphere MO, Calvert AT, Houghton BF, Weaver SD,  
 1379 Cole JW (2007) A multi-approach radiometric age estimate for the Rotoiti and  
 1380 Earthquake Flat eruptions, New Zealand, with implications for the MIS 4/3  
 1381 boundary. Quat Sci Rev 26:1861-1870  
 1382  
 1383 Wilson G, Wilson TM, Deligne NI, Cole JW (2014) Volcanic hazard impacts to  
 1384 critical infrastructure: a review. J Volcanol Geotherm Res 286:148-182  
 1385  
 1386 Zawalna-Geer A, Lindsay JM, Davies S, Augustinus P, Davies S (2016) Extracting a  
 1387 primary Holocene cryptotephra record from Pupuke maar sediments, Auckland,  
 1388 New Zealand. J Quat Sci 31:442-457  
 1389



## 1 **Figure Captions**

2 **Figure 1.** (A) Map of the Auckland Volcanic Field and its eruptive centres (from  
 3 Hayward et al. 2011). The locations of maar craters from which cores documented here  
 4 were collected are highlighted by red symbols and red font: Pupuke, Onepoto, Glover  
 5 Park, Orakei, Hopua and Pukaki. Although the Glover Park core is from St Heliers  
 6 volcano, to avoid confusion here the core location will continue to be called Glover Park.  
 7 (B) General location of the AVF within the North Island, New Zealand. Highlighted are  
 8 other key volcanic centres including the South Auckland Volcanic Field (SAVF), and the  
 9 key rhyolitic sources from the Taupo Volcanic Zone (TVZ) (Taupo Volcanic Centre  
 10 (TVC), Okataina Volcanic Centre (OVC)) and andesitic (Tongariro Volcanic Centre  
 11 (TgVC), Mt. Taranaki (Tk/Eg)) sources of tephra found in Auckland maar crater cores.

12  
 13 **Figure 2.** Age-depth profiles for rhyolitic marker horizons (RMHs) and basaltic tephra  
 14 deposits within the cores, and individual sedimentation rate profiles for each core.  
 15 Abbreviations, errors, and references for the RMHs ages are in **Table 2**. Age envelopes  
 16 are highlighted in light grey based on the errors associated with the RMH ages. AVF  
 17 basaltic deposits are plotted as red triangles at the appropriate depth in the core, and  
 18 horizon Eg36, an andesitic marker horizon from Mt Taranaki, is plotted in green.

19  
 20 **Figure 3.** Representative major and trace element variation diagrams (in wt%) for AVF  
 21 volcanic rocks (n=744; data in **supplementary material**). Highlighted are those which  
 22 show examples of the distinct patterns seen within individual centres, grey symbols  
 23 show all other data.

24  
 25 **Figure 4.** Primitive mantle-normalised trace element plots for whole rock (shaded grey)  
 26 and glass from selected tephra horizons (coloured lines) from a range of cores showing  
 27 a range of geochemistries and ages (high AVF#s = young, low AVF# = old). Values are  
 28 normalised to primitive mantle after McDonough and Sun (1995).

29  
 30 **Figure 5.** Comparison plot for concentrations of major and trace elements for whole  
 31 rock and glass for the full sample suite (all data in **supplementary material**). (A) MgO  
 32 vs. SiO<sub>2</sub> indicating an example of elements that do not correlate, and (B) (Zr/Yb)<sub>N</sub> vs.  
 33 (Gd/Yb)<sub>N</sub> indicating an example of trace element ratios that do correlate for glass and  
 34 whole rock samples.

35

**Figure 6.** Multi-element plots to show geochemical comparison between glass from a known Mt. Wellington tephra deposit from the Hopua maar core, a simulated glass (matrix-derived glass) made from Mt. Wellington whole rock sample AU62394, and whole rock analyses from Mt Wellington. (A) Glass comparison of MgO vs. Al<sub>2</sub>O<sub>3</sub>, (B) glass comparison for Gd vs. Zr, (C) example of glass and whole rock concentrations for major elements which are not comparable (MgO vs Al<sub>2</sub>O<sub>3</sub>), (D) example of glass and whole rock major element concentration that are comparable (CaO vs FeO), (E) example of glass and whole rock trace elements that are comparable (Tm vs. Gd), (F) example of glass and whole rock trace element ratios that are comparable ((Zr/Yb)<sub>N</sub> vs. (Gd/Yb)<sub>N</sub>). Individual analyses are shown by symbols, field-wide geochemical concentrations of glass are outlined by orange dashed area and field-wide geochemical whole rock concentrations are shown by black dashed area.

**Figure 7.** Selected whole rock and glass sample concentrations to show the effects of crystal removal. (A) MgO vs. Ni for glass and, (B) whole rock. Both show a high r<sup>2</sup> value suggesting a statistically significant relationship between the two elements. In comparison (C) MgO vs. La for glass and, (D) for whole rock. Both show r<sup>2</sup> values near zero, indicating no statistically significant relationships between the elements.

**Figure 8.** Graphs showing the variations and comparability of the geochemical signatures observed through the eruptive products of Motukorea volcano (from McGee et al. 2012), coupled with the geochemical signatures for the distal glass composition found within the Orakei Basin core (horizon AVF15). (A) SiO<sub>2</sub> (wt%) vs. Zr (ppm) and (B) (Zr/Yb)<sub>N</sub> vs. (Gd/Yb)<sub>N</sub> normalised to primitive mantle values (McDonough and Sun 1995). Similar relationships are also seen for (La/Yb)<sub>N</sub>, (Ce/Yb)<sub>N</sub>, (Nb/Yb)<sub>N</sub>, and (Nd/Yb)<sub>N</sub> (data from **supplementary material**).

**Figure 9.** Example plots of geochemical correlations. Glass values are shown in coloured symbols that indicating different cores, whole rock values are shown by coloured triangles for each centre, and the grey field shows the geochemical spread for the entire AVF, both whole rock and glass compositions. (A) Example of a confidence level 1 correlation for the Three Kings centre with tephra layer AVF7, showing selected major element and normalised trace element ratios. (B) Example of an ambiguous geochemical correlation for Crater Hill centre and tephra horizon AVF8 due to limited trace element geochemistry for some centres. (C) Example of centres that are of an appropriate age but show no geochemical correlation to the tephra horizon AVF13.

**Figure 10.** Data for all correlations with a confidence rating of level 1 or 2 (data in **Table 6**). (A) Horizon thickness vs. distance from source, showing the thinning of deposits increases away from source. Grey shaded area marks <6 km, within which all the deposits >100 mm thick are found. (B) % Shard size vs. distance from source, indicating the fining of away from source.

**Figure 11.** Example of the correlation of Mt. Eden eruption to tephra deposit AVF12. (A) Graph to show change in deposit thickness away from source, note the extreme decline in thickness after ca. 6 km distance. Also shown on (A) are backscatter electron images of the glassshards from each core site taken on EMPA. All pictures are at the same scale with the bar at the base of the images representing 200  $\mu\text{m}$ . (B) Inferred isopach map of the tephra dispersal from Mt. Eden based on the deposit thicknesses found in the cores. Dispersal is skewed to the east to reflect the westerly winds likely to have been present at the time of eruption (Hayward et al. 2011).

**Figure 12.** Age range chart for all centres (data from **Table 5.1**). Those in red are  $^{40}\text{Ar}/^{39}\text{Ar}$  (from Leonard et al. 2017 or Cassata et al. 2008) (2 sd error) or  $^{14}\text{C}$  ages (from Lindsay et al. 2011). Markers show the mean ages measured by these techniques with lines showing the age ranges measured. Lines in orange have their ages based only on morphostratigraphy, and those in grey have no ages associated with them. Of note is the number of centres which, based on errors, could have erupted at a given time. For example there are 18 potential centres whose age ranges include 50 ka (Mt. Cambria, McLaughlins Hill, Hopua, One Tree Hill, Mt. Victoria, Mt. Hobson, Waitomokia, Onepoto, St Heliers, Tank Farm, Domain, Grafton, Otuaataua, Puhinui Craters, Mt. Robertson, Cemetery Hill, Boggust Park, and Pigeon Mt.).

**Figure 13.** Figure to show the combined age data that allow the centres to be put in order. Core correlations are from Hopkins et al. (2015), AVF horizon correlations from this study, Ar-Ar ages and ranges from Leonard et al. (2017), and morphostratigraphic relationships from Allen and Smith (1994); Affleck et al. (2001); and Hayward et al. (2011). Key rhyolitic marker horizons are shown in colours, and highlight the chronostratigraphic age limits for the basaltic horizons. Age ranges depicted by error bars are not to scale, the ranges are drawn to the associated ages in the cores.

**Figure 14.** A comparison of relative and absolute age orders for 45 AVF centres from statistical modelled results (Bebbington and Cronin 2011) versus new data from this study. (A) Relative age order, (B) absolute age estimates, and (C) 10-50 ka for absolute age. The 1:1 ratio lines are shown in red on each chart for comparison purposes.

**Figure 15.** Comparison plots for whole rock geochemistry vs. eruptive volume for all data available from the AVF. Data are plotted versus eruptive volume estimates from both Kereszturi et al. (2013) and Allen and Smith (1994) for comparison. All data are shown in light grey symbols, with mean values for each centre highlighted for pre-existing data in grey triangles, and for new data in red triangles.

## Table Captions

**Table 1.** Catalogue of geochemical whole rock data (pre-existing and additions from this study) available for the AVF, ordered by the number of analyses, including those centres without any current data. After the addition of data in this paper, 44 centres now have 3 or more geochemical data points.

**Table 2.** Details of all 53 centres in the AVF, their eruption type; the current age estimate and method by which the ages are calculated, the relative age relationships where known including, and the morphological features which give age constraints. Sources are: a. Hayward et al. (2011); b. Allen and Smith (1994); c. Affleck et al. (2001); d. Sandiford et al. (2002); e. Lowe et al. (2013); f. Lindsay et al. (2011); g. Kermode (1992); h. Newnham et al. (2007); i. Agustín-Flores et al. (2015); j. Leonard et al. (2016); k. Hayward et al. (2016); the estimated dense rock equivalent (DRE) volumes for the total, tuff ring and scoria cone from Kereszturi et al. (2013); and the calculated tephra volumes using the equation reported in Kawabata et al. (2015). For the eruption types, (A) phreatomagmatic wet explosive eruption which produces maar craters and tuff rings, (B) dry magmatic eruptions including fire fountaining creating scoria cones, and (C) effusive eruptions resulting in lava flows, and shield building.

**Table 3.** The ages and associated errors calculated for each basaltic horizon using either, Monte Carlo simulations for those younger than the Maketu RMH, and sedimentation rate calculations for those older than the Maketu RMH (*italicised*). References: a. Needham et al. (2011); b. Lowe et al. (2013); c. Molloy (2008); d. D.J. Lowe *pers comm* (2016); and e. Leonard et al. (2016). AVF24 is split into Rangitoto (Ra)1 and 2 identified and dated ( $^{14}\text{C}$  in cal. yr. BP) by Needham et al. (2011), \*indicates nomenclature from Molloy et al. (2009) for the tephra horizons found in the Pupuke core. The ages for the rhyolitic marker horizons (shaded grey) are outlined in cal. yr. BP. The age of AVF17 is shown in grey text as an outlier, and the position of AVF16 also shown in grey text as out of sequence, both of these are discussed in the text. The age of deposit AVFd in the base of the Onepoto core is taken from the minimum  $^{40}\text{Ar}/^{39}\text{Ar}$  age estimation for Pupuke centre, see text for details. All errors are reported as 2 s.d., and the 95% confidence limits are also reported.

**Table 4.** Outline of correlations for individual tephra horizons to their source centre. Average age are calculated by this study (**Table 3**). Proposed centre is given in bold with

certainty value (scale 1-3). Ticks indicate where correlation satisfies the criteria of age (within error of radiometric age), chemistry, scale, and location, '?' indicated where centre ages are unknown. Alternative possible centres are outlined with their certainty value and criteria. See supplementary material for explanation of ambiguities in the table in relation to rating given.

**Table 5.** For those deposits with a correlation certainty of 1 or 2, the distance to the deposition site (core) (km), thickness of the deposit within the core (mm) and the average shard size of the tephra ( $\mu\text{m}$ ) are shown.

**Table 6.** Comparative global values for tephra dispersal, thickness and total dense rock equivalent (DRE) volume (in  $\text{km}^3$ ; from Kereszturi et al. 2013 to allow global comparisons) for monogenetic basaltic volcanoes. \* Cerro Negro is a polygenetic scoria cone, however it has a comparable total volume estimate from the 1995 basaltic eruption, and is therefore deemed applicable for comparison. In bold are examples from this study to allow a direct comparison.

**Table 7.** Relative order of eruptions with calculated mean ages, time and distance relationship between the  $n^{\text{th}}$ ,  $n+1$  and  $n+2$  centre. References include a. tephra horizon ages from this study; b.  $^{14}\text{C}$  from Lindsay et al. 2011; c. Ar-Ar from Leonard et al. 2016 or Cassata et al., 2008 (see **Table 3**); d. morphostratigraphic constraints (references in **Table 3**) and/or paleomagnetic constraints (from Shibuya et al. 1992). Absolute ages evaluated by this study are discussed in detail in the supplementary material. Note that for centres where morphostratigraphy suggests contemporaneous eruptions (e.g., no material between successive volcanic deposits) an arbitrary difference of 500 years is assigned based on a minimum time taken to form soil horizons.

Figure 1

[Click here to download Figure Figure 1.png](#)

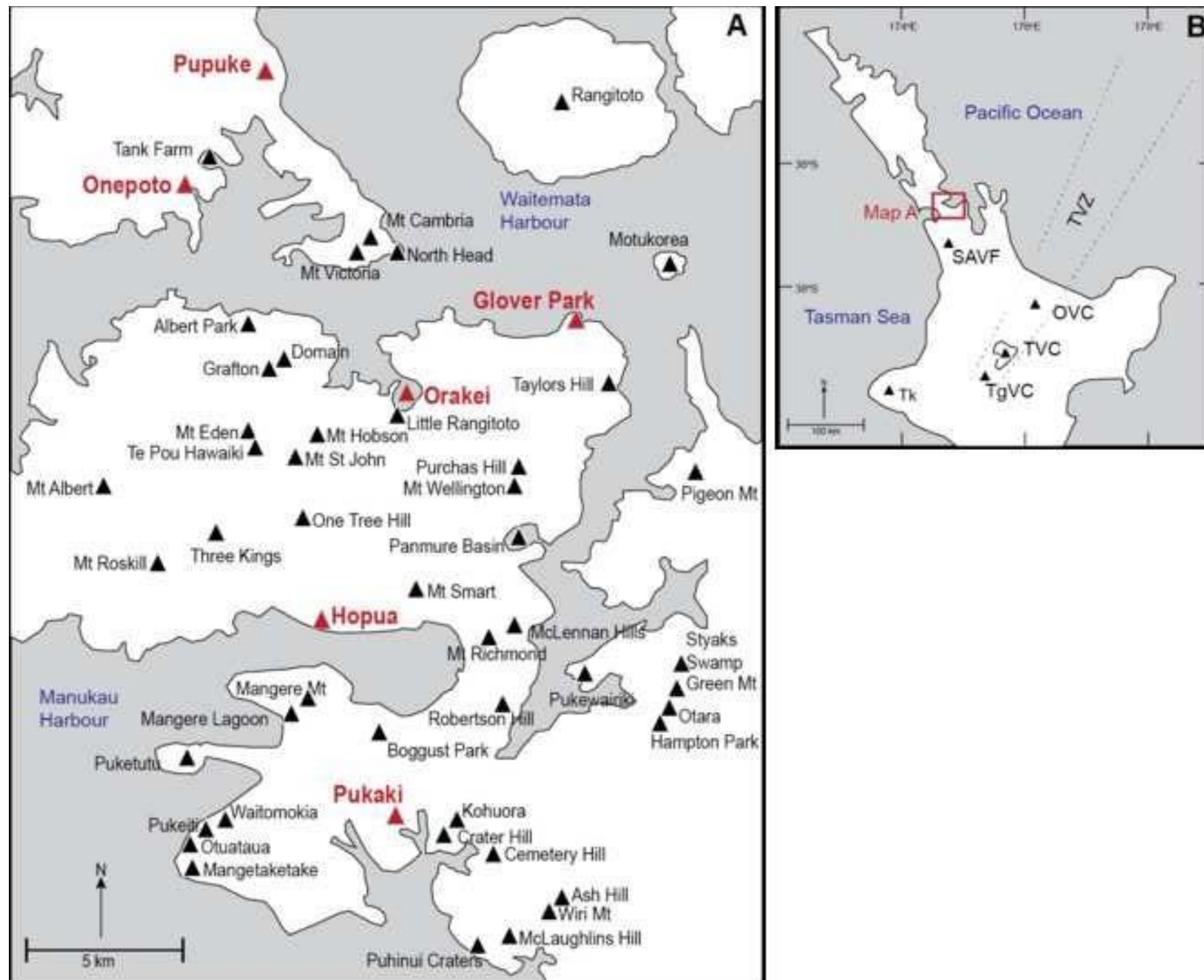


Figure 2

[Click here to download Figure Figure 2.png](#)

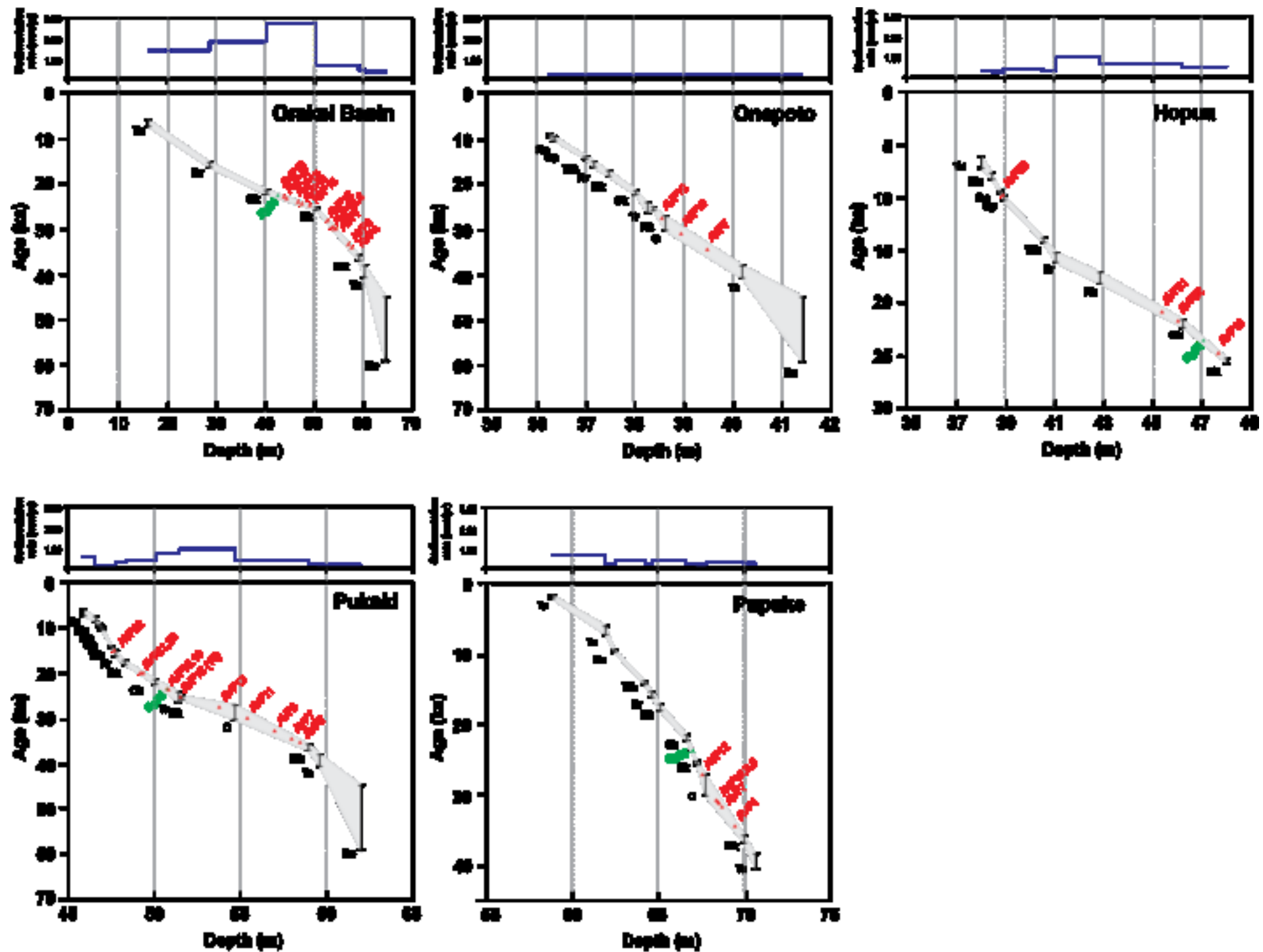




Figure 3

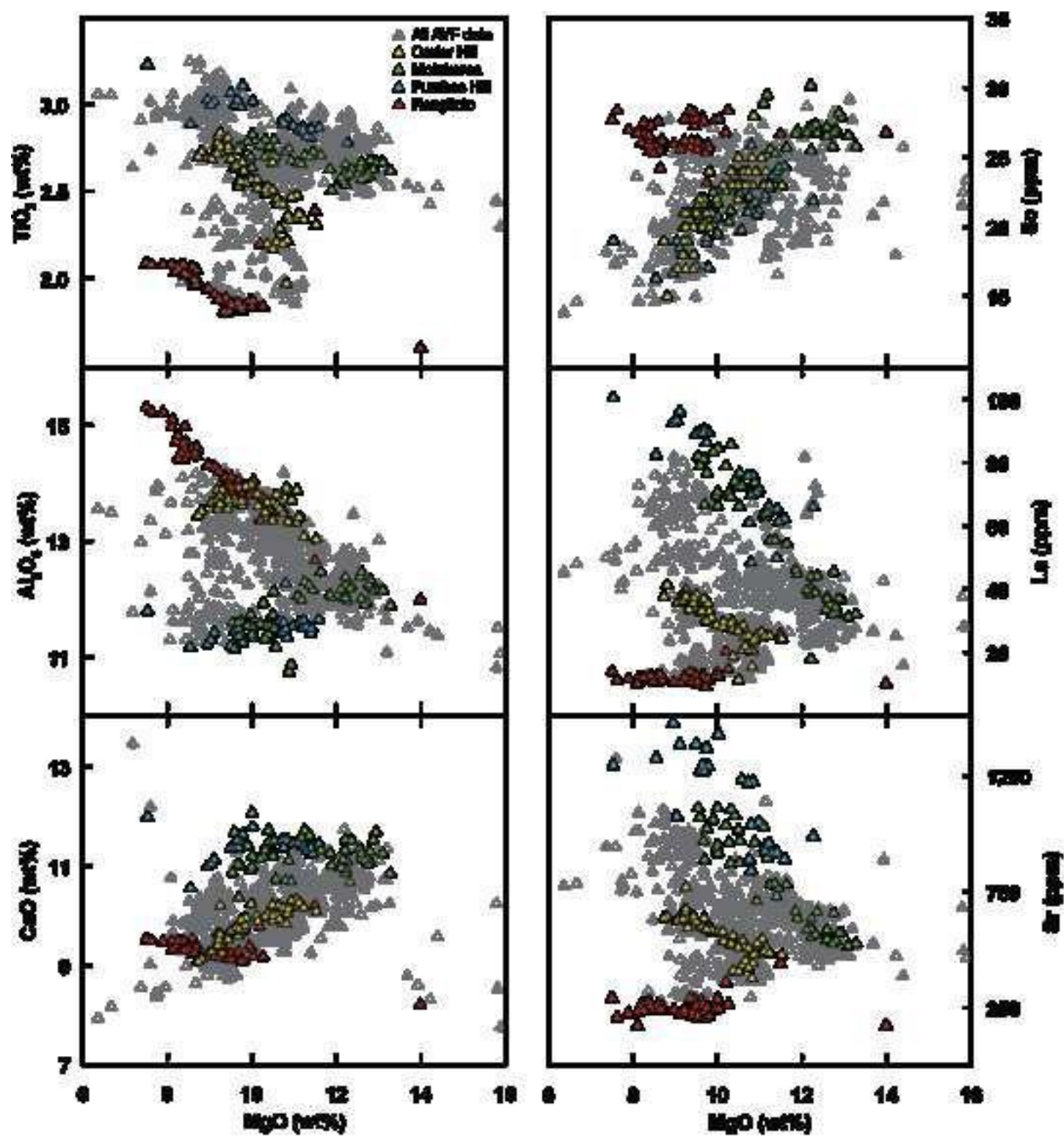
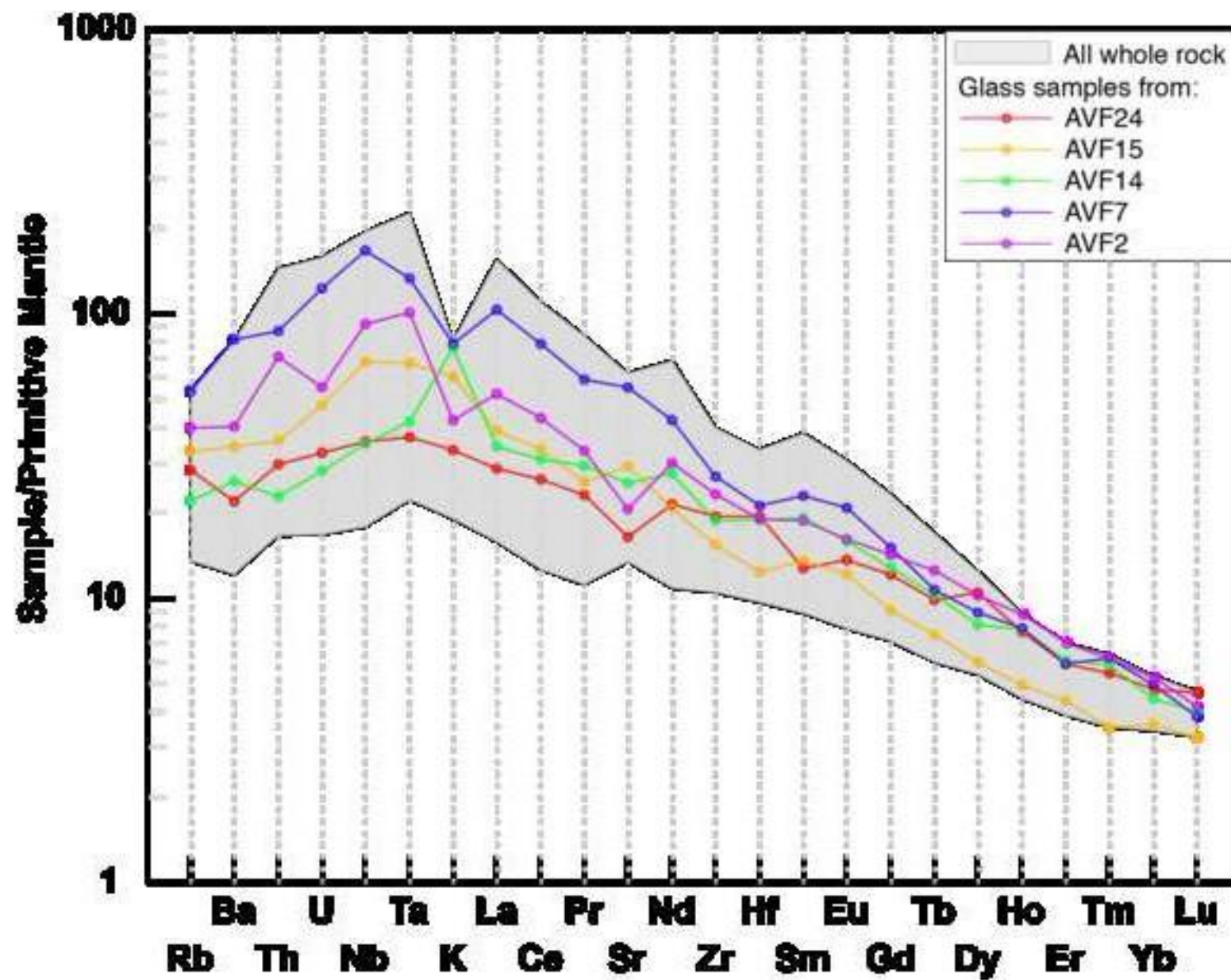
[Click here to download Figure Figure 3.png](#)

Figure 4

[Click here to download Figure Figure 4.png](#)

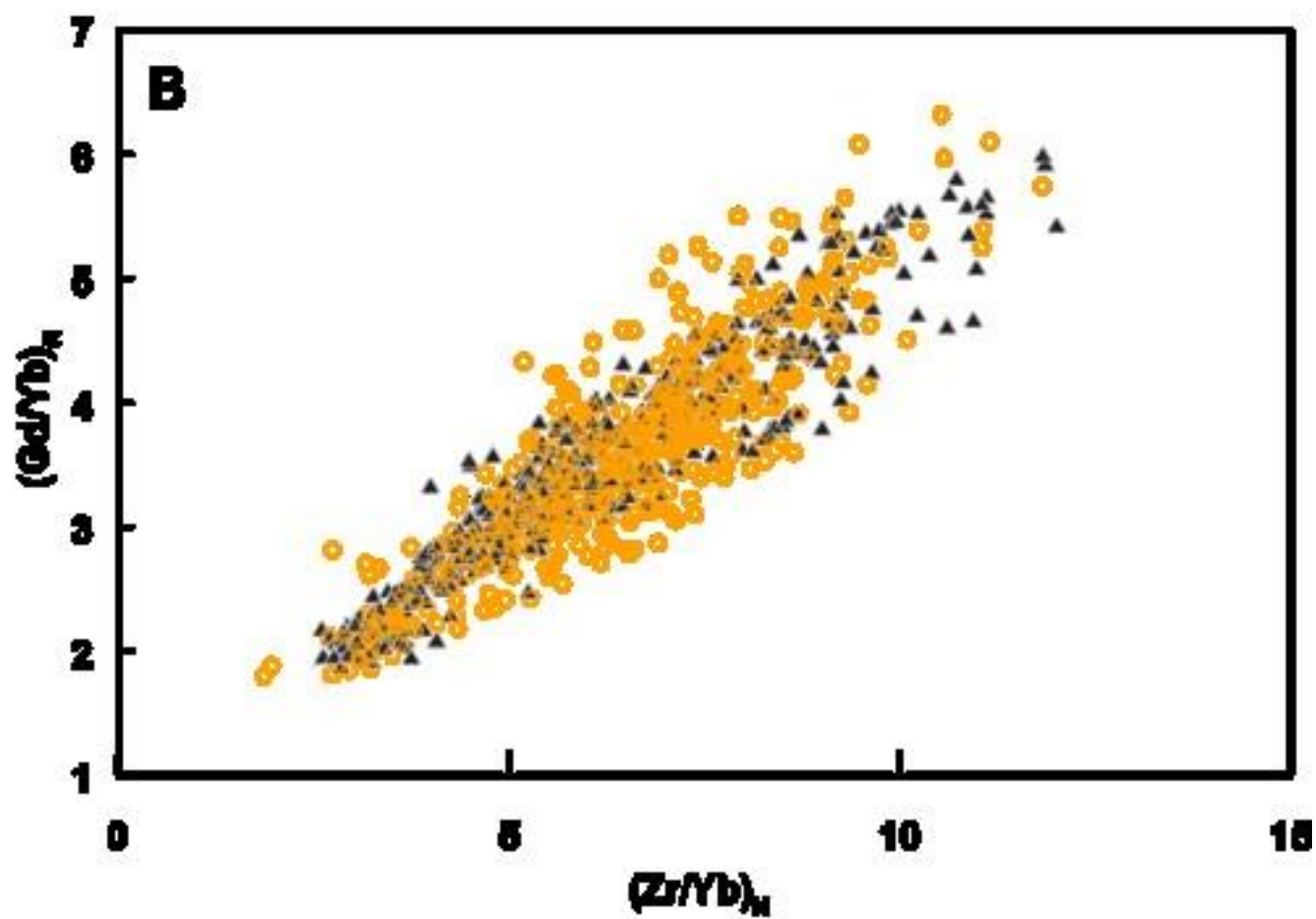
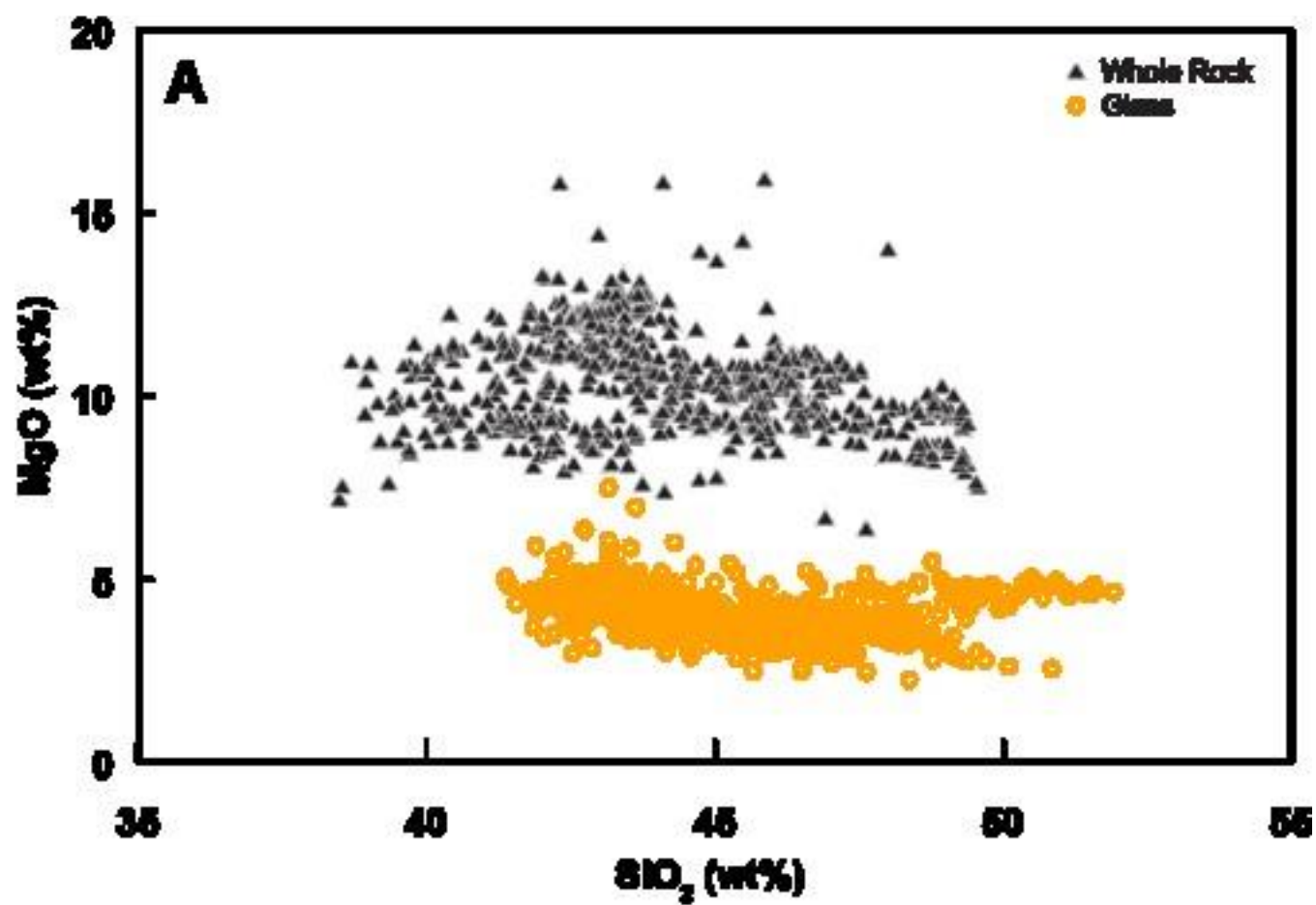


Figure 6

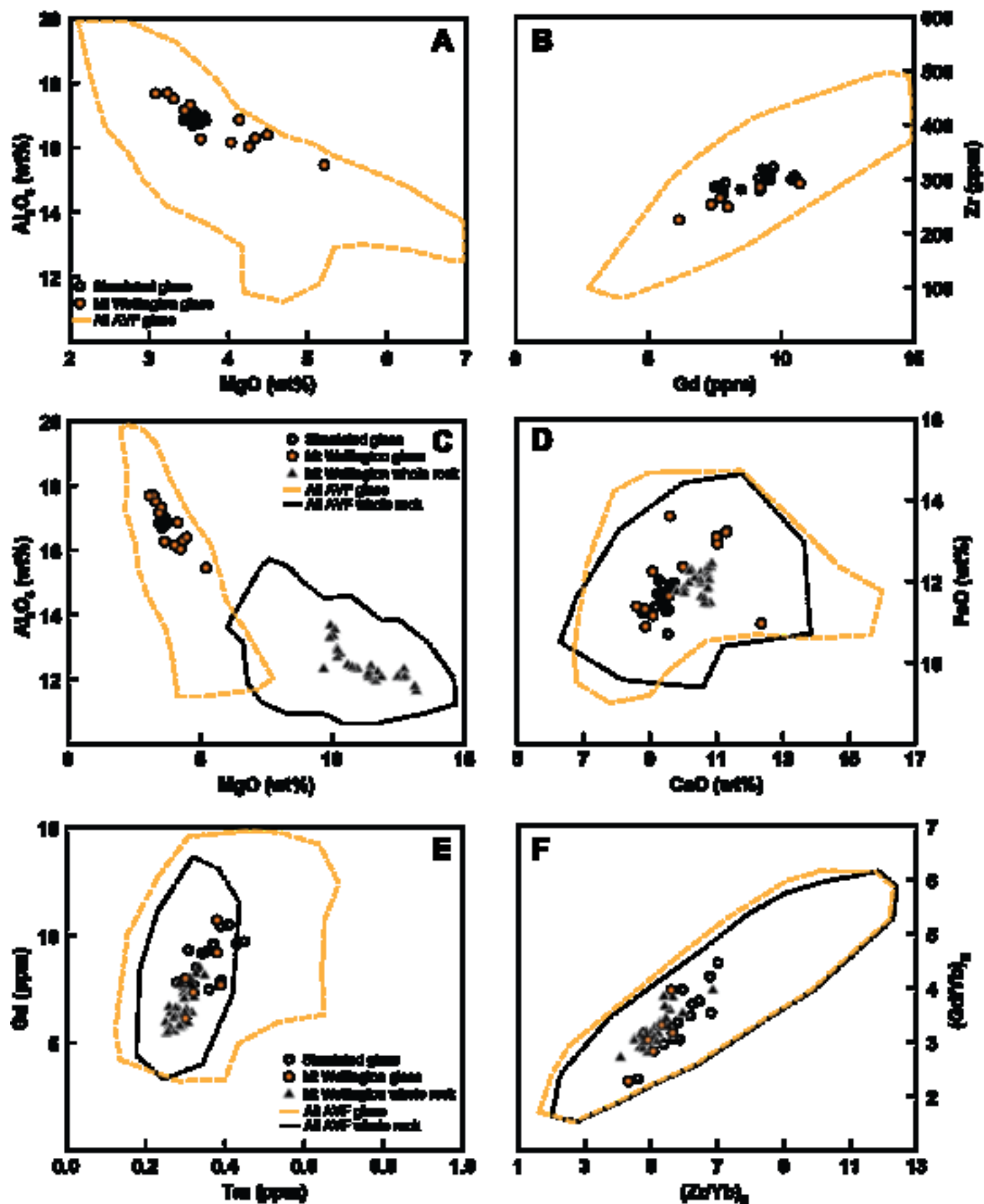
[Click here to download Figure Figure 6.png](#)

Figure 7

[Click here to download Figure Figure 7.png](#)

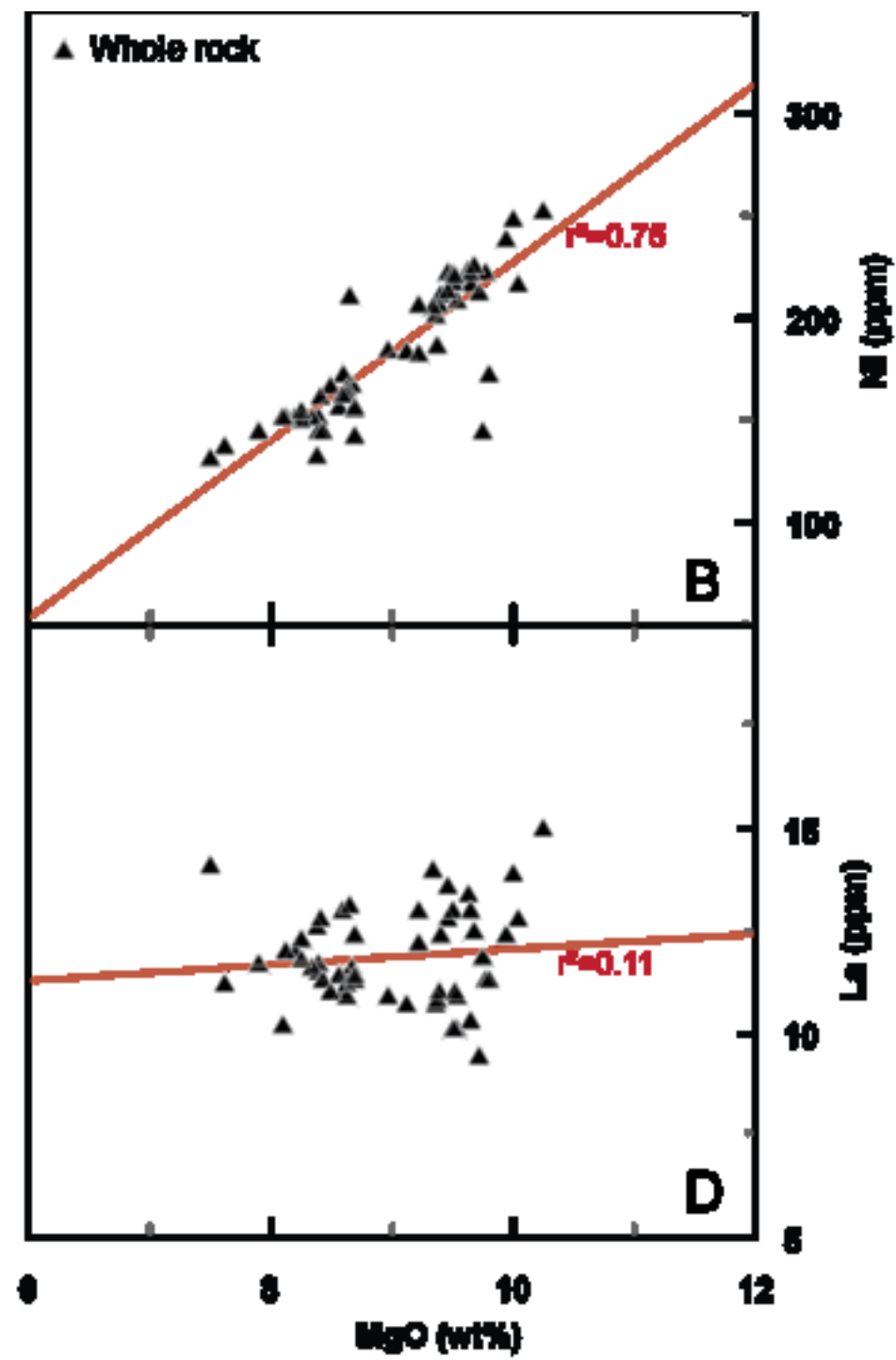
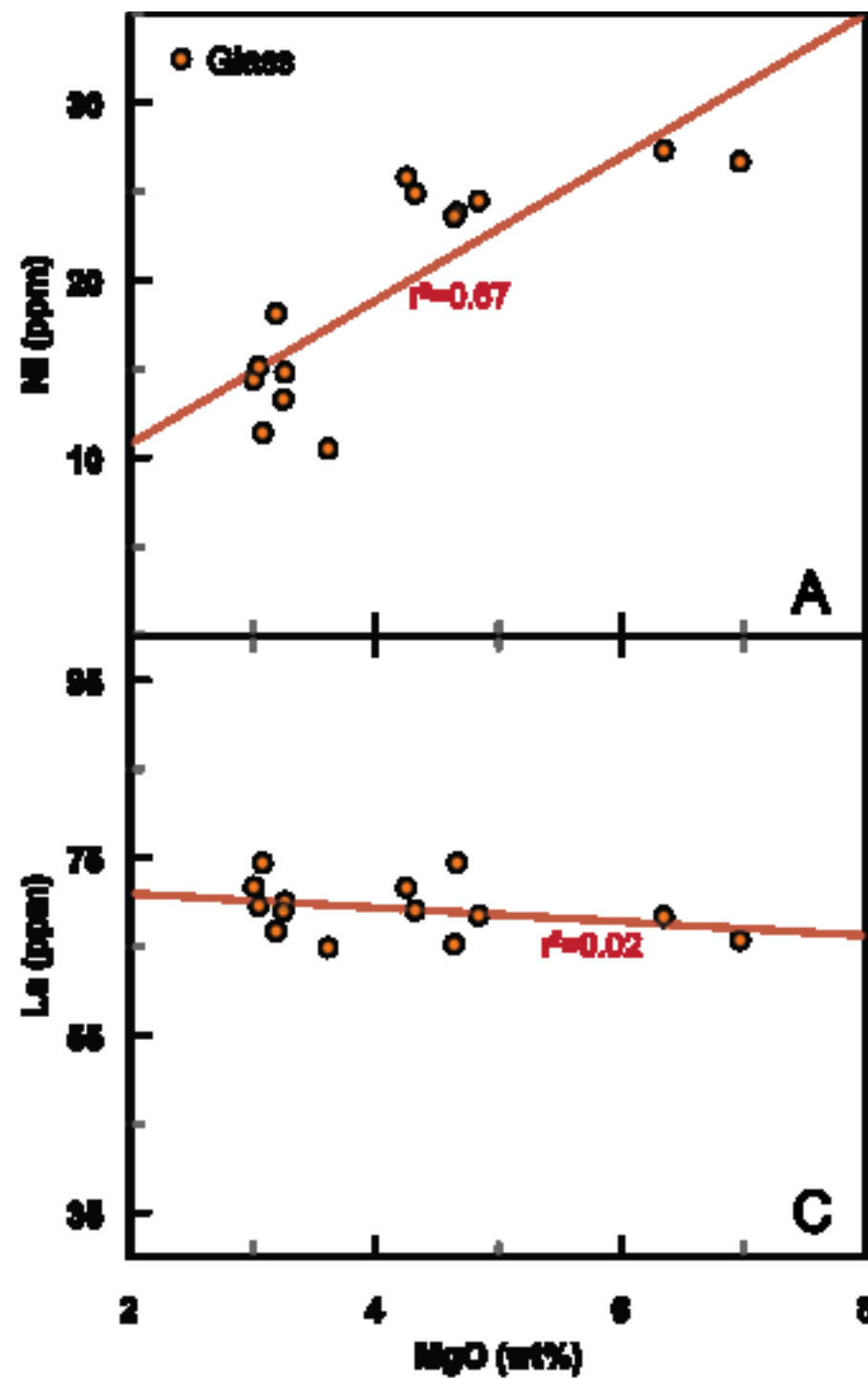


Figure 8

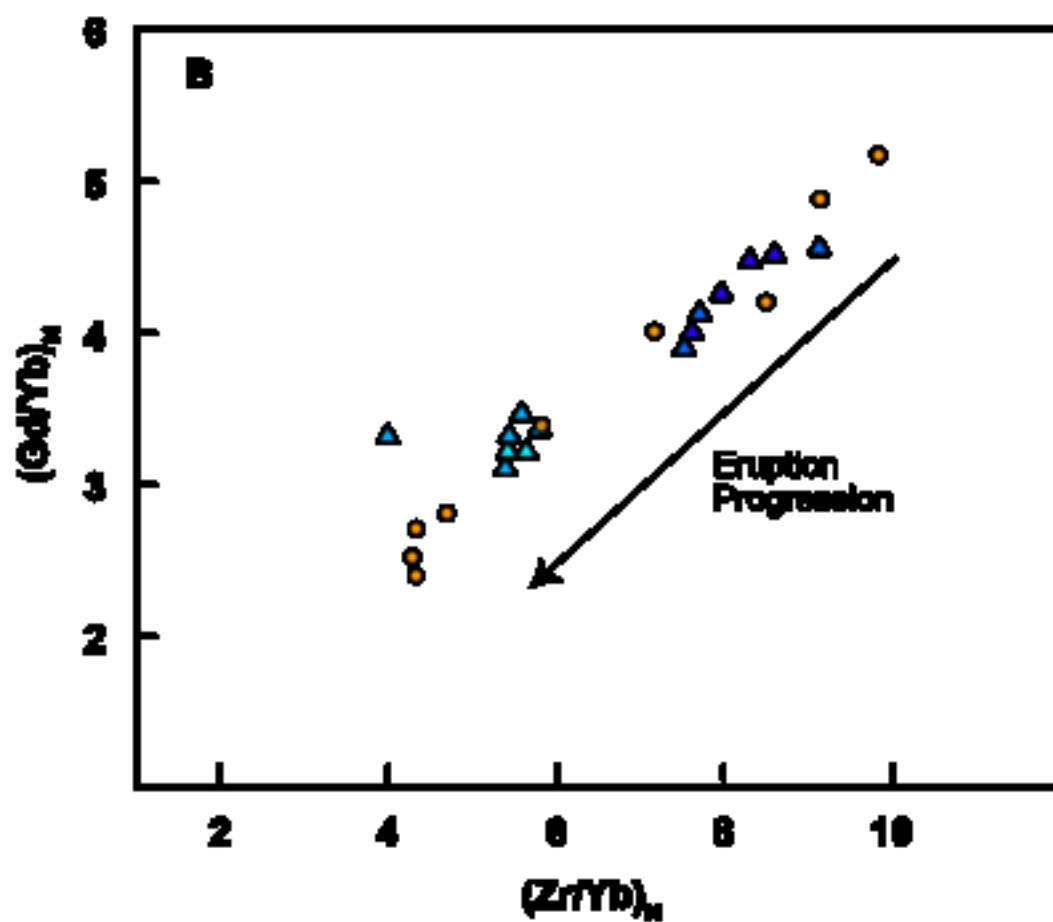
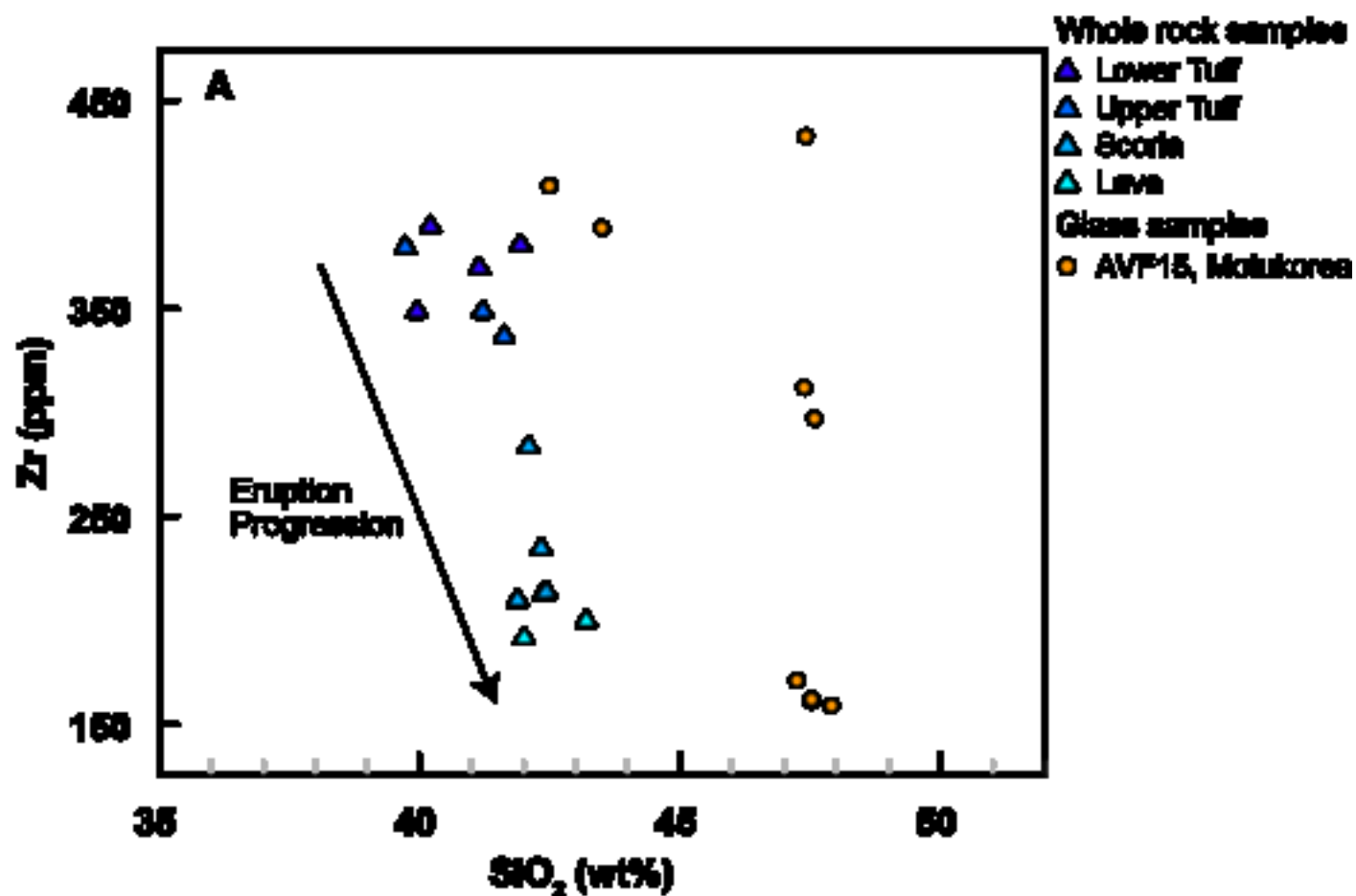
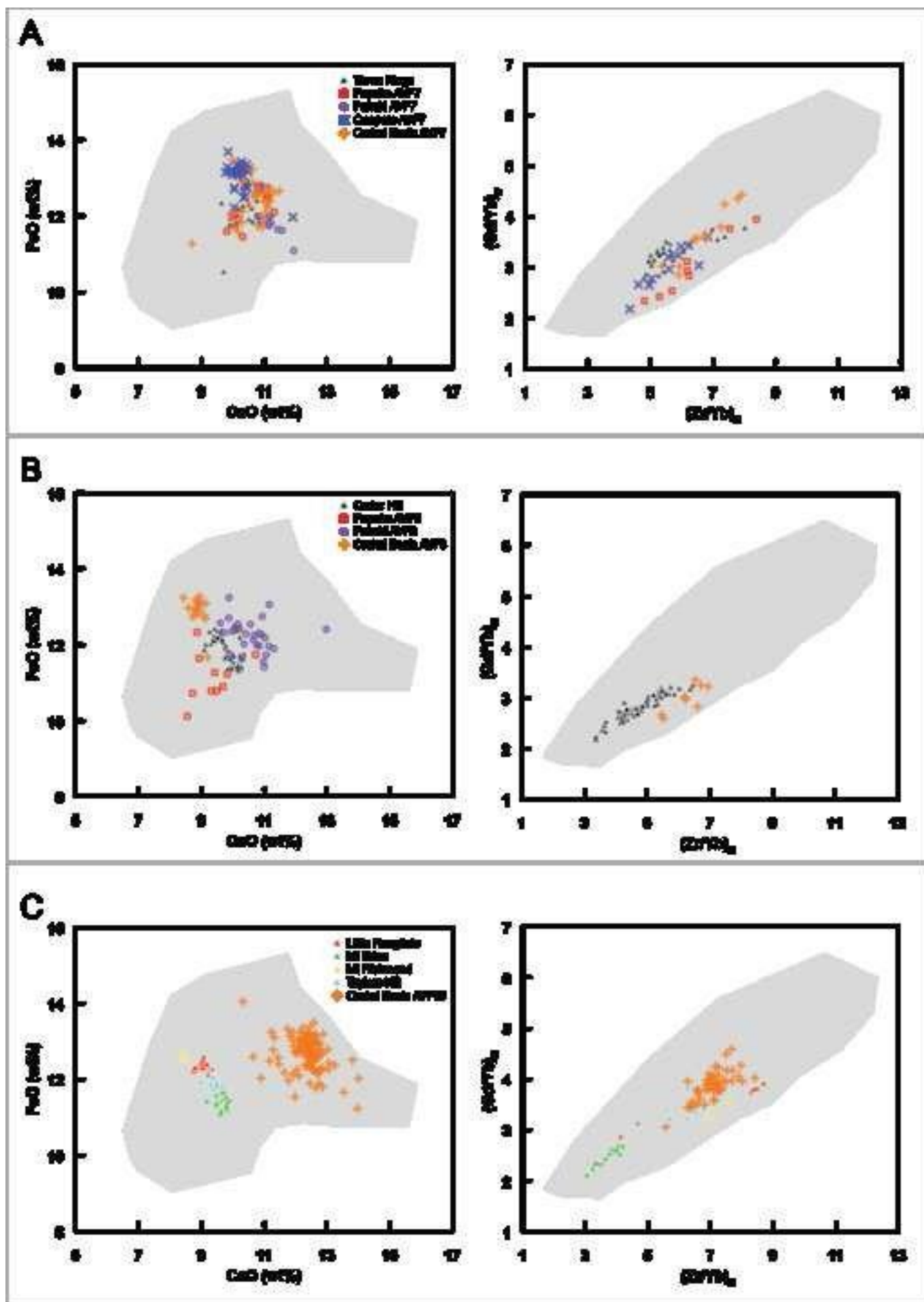
[Click here to download Figure Figure 8.png](#)



Figure 9

[Click here to download Figure Figure 9.png](#)

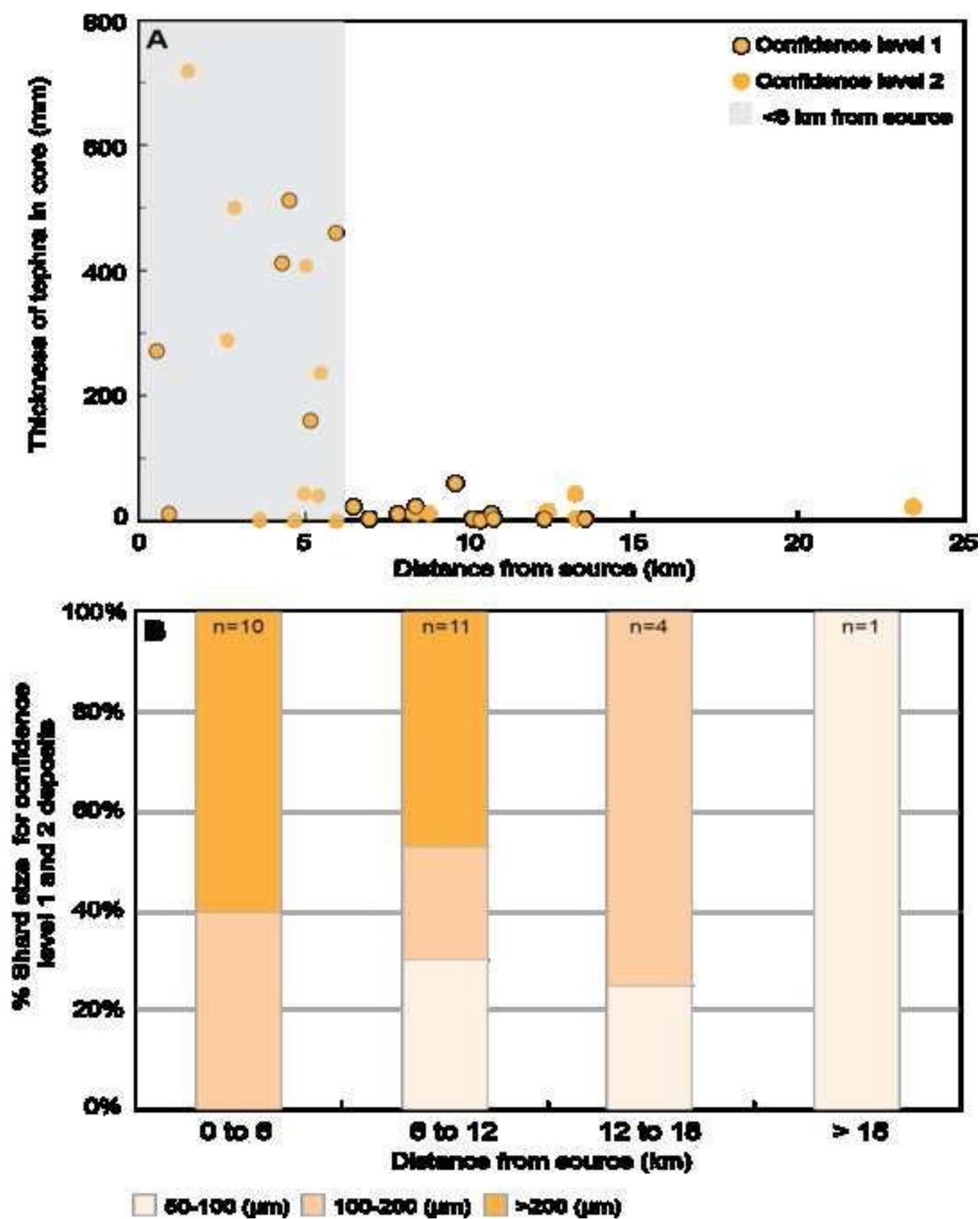




Figure 11

[Click here to download Figure Figure 11.png](#)

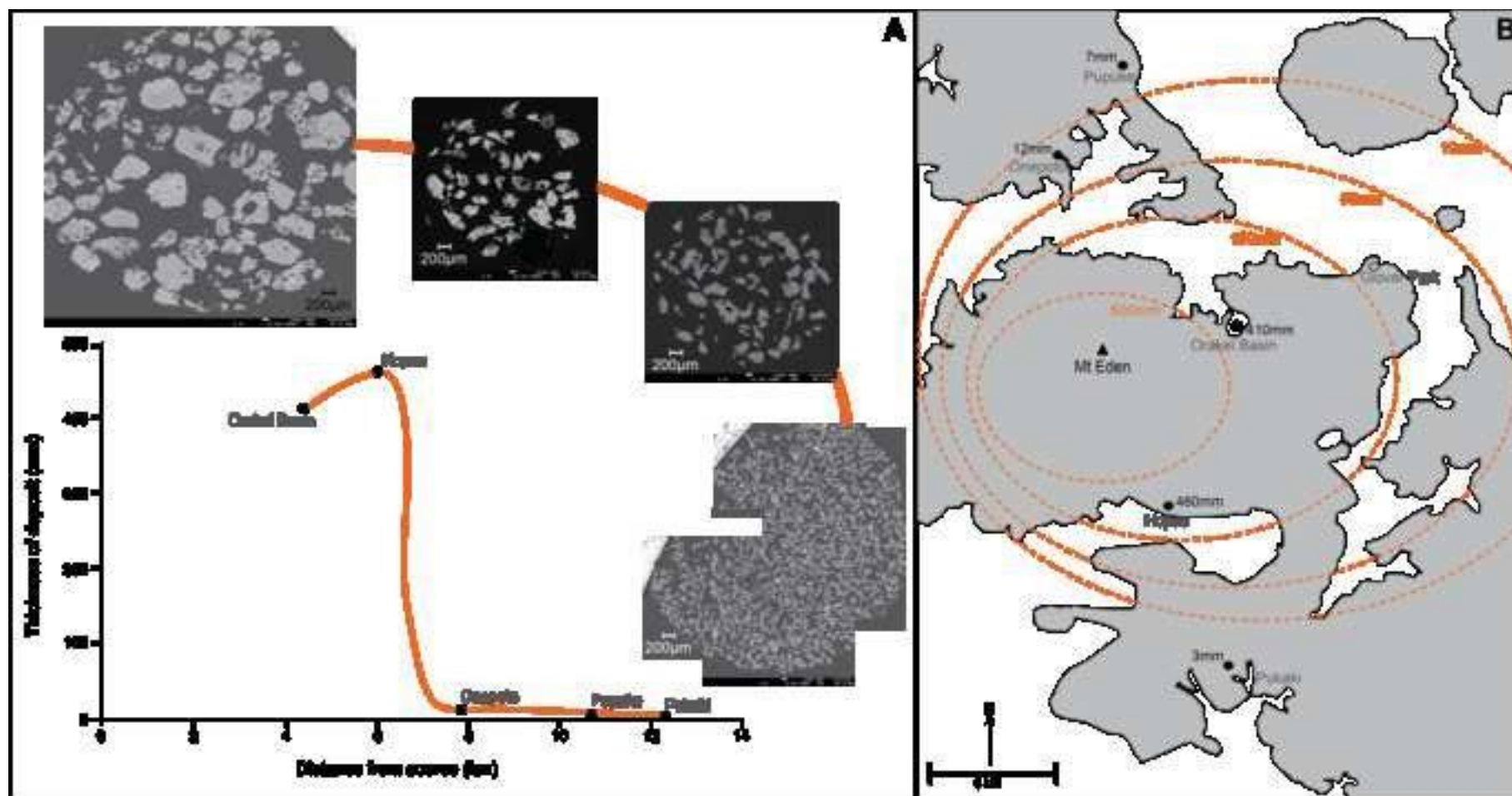
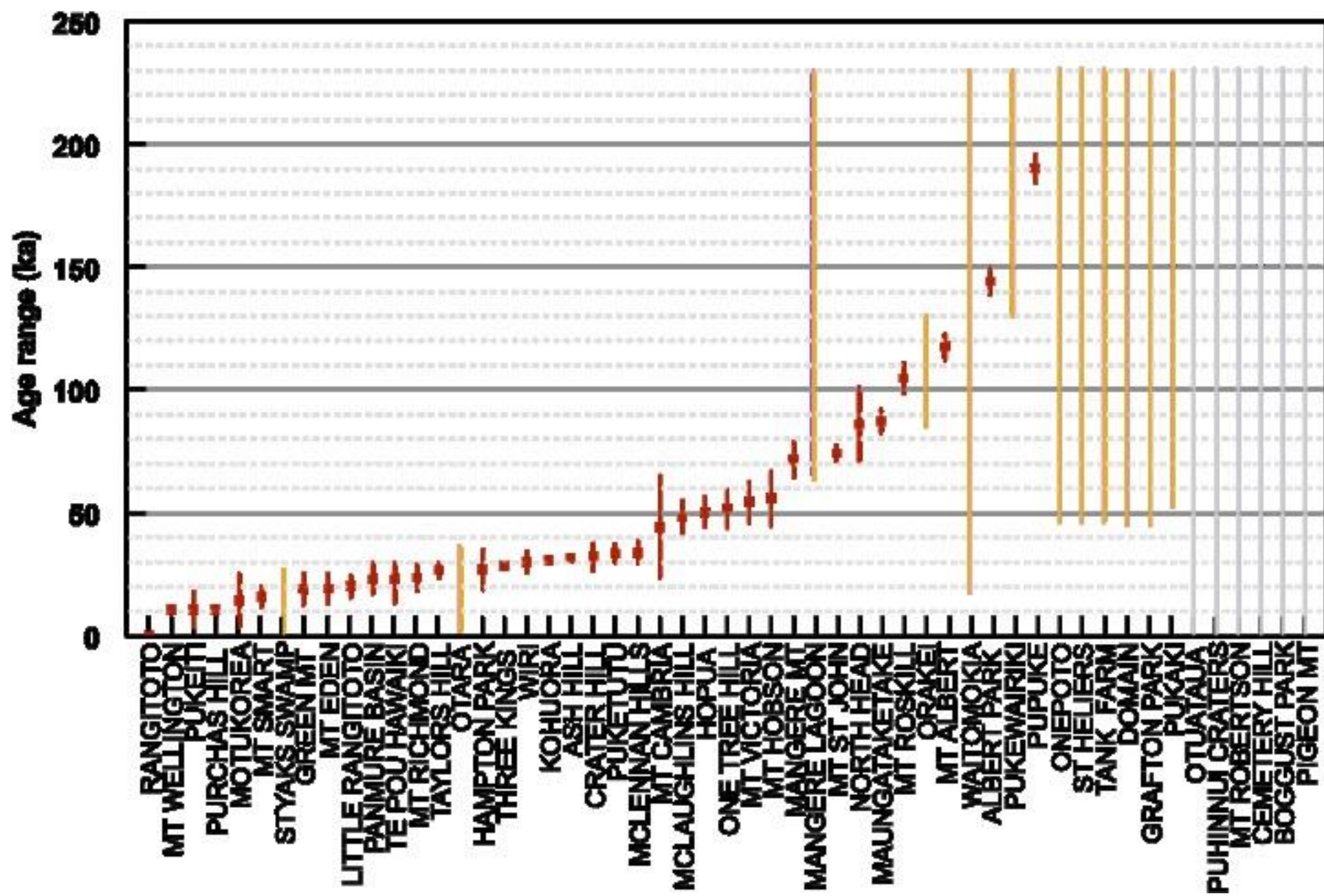
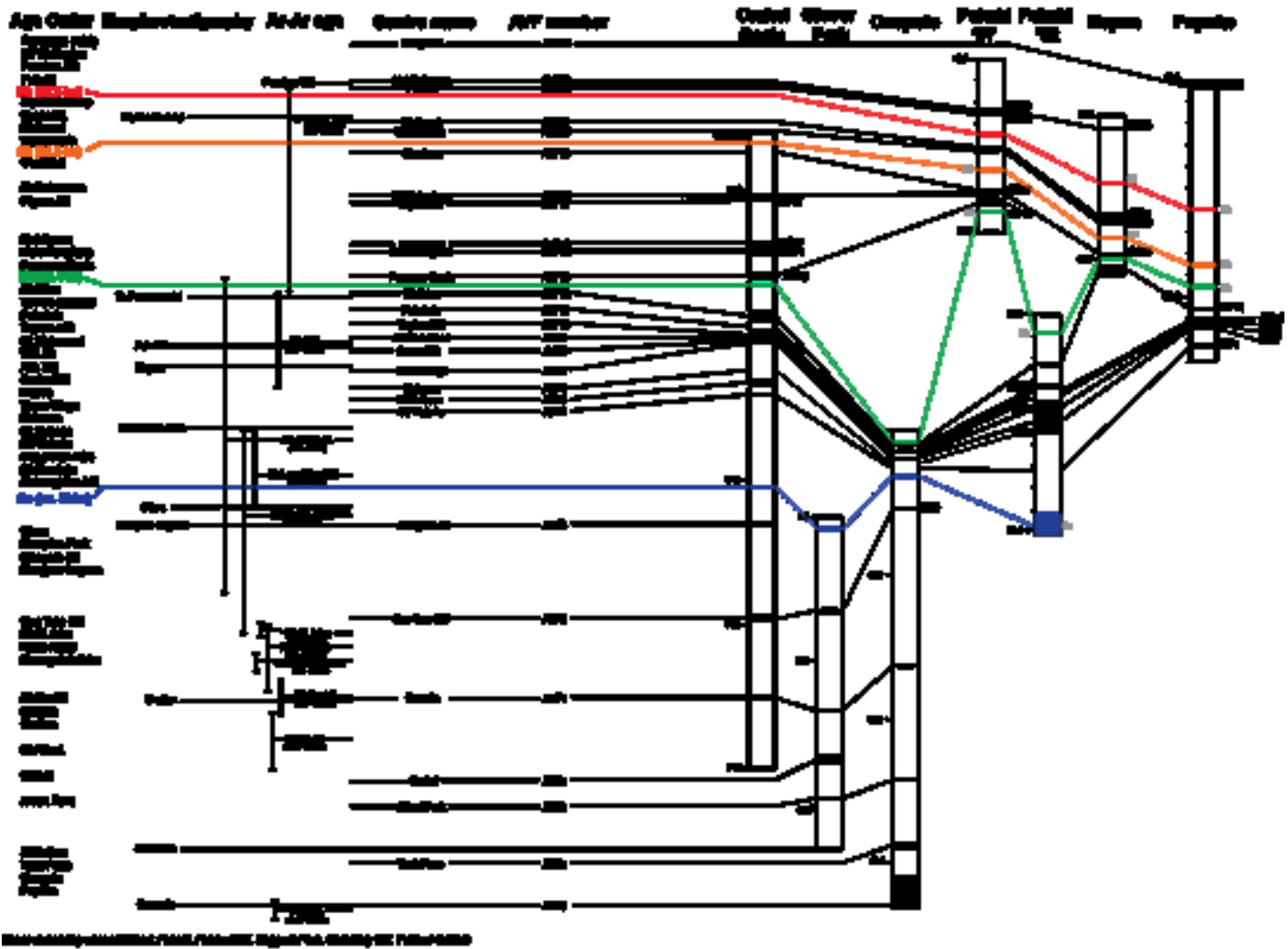
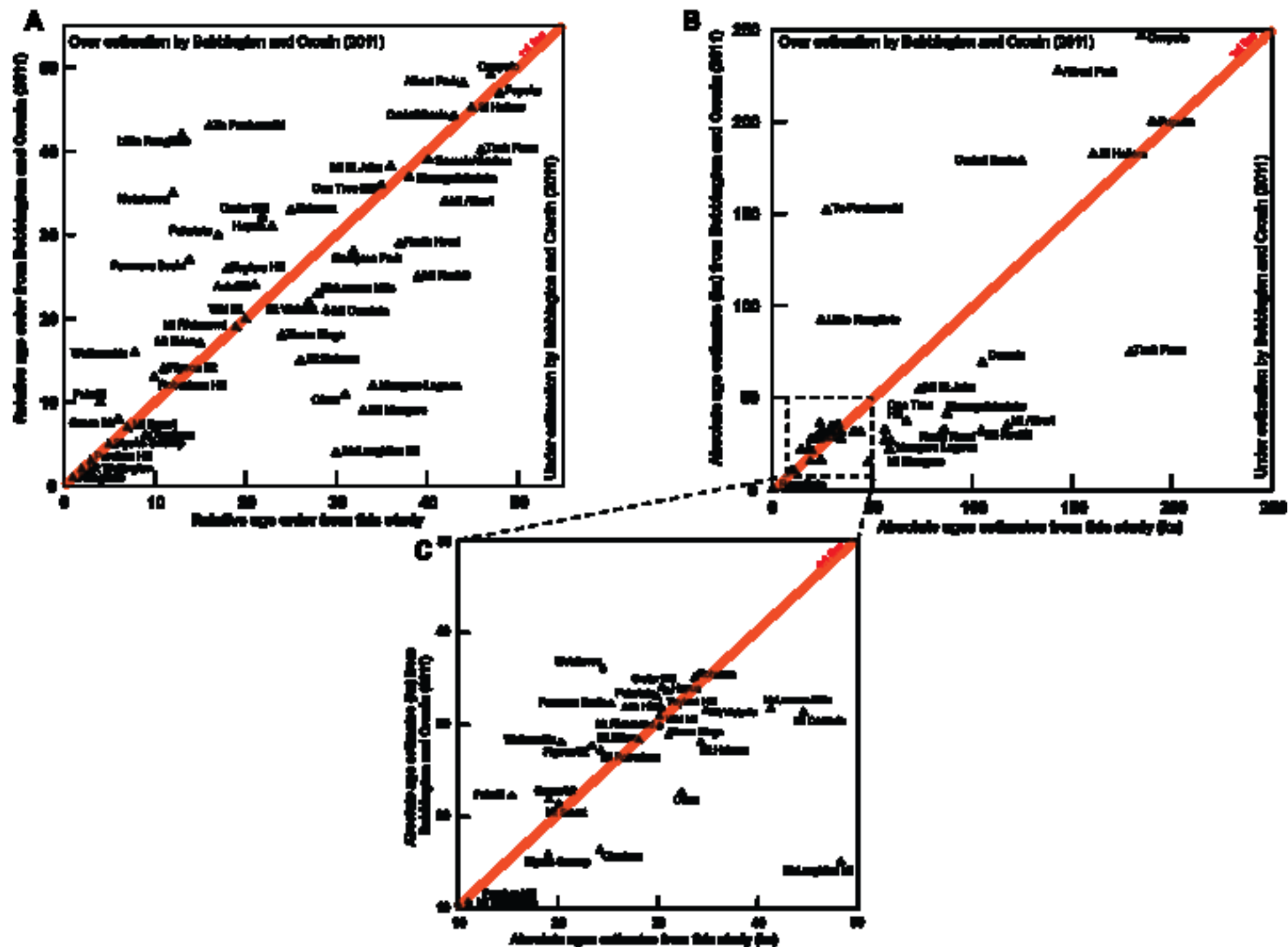


Figure 12







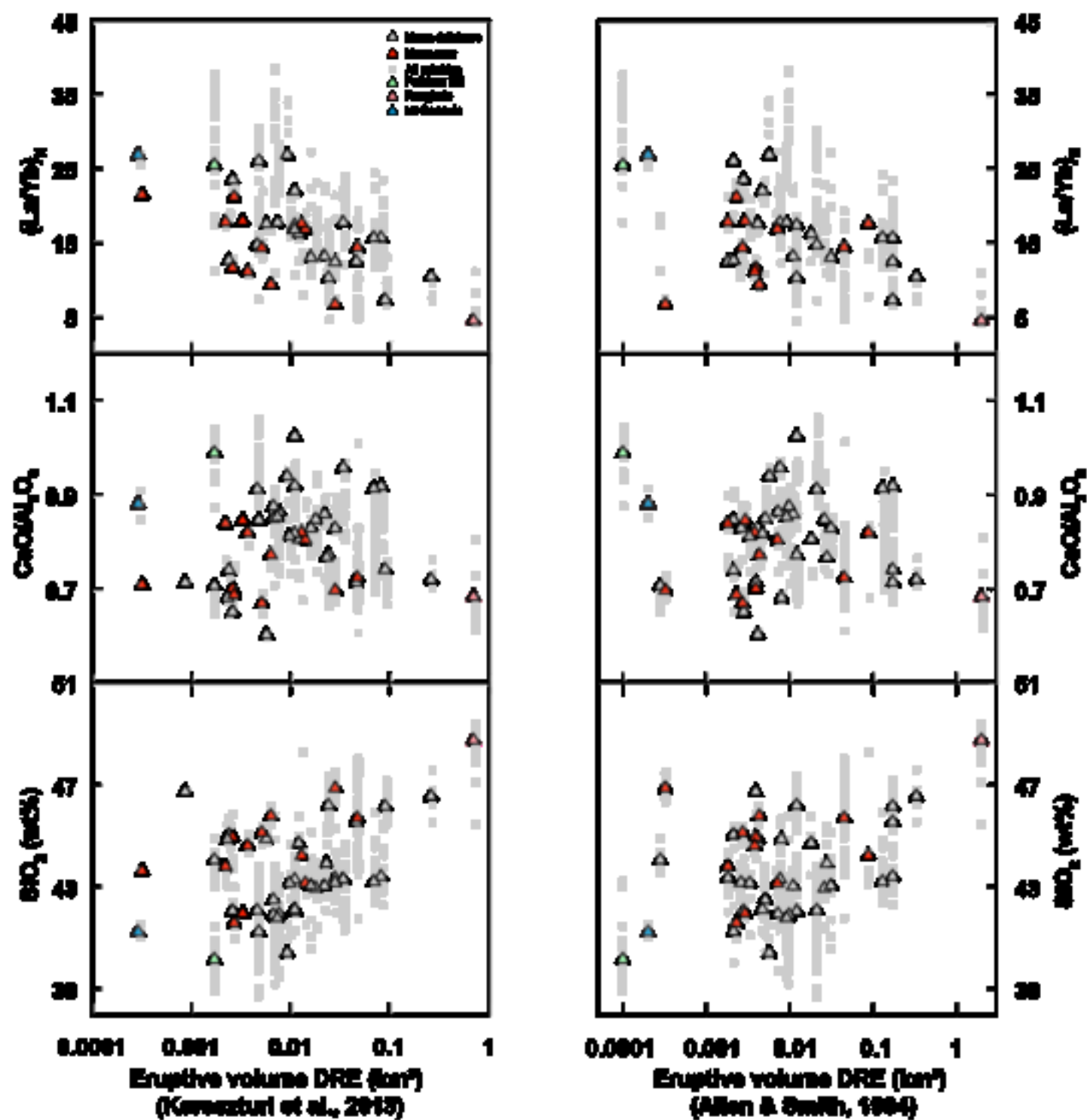


Table 1

Centre	Current whole rock data		References
	Major	Trace	
ALBERT PARK	4	4	McGee, 2012; Smith unpub data
ASH HILL	0	0	
BOGGUST PARK	0	0	
CEMETERY HILL	0	0	
CRATER HILL	61	61	Smith et al. 2008
DOMAIN	19	7	Smith unpub data
GRAFTON PARK	10	10	DEVORA group unpub data
GREEN HILL	3	1	Miller, 1996
HAMPTON PARK	4	0	Miller, 1996
HOPUA	1	1	Smith unpub data
KOHUORA	0	0	
LITTLE RANGITOTO	17	1	Franklin, 1999; Smith unpub data
MANGERE LAGOON	0	0	
MANGERE MT	7	2	Miller, 1996
MAUNGATAKETAKE	23	23	Smith unpub data
MCLAUGHLINS HILL	1	0	Heming and Barnet, 1986
MCLENNAN HILLS	6	3	Miller, 1996
MOTUKOREA	53	53	Bryner, 1991; McGee, 2012, McGee et al. 2012
MT ALBERT	2	4	Smith unpub data
MT CAMBRIA	1	1	Smith unpub data
MT EDEN	29	17	Eade, 2009; McGee, 2012
MT HOBSON	10	2	Smith unpub data
MT RICHMOND	6	3	Eade, 2009; McGee, 2012; Smith unpub data
MT ROSKILL	3	2	McGee, 2012
MT SMART	2	2	McGee, 2012; Smith unpub data
MT ST JOHN	22	13	Franklin, 1999; Eade, 2009
MT VICTORIA	4	2	Smith unpub data
MT WELLINGTON	34	34	McGee, 2012, McGee et al. 2013
NORTH HEAD	6	5	Smith unpub data
ONE TREE HILL	8	4	Eade, 2009; Smith unpub data
ONEPOTO	0	0	
ORAKEI	41	21	Franklin, 1999; Smith unpub data
OTARA	12	0	Miller, 1996; McGee, 2012
OTUATAUA	1	1	Heming unpub data
PANMURE BASIN	22	21	Smith unpub data
PIGEON MT	1	1	Smith unpub data
PUHINUI CRATERS	0	0	
PUKAKI	2	2	Zawalna-Geer, 2012
PUKEITI	1	1	Smith unpub data
PUKEKIWIIRIKI	4	3	Smith unpub data
PUKETUTU	23	13	Miller, 1996; McGee, 2012
PUPUKE	51	51	Spargo, 2007

PURCHAS HILL	27	27	McGee 2012; McGee et al. 2013
RANGITOTO	55	55	Hookway, 2000; Needham et al. 2011
ROBERTSON HILL	0	0	
ST HELIERS	1	1	Smith unpub data
STYAKS SWAMP	0	0	
TANK FARM	0	0	
TAYLOR'S HILL	3	3	McGee, 2012; Smith unpub data
TE POU HAWAIKI	13	0	Franklin, 1999
THREE KINGS	36	35	Eade, 2009; Smith unpub data
WAITOMOKIA	9	9	McGee, 2012
WIRI	12	12	McGee, 2012; McGee et al. 2013
<b>TOTALS</b>	<b>650</b>	<b>511</b>	

This study whole rock data	
Major	Trace

Surface exposure currently non-existent

3	3
new centre	

2  
4

Surface exposure currently non-existent

Surface exposure currently non-existent

6	6
	3
5	5
	3
1	1
5	5
5	5
6	6
6	6
	1
	2
2	2
	5
5	5
5	5
new centre	
4	4
4	4
	2
1	1



2	2
4	4
2	2
Surface exposure currently non-existent	
Surface exposure currently non-existent	
6	6
5	5
<hr/>	
<b>77</b>	<b>99</b>
<hr/>	

Table 2

Table\*. Over view of current volcanoes identified in the Auckland Volcanic Field, their age, relative age and Dense Rock Equivalent (DRE) values and geochemical analyses.

Centre name	Eruption types <sup>a</sup>	Age estimate (ka)			Method	Method reference	Relative ages and relationships based on morphology	DRE volumes x10 <sup>6</sup> m <sup>3</sup>			
		min 2sd	mean	max 2sd				Total	Tuff	Scoria Cone	Tephra
ALBERT PARK	A,B,C	141.3	146.9	152.5	Ar-Ar	Leonard et al. 2017		27.8	0.82	0.01	0.43
ASH HILL	A	31.4	31.8	32.2	14C	Hayward, 2008	older than Wiri Mt <sup>b</sup>	0.076	0.05	0.00	0.03
BOGGUST PARK	A? (new)							0.32	0.18	0.00	0.09
CEMETERY HILL	(new)							0.24	0.14	0.00	0.07
CRATER HILL	A,B,C	26.7	32.1	37.5	Ar-Ar	Cassata et al. 2008	Mono Lake' p.mag excursion <sup>l</sup> , younger than Kohuora <sup>a</sup>	24.5	5.88	0.76	4.09
DOMAIN	A,B	52.0			Rotoehu Tephra in drill core		younger than Grafton Park <sup>b</sup> one of the older centres in the	11.4	4.06	0.06	2.11
GRAFTON PARK	A,B	52.0			morphostratigraphy		AVF <sup>g</sup> older than Domain <sup>b</sup> one of the older centres in the AVF <sup>g</sup>	11.4	4.06	0.06	2.11
GREEN MT	A,B,C	13.0	19.6	26.2	Ar-Ar	Leonard et al. 2017	older than Styaks Swamp <sup>a</sup>	12.2	0.36	1.50	2.43
HAMPTON PARK	A,B,C	37.0	55.0	73.0	Ar-Ar	Cassata et al. 2008	unusual p.mag orientation <sup>l</sup> , just older than Otara <sup>a</sup>	2.41	0.11	0.40	0.65
HOPUA	A	45.2	51.6	58.0	Ar-Ar	Leonard et al. 2017	younger than One Tree Hill <sup>a</sup>	0.86	0.31	0.00	0.15
KOHUORA	A	32.0	33.0	34.0	14C	Lindsay et al. 2011	older than Crater Hill <sup>a</sup> , contains Kawakawa/Oruanui tephra (>25.4 ka) <sup>h</sup>	7.24	5.10	0.00	2.55
LITTLE RANGITOTO	B,C	16.3	20.7	25.1	Ar-Ar	Leonard et al. 2017	younger than Orakei <sup>a</sup>	1.71	0.00	0.50	0.75
MANGERE LAGOON	A,B	63.1			morphostratigraphy		just older than Mangere Mt <sup>k</sup>	2.04	0.71	0.01	0.37
MANGERE MT	B,C	63.1	70.3	77.5	Ar-Ar	Leonard et al. 2017	just younger than Mangere Lagoon <sup>k</sup> , younger than One Tree Hill <sup>a</sup>	46.2	0.00	15.01	22.51
MAUNGATAKETAKE	A,B,C	84.1	88.9	93.7	Ar-Ar	Leonard et al. 2017	sea cut platform from last interglacial <sup>a</sup>	33.6	4.40	0.87	3.51
MCLAUGHLINS HILL	A,B,C	41.8	48.2	54.6	Ar-Ar	Leonard et al. 2017	older than Wiri Mt <sup>a,b</sup>	7.58	0.51	0.43	0.90
MCLENNAN HILLS	A,B,C	29.9	34.7	39.5	Ar-Ar	Leonard et al. 2017	Laschamp p.mag excursion <sup>l</sup> , older than Mt Richmond <sup>a</sup>	21.9	0.42	3.79	5.90
MOTUKOREA	A,B,C	2.3	14.3	26.3	Ar-Ar	Leonard et al. 2017		4.56	0.66	1.31	2.30
MT ALBERT	A,B,C	113.6	119.2	124.8	Ar-Ar	Leonard et al. 2017	older than Mt Eden and Mt Roskill <sup>a</sup>	22.9	0.35	3.03	4.72
MT CAMBRIA	B,C	20.1	42.3	64.5	Ar-Ar	Leonard et al. 2017		0.29	0.00	0.29	0.44
MT EDEN	B,C	14.6	21.2	27.8	Ar-Ar	Leonard et al. 2017	much younger than Mt St John, younger than Three Kings, Mt Hobson <sup>a</sup> , One Tree Hill and Domain <sup>g</sup>	89.8	0.00	5.94	8.92
MT HOBSON	B,C	45.3	56.9	68.5	Ar-Ar	Leonard et al. 2017	older than Three Kings <sup>a</sup>	6.68	0.00	1.20	1.80
MT RICHMOND	A,B	24.7	34.3	43.9	Ar-Ar	Leonard et al. 2017	Mono Lake' p.mag excursion <sup>j</sup> , younger than McLennan Hills <sup>a</sup> , older than Okaia tephra (28.6 ka) <sup>d</sup>	5.67	1.17	3.04	5.14
MT ROBERTSON	A,B							2.72	1.01	0.24	0.87
MT ROSKILL	A,B,C	99.1	105.3	111.5	Ar-Ar	Leonard et al. 2017	post-Blake p.mag excursion <sup>l</sup> , younger than Mt Albert <sup>a</sup>	14.4	0.02	1.37	2.07
MT SMART	A,B,C	12.8	16.4	20.0	Ar-Ar	Leonard et al. 2017	younger than One Tree Hill <sup>a</sup>	13.4	0.00	2.34	3.52
MT ST JOHN	B,C	71.9	75.3	78.7	Ar-Ar	Leonard et al. 2017	much older than Mt Eden and Three Kings <sup>a</sup>	28.1	0.00	0.40	0.60
MT VICTORIA	B,C	42.8	57.6	72.4	Ar-Ar	Leonard et al. 2017		4.81	0.00	2.58	3.87
MT WELLINGTON	B,C	9.3	10.3	11.3	14C	Lindsay et al. 2011	just younger than Purchas Hill <sup>a</sup>	82.3	1.93	3.02	5.49
NORTH HEAD	A,B	72.3	87.5	102.7	Ar-Ar	Leonard et al. 2017	raised sea levels ca. 128-116 ka <sup>l</sup>	2.65	1.12	0.04	0.61
ONE TREE HILL	B,C	45.2	52.8	60.4	Ar-Ar	Leonard et al. 2017	older than Hopua, Mt Hobson, Mt Eden, Mt Smart, Three Kings, One Tree Hill <sup>a</sup>	260	0.00	5.70	8.56
ONEPOTO	A	52.0			Rotoehu Tephra in drill core		similar age to Pupuke and Tank Farm <sup>a</sup>	2.62	1.54	0.00	0.77
ORAKEI	A	85.0		130.0	sed. rate ages of tephra horizons	Molloy et al. 2009	not breached in last interglacial, older than Little Rangitoto <sup>a</sup>	6.70	3.77	0.00	1.89
OTARA	A,B,C	0.0		73.0	morphostratigraphy		unusual p.mag orientation, just younger than Hampton Park <sup>a</sup>	2.30	0.11	0.70	1.10
OTUATAUA	A,B,C							6.30	0.00	0.99	1.49
PANMURE BASIN	A,B	17.5			Rerewhakaaitu tephra in drill core		older than Rerewhakaaitu (17 ka <sup>e</sup> )	7.44	4.65	0.30	2.77
PIGEON MT	A,B,C							3.31	1.33	0.28	1.08
PUHINUI CRATERS	A? (new)							-	-	-	-
PUKAKI	A	52.0			Core extent			9.19	7.10	0.00	3.55
PUKEITI	B,C	4.2	11.4	18.6	Ar-Ar	Leonard et al. 2017	younger than Otuaataua <sup>a</sup>	3.70	0.00	0.44	0.66
PUKETUTU	B,C	29.8	33.6	37.4	Ar-Ar	Cassata et al. 2008	paleomag excursion (32.4±0.3ka)	11.0	3.00	2.15	4.72
PUKEWAIRIKI	A,C	130.0			morphostratigraphy		sea cut platform from last interglacial <sup>a</sup>	17.5	2.29	0.00	1.15
PUPUKE	C,B,A	187.6	193.2	198.8	Ar-Ar	Leonard et al. 2017	similar age to Tank Farm and Onepoto <sup>a</sup>	46.7	20.11	0.00	10.06
PURCHAS HILL	A,B	10.7	10.9	11.1	14C	Lindsay et al. 2011	just older than Mt Wellington <sup>a</sup>	1.68	0.21	0.03	0.14
RANGITOTO 2	A,B,C	0.494	0.504	0.514	14C	Needham et al. 2011	youngest in the field <sup>a</sup>	699	4.65	41.60	64.73
RANGITOTO 1	A,B,C	0.539	0.553	0.567	14C; Needham et al. 2	Needham et al. 2011					
ST HELIERS	A,	52.0			Rotoehu Tephra in drill core			2.20	1.23	0.00	0.62
STYAKS SWAMP	A,	0.0		24.5	morphostratigraphy		just younger than Green Mt <sup>a</sup>	0.37	0.25	0.00	0.12
TANK FARM	A	52.0			morphostratigraphy		similar age to Onepoto and Pupuke <sup>a</sup>	5.87	4.13	0.00	2.06
TAYLORS HILL	A,B,C	24.2	27.4	30.6	Ar-Ar	Leonard et al. 2017	Mono Lake' p.mag excursion <sup>l</sup>	5.07	0.47	0.18	0.51
TE POU HAWAIKI	B	14.6			morphostratigraphy		older than Mt Eden <sup>c</sup>	28.1	0.00	0.08	0.12
THREE KINGS	A,B,C	27.7	28.7	29.7	14C	Lindsay et al. 2011	younger than One Tree Hill, Mt St John, Mt Hobson, older than Mt Eden <sup>a</sup>	69.3	0.00	3.00	4.51
WAITOMOKIA	A,B	15.6			morphostratigraphy		core contains Rotorua tephra, older than Pukeiti <sup>a</sup>	9.79	2.30	0.11	1.31
WIRI	A,B,C	25.6	30.2	34.8	Ar-Ar	Cassata et al. 2008	Mono Lake' p.mag excursion <sup>l</sup> , younger than Ash Hill <sup>b</sup>	16.4	0.08	0.86	1.34

Table 3

Source	abv	Age	error	ref	interpreted age (yr)	error	95% confidence limits	
AVF24 [P48]*	Ra2	504	5	a				
AVF24 [P49]*	Ra1	553	7	a				
Taupo	Tp	1,718	30	b				
Tuhua	Tu	6,577	547	b				
Mamaku	Ma	7,940	257	b				
Rotoma	Ro	9,423	120	b				
AVF23					9,950	300	9,650	10,240
Opepe	Op	9,991	160	b				
Waiohau	Wh	14,009	155	b				
AVF22					15,310	650	14,660	15,960
Rotorua	Rr	15,635	412	b				
Rerewhakaiaitu	Rk	17,496	462	b				
AVF21					20,080	100	19,080	21,070
AVF20					20,310	142	18,890	21,740
Okareka	Ok	21,858	290	b				
AVF19					24,200	880	23,320	25,090
AVF18					24,260	400	23,860	24,650
AVF17					23,350	350	23,000	23,700
AVF15					24,410	290	24,120	24,700
AVF14					24,550	290	24,270	24,840
Te Rere	Tr	25,171	964	b				
AVF16					25,230	860	24,370	26,090
AVF13					25,230	310	24,920	25,540
Kawakawa/Oruanui Kk		25,358	162	b				
AVF12					28,030	260	27,760	28,290
Okaia	O	28,621	1428	b				
AVF11					29,770	2240	27,530	32,010
AVF10					30,200	120	30,080	30,320
AVF9					30,200	2080	28,120	32,280
AVF8					30,400	400	30,000	30,810
AVF7					31,040	900	30,140	31,940
AVF6					33,710	1160	32,550	34,870
AVF5					34,200	860	33,340	35,070
AVF4					34,780	2000	32,780	36,780
Maketu	Mk	36,320	575	c				
Tahuna	Ta	39,268	1193	c				
Rotoehu	Re	52,000	7000	d				
AVF3					59,230	10,230	49,000	69,460
AVF2					67,200	6,250	60,950	73,450
AVF1					106,170	4,300	101,870	110,470
AVFa					126,150	3,320	122,830	129,470
AVFb					144,870	2,400	142,470	147,270
AVFc					181,430	580	180,850	182,010
AVFd		193,200	2,800	e				

Core	Sample name	New Horizon#	Depth (m)	Thickness (mm)	Average age (ka)	Proposed Centres	Confidence level	Age	Correlation criteria Chem	Scale	Location	Alternative(s)	Confidence level	Age	Correlation criteria Chem	Scale	Location
Post Rerewhakaia (c17.8ka)																	
	Pupuke	T21-1-48/5829	24	57.80	22	0.6	Rangitoto	1	✓	✓	✓	✓	-	-			
	Hopua	T4-2-H1-2/58839	23	38.95	3	9.95 ± 0.3	Mt Wellington	1	✓	✓	✓	✓	-	-			
	Pukaki	T14-47-72m	22	47.72	1.0	15.31 ± 0.65	Pukaki	2	✓	✓	✓	✓	-	-			
Rerewhakaia to Okareka (17.8 - 21.9ka)																	
	Pukaki	AT209-43.15m	21	49.15	3.0	20.08 ± 0.1	Mt Smart	2	✓	✓	✓	✓	Mt Eden	3	✓	✓	✓
	Hopua	T5-2-H1-18/58855/-58856	21	45.17	290							Paimuru Basin	2		✓	✓	✓
												Boggs Pt	3	?		✓	✓
	Pukaki	AT210-49.17m	20	49.17	2.0	20.3 ± 0.14	Waikomaka	2	✓	✓	✓	✓	Mt Robertson	3	?	✓	✓
	Hopua	T6-5-H1-20/58871/-58858	20	45.51	235							Chatawa	3	?		✓	✓
Okareka to Onumet (21.9 - 25.4ka)																	
	Pukaki	T42-51.05	19	51.05	1.0	24.2 ± 0.88	Chatawa	3	?	✓	✓	✓	Wiri Mt	3	✓	✓	✓
												Boggs Pt	3	?		✓	✓
												Mt Robertson	3	?		✓	✓
	Orakei Basin	OB1-450-4.44-99	18	44.22	8		Mt Robertson	3	?				Paimuru Basin	3	✓		
	Hopua	T5-6-H1-32/58869	18	47.81	40	24.26 ± 0.4						Boggs Pt	3	?			
	Pukaki	T45-51.19	18	51.19	0.5												
	Orakei Basin	OB1-455-4.44-99/-455-4.44-99A	17	44.65	5	23.35 ± 0.35	Pigeon Mt	3	?	✓	✓	✓	Little Rangitoto	3	✓	✓	✓
												Motukorea	2	✓	✓	✓	✓
												Mt Cambria	3	✓	✓	✓	✓
												Paimuru Basin	3	✓	✓	✓	✓
												Taylor's Hill	3	✓	✓	✓	✓
	Orakei Basin	OB1-453-4.44-99	15	47.72	12	24.41 ± 0.29	Motukorea	2	✓	✓	✓	✓	Pigeon Mt	3	?	✓	✓
												Mt Cambria	3	?	✓	✓	✓
	Orakei Basin	OB1-453-2-48-12/-48-12B	14	48.13	12	24.55 ± 0.29	Little Rangitoto	1	✓	✓	✓	✓	-	-			
	Orakei Basin	OB1-453-2-48-19/-48-27B	newB	48.28	10		?										
	Orakei Basin	OB1-453-4-43-14/-49-46	newA	49.46	45												
	Orakei Basin	OB1-454-3-50-08B/-49-55A	13	50.09	160	25.23 ± 0.86	Paimuru Basin	1	✓	✓	✓	✓	Mt Eden	2	✓	✓	✓
	Pukaki	T42-45-51.52	13 (16)	51.52	50.0							Little Rangitoto	2	✓	✓	✓	✓
												Mt Richmond	2	✓	✓	✓	✓
												Taylor's Hill	2	✓	✓	✓	✓
Onumet to Rotonehu (25.4 - ca. 52 ka)																	
	Orakei Basin	OB1-456-3-52-817/-53-02B	12	53.03	410							Three Kings	2	✓	✓	✓	✓
	Onepoto	On2-84-39.06	12	38.09	12							Ta Pou/Hawaki	3	✓	✓	✓	✓
	Pukaki	S4-355m	12	54.36		28.03 ± 0.26	Mt Eden	1	✓	✓	✓	✓					
	Pupuke	P23-58947	12	67.59	7												
	Hopua	T6-5-H1-39/58876	12	48.80	460												
	Pukaki	c. 60-165m	11	55.34	<10	29.8 ± 2.2	Pukututu	2	✓	✓	✓	✓	Kohura	3	✓	✓	✓
													Chatawa	3	✓	✓	✓
													Mt Robertson	3	✓	✓	✓
													Wiri Mt	3	✓	✓	✓
	Orakei Basin	OB1-457-3-52-115/-52-91B	10	54.21	407		Taylor's Hill	2	✓	✓	✓	✓	Paimuru Basin	2	?	✓	✓
	Onepoto	On2-84-39.47	10	39.47	15	30.2 ± 0.12						Pigeon Mt	3	?	✓	✓	✓
	Pupuke	T18-7-P26/58951	10	68.09	3							Three Kings	3	✓	✓	✓	✓
												Mt Cambria	3	✓	✓	✓	✓
	Pukaki	P27-58963	9	68.15	6	30.2 ± 2.08	Mt Richmond	3	✓	✓	✓	✓	Mt Cambria	3	✓	✓	✓
												Mt Richmond	3	✓	✓	✓	✓
												Hopua	3	✓	✓	✓	✓
	Orakei Basin	OB1-457-3-52-94-77	8	54.27	40												
	Pupuke	P25-58953	8	68.24	20	30.4 ± 0.4	Crater Hill	2	✓	✓	✓	✓	Kohura	2	✓	✓	✓
	Pukaki	c. 56-4m	8	56.40	ca. 720												
	Orakei Basin	OB1-457-3-52-104 (AVP7)	7	54.34	20												
	Onepoto	On2-84-39.90/-39-91A	7	39.90	20	31.04 ± 0.9	Three Kings	1	✓	✓	✓	✓	-	-			
	Pukaki	c. 56.0	7	56.80													
	Pupuke	T19-3-P29/58954	7	68.49	2												
	Pukaki	c. 67.0	6	57.10	ca. 500	33.71 ± 1.18	Kohura	2	✓	✓	✓	✓	Crater Hill	2	✓	✓	✓
													Pukututu	2	✓	✓	✓
													Wiri Mt	3	✓	✓	✓
													Mt Robertson	3	?	✓	✓
	Orakei Basin	OB1-456-3-52-142/-47-44B	5	57.34	110	34.2 ± 0.86	Mt Hobson	3	✓	✓	✓	✓	Little Rangitoto	3	✓	✓	✓
													Mt Cambria	3	✓	✓	✓
													Mt St John	3	✓	✓	✓
													Mt Victoria	3	✓	✓	✓
													North Head	3	✓	✓	✓
													Paimuru Basin	3	✓	✓	✓
													Taylor's Hill	3	✓	✓	✓
Pre Rotonehu ca. 52 ka																	
	Orakei Basin	OB1-445-5-67-03B/-61-17	3	67.04	41	59 ± 10.0	Mangere Mt	2	✓	✓	✓	✓	Mt Cambria	3	✓	✓	✓
													Mt Hobson	3	✓	✓	✓
													Mt Victoria	3	✓	✓	✓
													One Tree Hill	3	✓	✓	✓
	Orakei Basin	OB1-450-2-73-055	2	73.56	510												
	Glover Park	GP6-9-10-38/-10-6	2	10.60	60	67 ± 6.0	One Tree Hill	1	✓	✓	✓	✓	-	-			
	Onepoto	On2-46-2-43-86	2	43.66	4												
	Orakei Basin	OB1-454-3-80-047	1	80.05	100								Mt Ruakiri	3	✓	✓	✓
	Onepoto	AB1-On2-81-1-51-30	1	54.30	15	106 ± 4.0	Domain/Grafton	3	?	✓	✓	✓	North Head	3	✓	✓	✓
	Glover Park	GP16-17-52/18-15	1	18.15	12												
	Glover Park	GP1/24-20-78-21.0	AVP6	21.00	40	128 ± 3.0	Orakei	2	✓	✓	✓	✓	Domain/Grafton	3	✓	✓	✓
													Mt Albert	3	✓	✓	✓
													Mt Ruakiri	3	✓	✓	✓
													North Head	3	✓	✓	✓
	Onepoto	On2-818-62-36	AVP6	62.00	45	145 ± 2.0	Albert Park	2	✓	✓	✓	✓	Domain/Grafton	2	?	✓	✓
	Glover Park	GP1/40-23.67	AVP6	23.67	10												
	Onepoto	On2-821-66-68	AVP6	66.68	270	181 ± 0.6	Tank Farm	1	✓	✓	✓	✓	Pupuke	3	✓	✓	✓

Table 5

Centre (eruption)	AVF#	Confidence level	DREkm <sup>3</sup> (2sf)	Orakei Basin			Glover Park			Onepoto			Pukaki		Hopua			Pupuke		
				Distance to (km)	Horizon thickness (mm)	shard size (µm)	Distance to (km)	Horizon thickness (mm)	shard size (µm)	Distance to (km)	Horizon thickness (mm)	shard size (µm)	Distance to (km)	Horizon thickness (mm)	Distance to (km)	Horizon thickness (mm)	shard size (µm)	Distance to (km)	Horizon thickness (mm)	shard size (µm)
Rangitoto	AVF24	1	0.70		n/a			n/a			n/a			n/a			n/a	8.4	22	>200
Mt Wellington	AVF23	1	0.082		n/a			n/a			n/a		10.4	1	7.0	3	>200		n/a	
Little Rangitoto	AVF14	1	0.0017	0.9	12	>200		n/a			n/a			n/a			n/a		n/a	
Panmure Basin	AVF13	1	0.0074	5.2	160	100-200		n/a			n/a			n/a			n/a		n/a	
Mt Eden	AVF12	1	0.090	4.4	410	>200		n/a		7.9	12	100-200	12.3	3	6.0	460	>200	10.7	7	50-100
Three Kings	AVF7	1	0.069	6.5	20	100-200		n/a		10.6	12	50-100	10.1	2		n/a		13.5	2	50-100
One Tree Hill	AVF2	1	0.26	4.6	510	>200	9.6	60	>200	10.8	4	100-200		n/a		n/a			n/a	
Tank Farm	AVFc	1	0.0059		n/a			n/a		0.6	270	>200		n/a		n/a			n/a	
Pukeiti	AVF22	2	0.0037		n/a			n/a			n/a		4.7	1		n/a			n/a	
Mt Smart	AVF21	2	0.013		n/a			n/a			n/a		7.0	3	2.7	290	>200		n/a	
Waitomokia	AVF20	2	0.010		n/a			n/a			n/a		3.7	2	5.5	235	100-200		n/a	
Motukorea	AVF15	2	0.0046	8.4	12	50-100		n/a			n/a			n/a			n/a		n/a	
Puketutu	AVF11	2	0.018		n/a			n/a			n/a		6.0	<10		n/a			n/a	
Taylor's Hill	AVF10	2	0.0051	5.1	407	>200		n/a		12.4	15	100-200		n/a		n/a		13.2	3	100-200
Crater Hill	AVF8	2	0.024	13.2	45	100-200		n/a			n/a		1.5	720		n/a		23.5	20	<50
Kohuora	AVF6	2	0.0072		n/a			n/a			n/a		2.9	500		n/a			n/a	
Orakei Basin	AVFa	2	0.0067		n/a		5.4	40	100-200		n/a			n/a		n/a			n/a	
Albert Park	AVFb	2	0.028		n/a		8.8	10	50-100	5.0	45	100-200		n/a		n/a			n/a	

1

2

3

4

5

6

Table 6

Centre Name	Region	Total DRE volume (km <sup>3</sup> )	Tephra thickness (cm)	Dispersal distance (km)
Paricutin	Michoacán-Guanajuato volcanic field, Mexico	2.5	25	7
Sunset Crater	San Francisco volcanic field, Arizona	0.58	10	20
<b>One Tree Hill</b>	<b>Auckland volcanic field, New Zealand</b>	<b>0.26</b>	<b>6</b>	<b>9.6</b>
Mt Gambier	Newer Volcanics province, south-eastern Australia	0.198	≤5	10 to 12
Lanthrop Wells	Southwestern Nevada volcanic field	0.12	1	10
Cerro Negro*	Nicaragua	0.16	0.5	16
<b>Three Kings</b>	<b>Auckland volcanic field, New Zealand</b>	<b>0.069</b>	<b>2</b>	<b>6.5</b>
Marcath Volcano	Lunar Crater volcanic field, Central Nevada	0.06	2	7
<b>Orakei Basin</b>	<b>Auckland volcanic field, New Zealand</b>	<b>0.0067</b>	<b>0.4</b>	<b>5.4</b>

---

**Reference**

---

Ort et al., 2008

Ort et al., 2008

**This study**

Lowe and Palmer, 2005; van  
Otterloo and Cas, 2013

Valentine et al., 2008

Hill et al., 1998

**This study**

Johnson et al., 2014

**This study**

---



Table 7

Relative Order	Centre Name	Mean age (t) in ka	Error (1sd)	Age ref.	Time relationship		Distance r d+1 (km)
					t+1 (ka)	t+2 (ka)	
0	Rangitoto 2	0.50	±0.05	b	-		-
1	Rangitoto 1	0.55	±0.07	b	0.05	-	0.1
2	Mt Wellington	10.00	±0.5	a	9.4	9.5	11.7
3	Purchas Hill	10.90	±0.14	b	0.9	10.3	0.6
4	Pukeiti	15.31	±0.65	a	4.4	5.3	13.4
<b>Rerewhakaaitu (ca. 17.5 ka)</b>							
5	Styaks Swamp	19.10	-	d	3.8	8.2	13.9
6	Green Mt	19.60	±3.3	c	0.5	4.3	0.6
7	Mt Smart	20.08	±0.1	a	0.5	1.0	8.1
8	Waitomokia	20.30	±0.14	a	0.2	0.7	7.6
<b>Okareka (ca. 21.9 ka)</b>							
9	Otuataua	24.20	±0.88	a	3.9	4.1	1.7
10	Mt Robertson	24.26	±0.4	a	0.1	4.0	8.8
11	Pigeon Mt	23.35	±0.35	a	-0.9	-0.8	8.5
12	Motukorea	24.41	±0.29	a	1.1	0.1	6.5
13	Little Rangitoto	24.55	±0.29	a	0.1	1.2	9.1
14	Panmure Basin	25.23	±0.86	a	0.7	0.8	4.8
<b>Oruanui/Kawakawa (ca. 25.4 ka)</b>							
15	Mt Eden	28.03	±0.26	a	2.8	3.5	8.3
16	Te Pou Hawaiki	28.53	-	d	0.5	3.3	0.7
17	Puketutu	29.80	±2.2	a	1.3	1.8	9.3
18	Taylors Hill	30.20	±0.12	a	0.4	1.7	8.0
19	Mt Richmond	30.20	±2.08	a	0.0	0.4	8.0
20	Wiri Mt	30.20	±4.6	c	0.0	0.0	8.5
21	Ash Hill	30.70	-	d	0.5	0.5	1.0
22	Crater Hill	30.40	±0.4	a	-0.3	0.2	4.4
23	Hopua	31.00	-	d	0.6	0.3	6.5
24	Three Kings	31.04	±0.9	a	0.0	0.6	4.6
25	Kohuora	33.71	±1.16	a	2.7	2.7	11.5
26	Mt Hobson	34.20	±0.86	a	0.5	3.2	12.0
27	Mt Victoria	34.78	±2.0	a	0.6	1.1	6.6
28	McLennan Hills	41.30	±1.2	d	6.5	7.1	12.2
29	Mt Cambria	42.30	±11.1	c	1.0	7.5	12.5
30	McLaughlins Hill	48.20	±3.2	c	5.9	6.9	21.5
<b>Pre Rotoehu (ca. 52 ka)</b>							
31	Otara	56.5	-	d	8.3	14.2	8.7
32	Hampton Park	57.0	±16.0	c/d	0.5	8.8	0.5
33	Mangere Mt	59.0	±10.0	a	2.0	2.5	5.4
34	Mangere Lagoon	59.5	-	d	0.5	2.5	0.9
35	One Tree Hill	67.0	±6.0	a	7.5	8.0	8.6
36	Mt St John	75.3	±1.7	c	8.3	15.8	8.2
37	North Head	87.5	±7.6	c	12.2	20.5	6.8
38	Maungetaketake	88.9	±2.4	c	1.4	13.6	19.4

39	Mt Roskill	105.3	±3.1	c	16.4	17.8	9.1
40	Domain	106.0	±4.0	a	0.7	17.1	6.7
41	Grafton	106.5	-	d	0.5	1.2	0.3
42	Mt Albert	117.6	±5.2	c	11.1	11.6	5.6
43	Orakei	126.0	±3.0	a	8.4	19.5	8.6
44	Albert Park	145.0	±2.0	a	19.0	27.4	4.4
45	St Heliers	161.0	±18.0	d	16.0	35.0	8.8
46	Tank Farm	181.0	±1.0	a	20.0	36.0	11.4
47	Onepoto	187.6	-	d	6.6	26.6	0.6
48	Pupuke	193.2	±2.8	c	5.6	12.2	3.3
<b>Undated centres</b>							
	Pukaki	>52.0					
	Pukewairiki	>130					
	Boggust Park	?					
	Cemetery Hill	?					
	Puhinui Craters	?					

---

relationship  
d+2 (km)

-

11.8

10.7

12.8

13.4

13.5

8.1

12.3

9.1

7.1

16.8

13.9

8.5

9.1

4.0

7.8

9.9

9.6

9.2

15.8

8.5

3.7

11.5

10.2

7.5

3.2

17.4

7.8

0.4

9.4

16.0

6.5

14.0

6.3

3.3

7.3

14.7

12.7

11.5

15.1

6.4

6.0

3.6

6.3

5.4

5.5

11.4

2.7

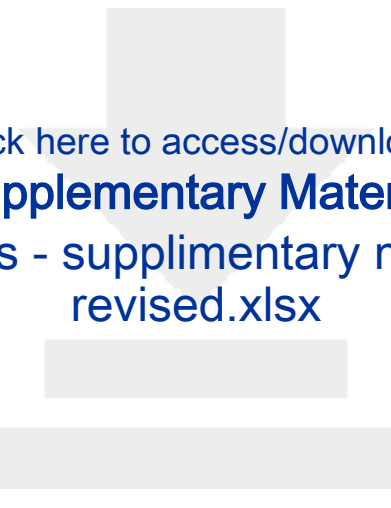




[Click here to access/download](#)

**Supplementary Material**

Correlation ms - Supplementary Material text  
final(2).docx



[Click here to access/download](#)

**Supplementary Material**

Correlation ms - supplimentary material tables  
revised.xlsx